1989

Multizone modeling of a fumigated diesel engine

Pradheepram Ottikkutti
Iowa State University

Order Number 9014936

Multizone modeling of a fumigated diesel engine

Ottikkutti, Pradheepram, Ph.D.

Iowa State University, 1989

U·M·I
300 N. Zeeb Rd.
Ann Arbor, MI 48106

Multizone modeling of a fumigated diesel engine

by

Pradheepram Ottikkutti

A Dissertation Submitted to the

Graduate Faculty in Partial Fulfillment of the

Requirements for the Degree of

DOCTOR OF PHILOSOPHY

Major: Mechanical Engineering

Approved:

Signature was redacted for privacy.

In Charge of Major Work

Signature was redacted for privacy.

For the Major Department

Signature was redacted for privacy.

For the Graduate College

Members of the Committee:

Signature was redacted for privacy.

Iowa State University
Ames, Iowa
1989

TABLE OF CONTENTS

ACKNOWLEDGEMENTS xii

1. INTRODUCTION 1

1.1 Research Goals 2

1.2 Dissertation Organization 3

2. REVIEW OF LITERATURE 4

2.1 Modeling of Diesel Combustion 4

2.1.1 Multidimensional models 4

2.1.2 Phenomenological models 6

2.1.3 Spray geometry 9

2.1.4 Fuel-air mixing 10

2.1.5 Ignition 19

2.1.6 Combustion 21

2.1.7 Heat transfer 23

2.1.8 Emissions 23

2.2 Fumigated Diesel Engines 25

2.2.1 Experimental studies 25

2.2.2 Analytical and modeling studies 26

2.3 Need for Present Research 29

3. DEVELOPMENT OF DIESEL COMBUSTION MODEL 30

3.1 Introduction 30

3.2 Thermodynamic Calculations 31

3.3 Transient Spray Calculations 41

3.3.1 Justification of gas jet assumption 48

3.3.2 Spray geometry 50

3.3.3 Fuel-air distribution correlations 60

3.3.4 Definition of zone boundaries 65

3.3.5 Evolution of zones 68

3.4 Phases of the Combustion Process 76

3.5 Initial Conditions for the Model 83

3.6 Nitric Oxide Sub-model 86

3.7 Summary 87

4. EXPERIMENTAL APPARATUS AND TEST PROCEDURE . 89

4.1 Experimental Apparatus 89

4.1.1 Engine 89

4.1.2 Fumigation system 92

4.1.3 Measurement of fuel flows, temperatures, pressures, and exhaust emissions 92

4.2 Data Acquisition System 94

4.3 Experimental Procedure 95

4.3.1 Test matrix 95

4.3.2 Alcohol and water mixture preparation 96
4.3.3 Test procedure 99
4.4 Data Analysis 101
5. RESULTS AND DISCUSSION 103
5.1 Capabilites of the Multizone Model 103
5.1.1 Model-predicted exhaust temperature 107
5.2 Comparison of Experimental Results and Model Predictions 114
5.2.1 Effect of speed and load 116
5.2.2 Effect of percent torque replacement 129
5.2.3 Effect of alcohol proof 136
5.2.4 Comparison of ethanol and methanol 143
5.2.5 Water injection 152
5.3 Discussion 155
5.3.1 Capabilities of the model 157
5.3.2 Failure to predict higher thermal efficiencies at lower loads . . 160
5.3.3 Large discrepancy in exhaust temperature predictions 162
5.3.4 Poor NO prediction 163
6. CONCLUSIONS 170
6.1 Summary 170
6.2 Recommendations for Future Work 172
6.2.1 Include heat transfer between individual zones 172
6.2.2 Improve the wall model 172
6.2.3 Include premixed burning of alcohol-air mixture 173

6.2.4 Verify spray geometry 174

6.2.5 Model other pollutants 174

7. REFERENCES 175

8. APPENDIX A: EVALUATION OF PROPERTIES OF EQUILIBRIUM COMBUSTION PRODUCTS 181

9. APPENDIX B: UNBURNED MIXTURE PROPERTY EVALUATION 185

9.1 Mixture Properties 185

10. APPENDIX C: BURNED GAS PROPERTY EVALUATION FOR TWO FUELS 195

11. APPENDIX D: INSTANTANEOUS BURNING OF NEWLY CREATED ZONES 200

12. APPENDIX E: WALL IMPINGEMENT MODEL 206

12.1 Division of the Combustion Period into Discrete Phases 206

12.2 Instantaneous Mixing in Zone D 208

12.3 Solution Procedure to Obtain Final Conditions 212

13. APPENDIX F: MODELING THE FORMATION OF NITRIC OXIDE 216

14. APPENDIX G: DIESEL FUEL PROPERTIES 221

LIST OF TABLES

Table 4.1: John Deere 4276 T Four Cylinder Engine Specifications . . . 91

Table 4.2: Methanol-Water Mixture Data 99

Table 5.1: Effect of Speed (1500 rpm and 2100 rpm) and Load (25%, 50%, 75% and 100% of full load) on IMEP and $\eta_{th,ind}$ for Diesel-only and Alcohol Fumigation (30% Torque Replacement from 80 Proof and 169.5 Proof Ethanol) 117

Table 5.2: Effect of Percent Torque Replacement (10%, 20% and 30%) on IMEP and $\eta_{th,ind}$, at 1500 and 2100 rpm, with 80 Proof and 169.5 Proof Ethanol 130

Table 5.3: IMEP and $\eta_{th,ind}$ at various Ethanol Proofs (40 Proof to 169.5 Proof), with 30% Torque Replacement, at 100% and 50% Load Conditions, at 1500 and 2100 rpm 137

Table 5.4: IMEP and $\eta_{th,ind}$ for Ethanol and Methanol Fumigation (40 Proof/Pr.EEM to 169.5 Proof/Pr.EEM), with 20% Torque Replacement at 1500 rpm, and 100% of Full Load 146

Table 5.5: IMEP and $\eta_{th,ind}$ for Ethanol and Methanol Fumigation (40 Proof/Pr.EEM to 169.5 Proof/Pr.EEM), with 30% Torque Replacement at 2100 rpm, and 100% of Full Load 146

Table 5.6: IMEP and $\eta_{th,ind}$ for Water Fumigation at 1500 rpm, 100% and 75% of Full Load 153

Table 5.7: Effect of Load on the Timing of Phase 3 at 1500 rpm 161

Table 13.1: Table of Reaction Rate Constants 218

LIST OF FIGURES

Figure 3.1: General Description of Zone Division in the Cylinder (Top View) 32

Figure 3.2: Spray Geometry in a Non-swirling Medium 42

Figure 3.3: Spray Geometry in a Swirling Medium 43

Figure 3.4: Zone Division at Incipient Ignition (θ_{ign}) 45

Figure 3.5: Zone Division at $\theta_{ign} + \Delta\theta$ 46

Figure 3.6: Zone Division at $\theta_{ign} + K_\theta(\Delta\theta)$. New Zone B_2 is Evolved . . 46

Figure 3.7: Plot of Spray Cone Angle 54

Figure 3.8: Modified Spray Geometry in a Swirling Medium 58

Figure 3.9: Diesel Concentration Profile Along the Spray Axis 62

Figure 3.10: Diesel Concentration Profile Across the Spray Axis 63

Figure 3.11: Phase 1: Free Jet 77

Figure 3.12: Phase 2: Wall Jet with Fuel Injection 78

Figure 3.13: Phase 3: Wall Jet following End of Injection 80

Figure 3.14: Phase 4: Wall Jet, Spray Plume Completely Transferred to Zone D 81

Figure 3.15: Phase 5: Cylinder Contents are Homogeneous 82

Figure 3.16: Control Volumes for Intake Pipe and Engine Cylinder 84

Figure 4.1: Schematic of Experimental Apparatus 90

Figure 5.1: Model-predicted Pressure versus Crank Angle, at 1500 rpm, 100% Load, 30% Torque supplied by 140 Proof Ethanol . . . 105

Figure 5.2: Model-predicted Pressure versus Volume, at 1500 rpm, 100% Load, 30% Torque supplied by 140 Proof Ethanol 106

Figure 5.3: Model-predicted Nitric Oxide versus Crank Angle, at 1500 rpm, 100% Load, 30% Torque supplied by 140 Proof Ethanol 108

Figure 5.4: Exhaust Temperature versus Load, Diesel-only 119

Figure 5.5: Exhaust Temperature versus Load, at 1500 rpm, 30% Torque supplied by Ethanol 121

Figure 5.6: Exhaust Temperature versus Load, at 2100 rpm, 30% Torque supplied by Ethanol 122

Figure 5.7: Exhaust NO Concentration versus Load, Diesel-only at 1500 and 2100 rpm 124

Figure 5.8: Exhaust NO Concentration versus Load, at 1500 rpm, 30% Torque supplied by Ethanol 125

Figure 5.9: Exhaust NO Concentration versus Load, at 2100 rpm, 30% Torque supplied by Ethanol 126

Figure 5.10: Comparison of Model-predicted and Measured Nitric Oxide Emissions 128

Figure 5.11: Exhaust Temperature versus Percent Torque Replacement from Ethanol at 1500 rpm 131

Figure 5.12: Exhaust Temperature versus Percent Torque Replacement from Ethanol at 2100 rpm 133
Figure 5.13: Exhaust NO Concentration versus Percent Torque Replacement from Ethanol at 1500 rpm 134
Figure 5.14: Exhaust NO Concentration versus Percent Torque Replacement from Ethanol at 2100 rpm 135
Figure 5.15: Exhaust Temperature versus Ethanol Proof at 1500 rpm, 30% Torque Replacement 139
Figure 5.16: Exhaust Temperature versus Ethanol Proof at 2100 rpm, 30% Torque Replacement 140
Figure 5.17: Exhaust NO Concentration versus Ethanol Proof at 1500 rpm, 30% Torque Replacement 141
Figure 5.18: Exhaust NO Concentration versus Ethanol Proof at 2100 rpm, 30% Torque Replacement 142
Figure 5.19: Comparison of Model-Predicted and Measured Nitrogen Oxides Emission 144
Figure 5.20: Exhaust Temperature versus Alcohol Proof, at 1500 rpm 100% Load, 20% Torque Replacement 147
Figure 5.21: Exhaust Temperature versus Alcohol Proof, at 2100 rpm 100% Load, 30% Torque Replacement 148
Figure 5.22: Exhaust NO Concentration versus Alcohol Proof, at 1500 rpm 100% Load, 20% Torque Replacement 150

Figure 5.23: Exhaust NO Concentration versus Alcohol Proof, at 2100 rpm 100% Load, 30% Torque Replacement 151

Figure 5.24: Exhaust Temperature versus Water Injection Rate, at 1500 rpm, 100% and 75% Load 154

Figure 5.25: Exhaust NO Concentration versus Water Injection Rate, at 1500 rpm, 100% and 75% Load 156

Figure 5.26: Nitric Oxide History in the Cylinder, Experimental and Model-predicted Data 158

Figure 5.27: Nitric Oxide History in the Cylinder and the Wall Zone, at 1500 rpm, 80 Proof Ethanol, 30% Torque Replacement 164

Figure 5.28: Variation of Nitric Oxide History in the Wall Zone, at 1500 rpm, for four different Ethanol Proofs, 30% Torque Replacement 165

Figure 5.29: Equivalence Ratio History in the Wall Zone, at 1500 rpm, for four different Ethanol Proofs, 30% Torque Replacement . . . 167

Figure 5.30: Temperature History in the Wall Zone, at 1500 rpm, for four different Ethanol Proofs, 30% Torque Replacement 168

ACKNOWLEDGEMENTS

I would like to express my sincere thanks to Professor Jon H. Van Gerpen for his continuous inspiration and guidance in the pursuit of this research work.

I am appreciative of the immense patience and tolerance of my wife Lathalini Pradheepram during long hours of my research work, and for typing my dissertation on the computer conscientiously to meet deadlines. I am thankful to my parents who have been a constant source of encouragement throughout my educational career.

I would like to thank Professor Delmar B. Van Meter for providing me the opportunity to work as a graduate assistant on three of his research projects which was vital to complete my research and dissertation.

The help and support of my friends, Thiagaraj Subbian and Srikanth Padmanaban during my stay at Iowa State are greatly appreciated.

I wish to thank the technical staff of the Mechanical Engineering Department at Iowa State University: Gaylord Scandrett, James Dautremont, Brian Espeland and Robert Steed for their technical support and assistance in setting up the engine test facility and instrumentation. The computer consultancy services offered by Frank Poduska were very helpful in getting the engine data acquisition system to work and also in speeding up the modeling work.

I am grateful to the others who have directly or indirectly helped me in completing my Ph.D. studies at Iowa State.

1. INTRODUCTION

Public awareness of the need to maintain a clean environment is motivating extensive research into the sources of pollution and ways to reduce it. This research has confirmed that internal combustion engines are major contributors to air pollution. In addition to the environmental threat posed by these engines, their source of fuel, crude oil, is being depleted at an increasing rate. The development of less polluting and more efficient engines is a high priority for engine manufacturers.

Modern internal combustion engines can generally be divided into two types: spark-ignited and compression-ignited, or diesel, engines. Diesel engines operate with higher efficiency while producing lower levels of carbon monoxide and unburned hydrocarbons than spark-ignited engines. Although their emission of oxides of nitrogen are comparable to those from spark-ignited engines and their particulate emissions are much higher, diesel engines have become the dominant power source for trucks and buses. However, these vehicles have been identified as being important contributors to air pollution in urban areas. The Environmental Protection Agency has mandated that by 1991 urban buses must drastically reduce their emisssions of oxides of nitrogen and particulates. In 1994 these regulations will be extended to all diesel-powered vehicles [1].

Spraying methanol or ethanol into the intake air of the engine has been considered

as an option to reduce exhaust emissions from diesel engines. The amount of diesel fuel supplied to the engine is reduced, and the resulting decrease in power output of the engine is replaced by the alcohol. This technique, called fumigation, has been shown to provide significant reductions in oxides of nitrogen and particulates from the engine, although at the expense of higher carbon monoxide and unburned hydrocarbons.

With the more stringent regulations on exhaust emissions for diesels, engine manufacturers are faced with the challenge of developing better engines. Engine development is very expensive and requires a large amount of time. Engine manufacturers often resort to computer modeling of their engines to reduce development time and cost. Modeling is used as a tool to predict engine performance and pollution characteristics. Several attempts to model diesel engine behavior can be found in published literature. These models range from simple phenomenological models to very detailed multi-dimensional models. Complete prediction capability in terms of overall engine performance and pollution characteristics is yet to be achieved by these modeling efforts.

1.1 Research Goals

Very few attempts have been made to provide models for fumigated diesel engines. The objective of this study is to provide such a model. The model was intended to be a general diesel engine model capable of predicting the performance of single-fuel diesel engines as well. The goals of this study were;

1. to develop a computer model to predict engine performance parameters such as indicated mean effective pressure, indicated thermal efficiency, exhaust temper-

ature, and oxides of nitrogen in the exhaust, and

2. to verify the model using experimental data obtained by modifying an existing multi-cylinder turbocharged diesel engine to operate with ethanol fumigation. The experiments will determine the effect of speed, load, and fraction of torque derived from the fumigated alcohol on the thermal efficiency, and the exhaust levels of carbon monoxide, carbon dioxide, unburned hydrocarbons, oxides of nitrogen and smoke. The ability of the model to predict the effects of methanol fumigation on engine performance and exhaust emission, and the effect of water in the fumigated mixture will be investigated also.

1.2 Dissertation Organization

To recognize and understand work carried out by other researchers in the area of diesel modeling, a detailed review of the published literature was undertaken. Several modeling efforts including phenomenological and multi-dimensional models were reviewed. A summary of this review is provided in Chapter 2.

It was determined that the most suitable approach to meeting the research goals of this project was to develop a phenomenological multizone model. Details on the development of the multizone transient spray mixing model are provided in Chapter 3. Chapter 4 explains the experimental set-up used for the fumigation tests, the data-acquisition system, and the test procedure. Comparisons between model predictions and experimental data are discussed in Chapter 5. The conclusions are summarized in Chapter 6. Additional details on the important sub-models of the multizone model are provided in the Appendices.

2. REVIEW OF LITERATURE

This literature review is divided into two main sections. The first section is a review of recent diesel engine modeling efforts. The modeling efforts have been classified as either multidimensional, or phenomenological. The second section is a review of previous work fumigated diesel engines with particular emphasis on alcohol utilization. This section includes a discussion of both experimental and modeling studies on diesel engines operated on two fuels.

2.1 Modeling of Diesel Combustion

Numerous efforts have been made to model combustion processes in diesel engines. The present mathematical models can be classified under two main categories:

i. multidimensional or fluid mechanics models, and

ii. phenomenological models.

2.1.1 Multidimensional models

Multidimensional models are based on numerical solution of the fundamental differential equations which govern the fluid motions and the combustion process. These models are capable of providing detailed information in both space and time. The governing equations are developed and solved for the combustion chamber which

is divided into a fine geometric mesh. Such models require large amounts of computer time compared to phenomenological models.

A number of multidimensional models have been described in the literature. A typical example of a comprehensive code used for three-dimensional engine simulation is KIVA developed by Amsden et al. [2]. This code includes spray dynamics, fluid motion, mixing, chemical reactions and the resulting energy release. The turbulence model used is a subgrid scale transport model. The spray is represented by a number of groups of droplets, with constant physical properties assumed for droplets within each group. The model disregards thick spray effects. Although the spray model in the KIVA code compares well with experiments and has good numerical accuracy, the drop sizes and the spray cone angle must be supplied from correlations of atomizing liquid jets. This is a weakness of the KIVA code. In a study by O'Rourke and Amsden [3] the KIVA code was used to simulate a stratified charge diesel engine and the results were compared against experimental data. For the cases tested, the computed pressures were higher than measured pressures near top dead center, and the predicted peak pressures occurred about three to four degrees prior to the measured peak pressure location, indicating a faster burning rate. Amsden states that this discrepancy may be a result of one or more of the following weaknesses in their code: chemical conversion of the fuel being too fast, excessively rapid vaporization of the liquid fuel jet, high turbulence causing quick mixing of fuel, or the mesh division being too coarse. For the cases discussed the mesh size used created about 8000 to 10,000 cells and the computation time for one half of an engine cycle was about three hours on a CRAY-XMP processor. This indicates that if a finer mesh division is used

the resulting increase in computation time and cost would prohibit the use of such a code on a regular basis to address engine development related questions.

Recently McKinley et al. [4] and Zur Loye et al. [5] compared in-cylinder air motion measured in a motored two-stroke, high swirl engine using Laser Doppler Velocimetry with computed results obtained using the KIVA code. In the first investigation [4] comparisons were made for both circular and square shaped piston bowls. The mean radial and tangential velocity distributions were found to be in good agreement with measurements. The turbulence intensities also agreed well for most of the cycle, except during the expansion stroke. The model was found to respond correctly to the change in bowl geometry. McKinley stated that the differences in the turbulence intensities between the model and experiment are caused by shortcomings in the K-ε turbulence model used in the code. This is characteristic of most multidimensional modeling studies. There is a lack of reliable experimental data to provide good estimates of initial conditions, boundary conditions, and turbulence properties.

2.1.2 Phenomenological models

Phenomenological models are particularly well-suited for general engine simulation and the assessment of overall engine performance. Although phenomenological models lack the detailed spatial resolution that can be provided by the multidimensional models, they are capable of producing sufficient details for general engine development with significantly less computation time.

Phenomenological models are based on empirical relations to describe or quantify the individual processes that occur in an engine, such as: intake and exhaust, fuel

spray development, fuel-air mixing, ignition delay, combustion, heat transfer and formation of pollutants.

Phenomenological models can be further classified as: single zone, two zone, three zone, and multizone models. Single zone models are exemplified by the work of Lyn [6] and Shipinski et al. [7]. Single zone models treat the entire cylinder contents as homogeneous. Lyn [6] hypothesised that the major factors influencing the burning rate in diesel engines are: injection rate, engine speed, and combustion chamber design. Lyn developed a relationship between the rate of injection and the rate of burning in a direct-injection diesel engine with a central multihole nozzle, by dividing the injection diagram into elements according to their order of entry into the combustion chamber. A corresponding burning rate diagram that consisted of triangular shaped profiles that had been shifted in time by an amount equal to the ignition delay period was proposed. The model-predicted peak pressure, rate of pressure rise, and thermal efficiency matched closely with experimental data. The disadvantage of this technique is the need for prior knowledge of the injection diagram.

Shipinski et al. [7] developed an empirical relationship between the rate of injection and the heat release rate for a diesel engine. The correlations were based on actual engine data obtained under various operating conditions. Mathematical expressions relating the heat release to engine operating variables such as injection system settings and the fuel properties were developed. The method proposed by Shipinski also requires knowledge of the injection rate. The techniques suggested by Lyn [6] and Shipinski et al. [7] were not tried on other engines to confirm their capability to predict engine performance.

Two zone and three zone models are improvements over single zone models. The modeling work of Kouremenos et al. [8] on an indirect injection diesel engine, and the availability analysis of Van Gerpen and Shapiro [9] on a direct-injection engine are examples of two zone models. In two zone models the cylinder is divided into a product zone and a zone containing air alone or air mixed with unburned fuel. Combustion occurs instantaneously as air and fresh fuel are entrained from the unburned zone into the hot product zone. The pollutants are assumed to form in the product zone at the mass-averaged temperature of this zone. The capability of the two zone models to predict emissions is better than the single zone model, but it still assumes homogeneous properties for the entire product zone.

The three zone model of Gao [10] was used to model a fumigated diesel engine. The cylinder is divided into a zone containing a homogeneous mixture of unburned fumigated fuel and air, a second zone containing unburned diesel fuel, and a third zone containing burned products of combustion. The capability of this model to predict the oxides of nitrogen matched well with actual test data under a very limited range of engine operating conditions. Further details of this model are given in Section 2.

Multizone models account for the spatial variation in properties within the cylinder by dividing the cylinder into a number of smaller zones. The various multizone models developed for diesel combustion differ widely in their assumptions and the details of describing the individual processes. The phenomenological models of the following authors have been identified as important: Dent and Mehta [11], and Dent et al. [12], Meguerdichian and Watson [13], Lipkea and DeJoode [14], Chiu et al. [15], and Rife and Heywood [16]. These multizone modeling efforts are discussed in detail

below with particular reference to the types of sub-models used for the individual physical processes, and the capability of these models to predict diesel combustion.

The main purpose of the work described in this dissertation is to model the compression and combustion phases of the engine cycle. The intake and compression processes have been modeled by Jiang and Van Gerpen [17] and the exhaust process following the opening of exhaust valve can be modeled as a sudden decrease in the cylinder pressure to the exhaust back pressure. Details of the intake and compression model are given in Chapter 3, and a simple model used to estimate the exhaust temperature is described in Chapter 5.

2.1.3 Spray geometry

The development of a spray in a combustion chamber is characterized by the spray geometry. Spray penetration and cone angle are two of the most important parameters used to describe a spray. The spray penetration determines the distance traveled by the leading edge of the spray away from the injection tip. The cone angle describes the divergence of the spray as it leaves the injector. With appropriate assumptions for the concentration distribution in the spray, the penetration and cone angle can be used to determine the rate of air entrainment into the spray.

Dent and Mehta [11] developed a phenomenological model for a quiescent chamber diesel engine and later extended it to include swirl effects [12]. The spray penetration was obtained from the expression of Dent [18]. The penetration correlation of Hiroyasu et al. [19] was used for the early part of the injection period. The spray cone angle was not used to model mixing and entrainment in this work.

In their multizone modeling of a direct-injection diesel engine with swirl, Lipkea and DeJoode [14] used Dent's spray penetration correlation [18] for a quiescent chamber. The effect of air swirl was included by using the correlation of Patrick [20]. The spray cone angle was not required to model mixing and air entrainment.

The work of Chiu et al. [15] is the forerunner of other published efforts [21, 22] by researchers at the Cummins Engine Company to develop a phenomenological multizone model for a diesel engine. The spray penetration and cone angle were obtained from spray experiments and photographs in a constant volume combustion bomb. The spray width at each location along the spray centerline was calculated using a simple correlation based on Prandtl's mixing length theory.

In the multizone model of Meguerdichian and Watson [13] spray penetration for a straight fuel jet in the absence of swirl was obtained using Dent's equation [18]. The deflection of this straight jet in a swirling flow was calculated using Patrick's correlation [20]. Cone angle was not required for calculating fuel-air mixing rates and entrainment rates.

Although they were not used by their authors to model diesel combustion, the spray penetration and cone angle correlation of Wakuri et al. [23] are simple and easy to use for diesel spray modeling. The details of these correlations are given in Chapter 3.

2.1.4 Fuel-air mixing

The fuel spray injected into the cylinder entrains air as a result of the shear layer formed along the boundary of the spray. The air entrained into the spray

plume mixes with the atomized fuel particles to form a heterogeneous mixture of fuel and air. Combustion in a diesel engine is largely controlled by this mixing process. The representation of this mixing process is an important requirement for any diesel engine model. The mixing process itself can be considered to be comprised of a sequence of processes such as: fuel atomization, air entrainment due to jet mixing, fuel evaporation, wall impingement, and preparation of a combustible mixture. Some of the mixing models developed for diesel engines and their application in complete cycle modeling will be reviewed in this section.

Wilson and Wallace [24] developed a mathematical model of the mixing processes in swirling flows based on the work of Adler and Baron [25] describing jets of variable composition in a crossflow. The model assumes a two-phase spray in the form of a mist of fine droplets, moving at the speed of the entrained (swirling) air. The model assumes that the jet is turbulent and the jet growth results from a linear superposition of two mechanisms: a growing axisymmetric jet, and a growing vortex pair. The results of this mixing model were found to correctly describe both quantitatively and qualitatively the mean flow in jets injected into a crossflow. Wilson and Wallace [24] state that this jet mixing model will provide a fundamental basis for a sophisticated phenomenological combustion model, but the complete model has not yet been published.

The basic approach of the phenomenological model due to Dent and Mehta [11] and Dent et al. [12] has been extended to a multizone spray model by Gupta et al. [26]. The fuel spray is divided into a number of elements or zones. The spray region between the spray centerline and the spray periphery is divided into sixteen

equal radial divisions, and the number of axial divisions increases with the injection duration at the rate of one additional axial division for every 1 degree crank interval. The droplet number distribution is based on a binary droplet division model, which assumes sixteen classes of droplet sizes. The droplets of all sixteen sizes are assumed to be randomly distributed throughout the spray region. The radial distribution of fuel concentration is based on a profile due to Abramovich [27].

$$\frac{C'}{C'm} = 1 - \left(\frac{y}{b}\right)^{1.5} \tag{2.1}$$

where

C' = fuel concentration at any location (x,y) in the spray

$C'm$ = spray centerline fuel concentration at distance x from the nozzle

y = vertical distance from the spray centerline

b = radius of the spray cross section at x

The concentration along the spray centerline is obtained from the spray mixing process. The air-fuel vapor mixing is assumed to be controlled by the turbulent kinetic energy dissipation rate in the cylinder. Comparison of model results with experimental data indicate that the model overpredicts heat release for most of the combustion period. The peak cylinder pressure is also overpredicted. During the last phase of the combustion period, the model overpredicts air entrainment rates, but underpredicts heat release rate. Gupta et al. [26] attribute such behavior of the model to continuous air entrainment which results in leaning of air-fuel vapor mixtures in several spray elements below the lean flammability limit.

In the multizone model of Meguerdichian and Watson [13] the injected fuel was

divided into a number of zones or elements of equal fuel mass. The mixing model was based on several theoretical and experimental studies of liquid fuel jets in air at high pressure and temperature. The authors did not rely on the concept of droplet evaporation to obtain air entrainment rates. The mixture formation was based on jet-mixing theories for free jets before the spray reaches the wall, and on wall jet theory following impingement. Experimental correlations of mixing and flow in turbulent jets injected into a crossflow were used to obtain the deflection of the spray due to swirl and the resulting concentration distributions. Due to lack of adequate theoretical work on sprays in a swirling flow, it was assumed that for every zone in the straight jet and the radial wall jet, there is a corresponding zone in the deflected jet with a higher mass of entrained air. The actual entrainment was expressed as a function of the position of the zone. Experiments on jets in crossflows, reported by other researchers, were applied to determine the deflection and concentration along the spray plume. The concentration profile across the jet was based on that given by Abramovich [27]. At transition from free jet to wall jet, fuel and air flows and the cross-sectional area were assumed equal to that of the free jet. The concentration profile along the boundary of the wall jet was assumed equal to that of the free jet. The air entrainment rates for the individual zones were obtained from the mixture formation process. Comparisons of model results with actual engine data indicate that the model does not accurately predict combustion. The authors suggest that small adjustments to the equation for the centerline concentration of a deflected jet in swirling flow reduced the discrepancies between the model and experimental data. Such adjustments could not be explained theoretically, and hence they suggested that

more work is needed to model air-fuel mixing in burning fuel sprays.

The zone division and mixing model approach of Lipkea and DeJoode [14] is similar to that of Meguerdichian and Watson [13]. Lipkea and DeJoode modeled the fuel jet injected into the swirling cylinder air as a jet in a cross flow. After wall impingement, the wall jet was assumed to flow along the solid boundary and entrain air from the part of the surface exposed to the surrounding cylinder air. The fuel spray is considered as an unsteady turbulent jet, and the mixing of fuel and air is modeled as entrainment of air into the jet due to the momentum exchange between the jet and the surroundings. The mixing process is based on the velocity gradient created by turbulent exchange across the shear layer. The zones reaching the wall are assumed to move sideways to form the developing wall jet boundaries. Model-predicted cylinder pressure data have been reported to compare well with experimental data.

Rife and Heywood [16] carried out photographic and performance studies of diesel combustion with a rapid compression machine to develop insight into the role of mixing in diesel engine combustion. Their experiments simulated a single fuel spray in a direct-injection open-chamber diesel engine, with and without swirl. From the photographs of the fuel jet, the authors deduced that the jet explodes into droplets at the nozzle orifice and no liquid core exists beyond a few orifice diameters downstream of the nozzle exit. The velocity of these droplets relative to the surrounding air decays rapidly and the droplets move with the entrained air. Based on the above arguments the fuel spray is considered to be a vapor jet, and the solution of Abramovich [27] for a two-phase turbulent submerged jet is applied to the fuel jet in a quiescent diesel engine. The velocity and concentration profiles across the spray centerline are

given by Abramovich's solution [27]. Abramovich proposed that the jet flow of liquid particles in air can be treated as a gaseous jet. To apply the Abramovich model [27] to analyze the spray mixing, the authors assumed that the jet flow is quasi-steady and the tip of the jet develops in the same way as the motion of any fuel injected following the start of injection.

In the quasi-steady modeling work of Rife and Heywood [16] spray penetration was calculated by combining the equations for the concentration profile and fuel mass contained in the spray. The concentration profile across the spray centerline due to Abramovich [27] given in Equation 2.1, was used by Rife and Heywood [16]. For the jet in a non-swirling flow, the centerline concentration, $C'm$, was given by

$$C'm = \frac{0.134(u_m/u_o)}{0.18 - 0.108(u_m/u_o)} \tag{2.2}$$

where u_m is the velocity at the jet axis, and u_o is the initial jet velocity. For the jet in a cross flow, the values of the entrainment parameters along and across the spray were obtained from those suggested by Hoult and Weil [28].

The mass flow rate of fuel across a surface of constant equivalence ratio in the jet flow was used as a means to characterize the rate at which the fuel-air mixture is prepared for combustion. A limiting equivalence ratio of 2.0 was chosen by Rife and Heywood [16] to identify the boundary of the combusting fuel-air mixture. The rate form of the fuel mass conservation equation is given by

$$\dot{m}_f(t) = 2\pi u_o \rho_o C' {r_o}^2 \int_{\psi(t-\Gamma_{inj})}^{\psi(t)} F(\psi) dy \tag{2.3}$$

where

$\dot{m}_f(t)$ = fuel injection rate, on a mass basis

u_o = initial jet velocity

ρ_o = density of the medium surrounding the jet flow

C = local fuel concentration

r_o = nozzle orifice radius

ψ = dimensionless radial distance (y/b)

y = vertical distance from the spray centerline

b = radius of the spray cross section at x

F = cross section area of the circular jet, expressed as a function of ψ

t = time

Γ_{inj} = injection duration.

The mixing rate was obtained by numerically integrating the above equation with a value of 2.0 for C. The entrainment rates were not directly used in the combustion model developed by Rife and Heywood [16].

In the published discussion of Rife and Heywood's paper [16], Chiu commented that in his work at Cummins Engine Company, the use of a quasi-steady spray mixing model resulted in jet penetration rates and heat release rates that did not agree well with experimental data.

The work of Chiu et al. [15] was based on the assumption of a growing transient fuel vapor jet injected into the cylinder air. By applying the law of conservation of mass for the injected fuel, the spatial and temporal fuel-air distribution was obtained. The entire combustion chamber was divided into a number of smaller zones defined by constant equivalence ratio boundaries. The mixing process is mainly based on

the turbulent jet theory of Abramovich [27]. The similarity profile for concentration across the spray is given by the steady jet profile of Abramovich given in Equation 2.1. Along the spray centerline, the fuel concentration is assumed to decay hyperbolically:

$$Cm = \frac{1}{\xi(t)x + 1} \tag{2.4}$$

where, $\xi(t)$ is the time dependent overall fuel concentration in the spray.

In the multizone approach of Chiu et al. [15] a set of continuously evolving combustion zones are superimposed on the spray plume. Combustion is assumed to occur in the zones subject to prescribed lean and rich flammability limits of the injected fuel. The fuel-air mixture over the rich flammability limit is contained in a core zone, and fresh fuel is injected into this zone. Air from the lean zone surrounding the spray is entrained into the core zone and mixed with the fuel. The freshly prepared mixture is assumed to evolve into a new burning zone along the outer skin of the core zone. Additional zones are evolved based on a predefined mass of diesel fuel required in the burning zones. Each zone is bound by two iso-equivalence ratio lines. The inner boundary closer to the nozzle is represented by ϕ_1, and the outer boundary by ϕ_2. According to Chiu et al. [15] the mass of diesel fuel contained in any individual zone is given by

$$m_{dsl} = 2\pi \int_{X_l}^{X_t} \int_{y(\phi_1)}^{y(\phi_2)} C\ \rho\ y\ dy\ dx \tag{2.5}$$

where

X_l = spray tail location

X_t = spray penetration

$y(\phi_1)$ = ordinate of the inner iso-equivalence ratio boundary for the zone

$y(\phi_2)$ = ordinate of the outer iso-equivalence ratio boundary for the zone

C' = local mass concentration of diesel fuel

ρ = local air-fuel mixture density

In the work of Chiu et al. [15] the local diesel fuel mass concentration C' was calculated from the similarity profiles prescribed for the fuel-air distribution in the spray. The mass of air entrained into the individual zones is obtained by calculating the difference in the mass of air in that zone between two consecutive crank positions, θ_1 and θ_2. The mass of air in an individual zone is given by the double integral:

$$m_{air} = 2\pi \int_{X_l}^{X_t} \int_{y(\phi_1)}^{y(\phi_2)} (1 - C')\ \rho\ y\ dy\ dx \tag{2.6}$$

Comparisons of the model-predicted cylinder pressure with experimental data revealed the usefulness of the model in understanding the combustion process in direct-injection diesel engines. Wall effects were not included in this model. More detailed comparisons between model predictions and actual engine test data have been discussed by Shahed et al. [21].

The models described above provide information about the fuel-air mixing. The mixing process continues after ignition and sustains the combustion process in the cylinder. The time between the start of fuel injection and the start of combustion is the ignition delay period. Several ignition delay correlations have been proposed for diesel combustion. The suitability of these ignition correlations to modeling engine

cycle, and their application in existing diesel engine models is discussed next.

2.1.5 Ignition

During the ignition delay period in a diesel engine, fuel and air are mixed and compressed to high pressure and temperature. Ignition takes place at locations in the spray that are within the flammability limits of the fuel. Several researchers have conducted experimental studies on the ignition delay of diesel fuel and air mixtures. Data obtained from such experiments in constant volume bombs, rapid compression machines, and actual engines have been used to develop ignition delay correlations. Important parameters such as cylinder pressure and temperature of the fuel-air mixture are used as inputs to the correlations. Other parameters such as the activation energy of the fuel and the cetane number have also been included in some of these correlations.

Dent and Mehta [11] and Gupta et al. [26] used the ignition delay correlation of Hardenberg and Hase [29]. The ignition delay correlation of Hardenberg and Hase [29] is given by

$$\theta_{id} = (0.36 + 0.22 S_p) exp \left[Ea \left(\frac{1}{RuT_{cyl}} - \frac{1}{17,190} \right) \left(\frac{21.2}{p_{cyl} - 12.4} \right)^{0.63} \right] \quad (2.7)$$

where

θ_{id} = ignition delay, in degrees crank angle

Sp = mean piston speed, in m/sec

Ru = universal gas constant, in kJ/kmole/K

p_{cyl} = cylinder pressure at the start of injection, in bars

T_{cyl} = cylinder temperature at the start of injection, in Kelvin

Ea = activation energy, in kJ/kmole.

The activation energy Ea is given by $Ea = 618{,}840/(CN+25)$, where CN is the cetane number of the fuel. The average cetane number for the No. 2 diesel fuel used for the engine tests is specified to be 45 [30]. The premixed heat release spike obtained by their models [11, 26] closely matched the premixed spike of the experimental heat release diagrams, indicating that the amount of fuel prepared for combustion during the ignition delay period is nearly equal to that in the actual engine.

The multizone model of Meguerdichian and Watson [13] assumes an Arrhenius type fuel mass burning rate with constant values of activation energy and steric factor. The zone equivalence ratio, temperature, and air density are used as inputs to the burning rate equation. Ignition is defined as the moment at which the pressure begins to rise rapidly. Ignition delay is not supplied to their multizone model by a separate correlation, but results from the effects of fuel-air mixing and the fuel kinetics. The multizone model of Meguerdichian and Watson [13] predicted incipient ignition at a crank position prior to that obtained from measurements on the engine. Lipkea and DeJoode [14] used an approach similar to that of Meguerdichian and Watson [13].

C'hiu et al. [15] used the experimental data of Lyn and Valdmanis [31] to obtain the ignition delay for their multizone model. The authors suggest that when a better

ignition prediction model becomes available, it can be easily substituted into their multizone model.

2.1.6 Combustion

In a diesel engine, combustion extends from the moment of ignition to the point where the fuel has been burned to final products. During the initial phase of combustion the fuel-air mixture is generally rich but the entrainment of fresh air continues until the lean overall cylinder equivalence ratio is reached. Close agreement between experiments and the model-predicted cylinder pressure curves, heat release diagrams, indicated mean effective pressure, and indicated specific fuel consumption can be used to assess the validity of the combustion model.

Different methods of modeling combustion have been used by phenomenological models. The droplet vaporization and burning model of Dent et al. [11, 12] and Gupta et al. [26] assumed combustion based on fuel-air stoichiometry to occur in each of the burning regions. Local regions in the droplet stream which were within an artificially prescribed flammability limit were assumed to burn spontaneously. Reasonable agreement in the heat release diagram and pressure curves between model predictions and experimental data were reported.

Meguerdichian and Watson [13] used an Arrhenius equation to represent the diesel fuel burning rate:

$$\frac{dm_{f,b}}{dt} = K_A \rho_a (1 - b_f)(1 - \phi b_f) exp(-Ea/Ru\ T) \tag{2.8}$$

where

$m_{f,b}$ = mass of fuel burned, in kg

K_A = 5×10^7, in $m^3/kg/sec$

ρa = zone air density, in kg/m^3

ϕ = equivalence ratio

b_f = mass of burned fuel in the zone/total mass of fuel in the zone

Ea = activation energy of diesel fuel = $1.25 \times 10^8 J/mole$

Ru = universal gas constant, in $J/mole/K$

T = zone temperature, in Kelvin

In this multizone approach the spray plume is divided into zones of equal mass. The initial rate of pressure rise and the peak cylinder pressure were underestimated by the model, and the authors noted that further refinements were necessary. The multizone model of Lipkea and DeJoode [14] also used a global hydrocarbon fuel kinetic scheme for the burning process. A second order fuel burning rate equation similar to Equation 2.8 was used for each zone. The pressure curves, and the work output predicted by the model matched closely with experimental data.

Chiu et al. [15] assumed instantaneous combustion of the zones within the artificially prescribed flammability limits. The model-predicted pressure curves and work output matched closely with the test data.

The use of hydrocarbon kinetics for engine models resulted in poor combustion prediction in the work of Meguerdichian and Watson [13]. Also, the published constants for hydrocarbon fuel kinetics have not been well tested for use in diesel engines. Although the work of Lipkea and DeJoode [14] is a successful example of this approach, the use of instantaneous burning of combustible regions has been used

in several engine modeling efforts [11, 12, 15, 21, 22].

2.1.7 Heat transfer

The representation of heat transfer in the engine cylinder is an important aspect of engine modeling. The instantaneous bulk cylinder temperature is dependent on the heat transfer correlation used. Several heat transfer correlations are available in the literature. The three best known are those of Eichelberg [32], Woschni [33] and Annand [34].

The heat transfer correlation of Woschni [33] was used by Dent and Mehta [11], Dent et al. [12], and Gupta et al. [26]. Meguerdichian and Watson [13] used Eichelberg's correlation [32]. Due to inherent problems pertaining to proper cylinder pressure prediction in their combustion model, it is difficult to assess the usefulness of Eichelberg's equation in their model. Lipkea and DeJoode [14] and Chiu et al. [15] used Annand's heat transfer correlation [34]. Annand's correlation includes an explicit radiation term, whereas Eichelberg and Woschni combine the radiation effect into the constants in their correlations. Details on the use of Annand's correlation, and the calculation of instantaneous heat transfer rates are given in Chapter 3.

2.1.8 Emissions

The capability of any engine model to predict emissions is an important requirement. Many of the models referred in this literature review have the capability to predict oxides of nitrogen emission. A few attempts have been made to model soot and unburned hydrocarbons in a diesel engine. The formation mechanisms for these

pollutants are not well understood, and good correlation between measurements and model have not been achieved.

The spray droplet evaporation and combustion model of Kyriakides et al. [35] is based on the previous work of Dent and Mehta [11], and Dent et al. [12]. A two reaction Zeldovich mechanism was used to model the nitric oxide kinetics in the cylinder. The model predictions of NO_X were from 30% lower to 50% higher than the actual test data, for engine speeds of 1300 and 1900 rpm, and a fixed air to fuel ratio of 25.

The work of Lipkea and DeJoode [14] also included a two reaction Zeldovich mechanism for nitric oxide and the model-predicted levels of exhaust nitric oxide compared well with measured values. The predicted values of nitric oxide were within $\pm 5\%$ of the measured values, at engine speeds of 1500 rpm and 2500 rpm, for air to fuel ratios between 23 and 33.

Chiu et al. included a nitric oxide sub-model in their work [15]. The standard two reaction kinetics model was used. Reasonable comparison between model predictions and experimental data was reported. The model-predicted exhaust nitric oxide concentration was within -40% to +60% of the actual test data, for twenty-five different operating conditions. The speed and load data for these operating conditions are not clearly stated in their paper [15].

The sub-models used by other researchers to describe the individual processes such as spray development, ignition delay, combustion, heat transfer, and the formation of pollutants have been reviewed. The multizone model developed as part of the present study is discussed in detail in Chapter 3, and the specific assumptions and

solution procedures for some of the sub-models are given in the appendices. Previous research efforts on alcohol fumigated diesel engines are reviewed in the next section. Reference is made to both experimental and analytical work in the area of fumigated diesel engines.

2.2 Fumigated Diesel Engines

A review of previously conducted experimental and modeling studies on fumigated diesel engines are discussed in this section.

2.2.1 Experimental studies

Fumigation of alcohols in existing diesel engines has been studied by several researchers. Hayes et al. [36] studied fumigation of low proof ethanol in a six cylinder diesel engine. Individual ethanol injectors for each cylinder were mounted on the cylinder head, close to the intake valve location. Ethanol proofs in the range of 100 to 200 were tested and cylinder pressure data were recorded. The nitric oxide emission levels were found to be less than normal diesel operation for proofs below 150. The water injected with the alcohol reduced the peak temperature and pressure in the cylinder resulting in a reduction of 30% to 60% in the nitric oxide levels. Carbon monoxide levels increased with increasing flow rates of ethanol due to incomplete combustion of the ethanol-air mixture. The unburned hydrocarbon emissions also increased considerably. An increase of 7.2 times that of diesel operation was observed at low loads, and at high loads the increase was 3.8 times.

Van Meter et al. [37] studied the effect of fumigating a mixture of methanol and

water on the performance and emission characteristics of a four-cylinder, four-stroke, turbocharged diesel engine. Actual engine tests were conducted at three different speeds: 1000, 1500 and 2100 rpm, and four different load conditions: 25%, 50%, 75% and 100%, at each speed. The amount of fumigated mixture of methanol and water was varied to provide up to 30% of the net brake power output of the engine. The researchers observed a consistent reduction in exhaust nitric oxide with increased fraction of power from the fumigated mixture, at all speeds and loads. Approximately 50% reduction in nitric oxide was achieved by fumigating a methanol and water mixture sufficient to supply 20% of the net brake power.

Valdmanis and Wulfhorst [38] studied the effect of pure water induction on a diesel engine. Their study is of relevance to determine the effect of water contained in the lower proof alcohols. The authors indicate that water induction reduced nitric oxide emission substantially, carbon monoxide and smoke levels decreased slightly, and hydrocarbon levels increased slightly.

2.2.2 Analytical and modeling studies

Very few attempts have been made to model fumigated diesel engines. Gao et al. [10] carried out an ignition delay and heat release analysis on a turbocharged diesel engine fumigated with ethanol. The ethanol and water contained in the fumigated ethanol-water mixture were vaporized before induction into the intake manifold. The effect of ethanol fumigation on ignition delay and heat release rate were investigated through the analysis of engine pressure data. The oxides of nitrogen emissions in the exhaust were also recorded. A three zone model, including two zones of fuel-air

mixture and a third product zone, incorporated the first law rate equation and mass conservation equation to obtain the heat release rate. The model assumed that the diesel spray entrained the same amount of ethanol and air mixture at all conditions. One of the fuel-air mixture zones, the one containing diesel fuel, is assumed to burn first. After the diesel zone is completely converted to products of combustion, the ethanol-air zone is mixed with the products of this burned diesel zone. Due to this mixing of products, only two zones are present during the last phase of combustion. Model-predicted NO_X histories showed that for equivalence ratios greater than unity, a first plateau is reached as the NO_X reactions approach equilibrium for the rich mixture. A second plateau was reached as the air continued to mix with the rich products resulting in additional heat release. The value of NO_X corresponding to the second plateau, agreed well with measured exhaust levels. The NO_X predictions matched the experimental data closely for 1500 rpm engine speed, and 25% load operation. At other load conditions at 1500 rpm, the model predictions exaggerated the trends in NO_X levels. At full load, the predicted values of NO_X were more than twice the measured values. The authors comment that the two step mechanism of NO_X formation is not correct and that a physical model for the mixing rates would be required to correct this discrepancy.

Karim and Zhaoda [39] developed an analytical model for a two fuel compression ignition engine. The analysis is based on modeling the chemical reactions of the homogeneous fumigated air-fuel mixture during the compression and burning following ignition of the pilot fuel. Methane was used as the secondary fuel in their experiments and modeling efforts. A complex set of combustion reactions for the

methane-oxygen system was simplified to a thirty two reaction scheme. The reaction scheme was combined with the differential form of the first law energy equation and the cylinder volume constraint to obtain the instantaneous cylinder pressure and the instantaneous temperature of the bulk gases in the cylinder. The indicated thermal efficiency, ignition delay, and the maximum cylinder pressure matched within $\pm 5\%$ of the measured values. The operating conditions of the engine used for such comparisons are not clearly stated in their paper [39]. The authors note that the features of the transient pilot spray injection will introduce errors in the model predictions of engine performance, particularly when the pilot quantity is not small.

Mathur et al. [40] developed a thermodynamic cycle simulation model for a diesel engine fumigated with biogas. The biogas mixture was composed of 60 to 65 percent methane gas, and 35 to 40 percent carbon dioxide with traces of hydrogen sulphide. Biogas was fumigated into the intake manifold. Both experimental and modeling work were carried out and the results compared. The model is based on a single zone approach and assumes that the temperature is uniform throughout the cylinder. A homogeneous mixture of biogas, air and residual gas is considered to surround the fuel spray. The mixture of air and biogas is entrained into the pilot fuel spray for fuel preparation. The spray geometry of the injected diesel fuel was based on Hiroyasu's correlations for penetration and cone angle in a swirling flow [19] and the entrainment rate of biogas and air mixture was obtained from the correlations used by Dent and Mehta [11] from the mass of fuel injected, spray penetration, orifice diameter, and density ratio of diesel fuel to cylinder air. Fuel preparation was defined. based on the correlation of Whitehouse and Way [41] as a function of the mass of fuel

injected, mass of unprepared fuel, and the partial pressure of oxygen. The burning rate was expressed, using an empirical relation, as a function of the rate at which the fuel is prepared. The total heat released due to combustion is the sum of the heat released by the pilot diesel fuel and the biogas. Comparisons between actual test results and model predictions show agreement within $\pm 10\%$ in cylinder pressure data, bulk cylinder temperature, and heat release rate. Their simulation work did not include the modeling of emissions.

2.3 Need for Present Research

Despite the fact that several models have been reported in the literature for fumigated diesel engines, there is a scarcity of models that use the multizone approach necessary for accurate emissions modeling. At the beginning of the present research, the need for a more detailed combustion model for fumigated diesel engines was identified. During the development of this model, the need to develop the model on a fundamental basis with a clear description of the underlying physical principles was emphasized.

3. DEVELOPMENT OF DIESEL COMBUSTION MODEL

3.1 Introduction

The need for a multizone model to predict the performance and emission characteristics of a fumigated diesel engine has been established in Chapter 1. The steps followed to develop the mathematical equations to describe the processes in the engine, and their solution procedures are discussed in this chapter. The instantaneous values of the important physical quantities such as: cylinder pressure, spatially-resolved temperature, bulk cylinder temperature, cumulative heat transfer, cumulative work output, and the nitric oxide in the cylinder are required from the model.

This chapter is divided into six major sections. The first section describes the development of the thermodynamic equations that can be solved for cylinder pressure, individual zone temperatures, and individual zone volumes. The transient spray calculations to obtain the instantaneous mass of diesel fuel and alcohol, water, and air mixture in each zone, and the entrainment of alcohol, water, and air from the lean zone to the rich core zone, and the burning zones is developed in the second section. The injection and combustion phase of the multizone model is divided into five discrete phases. The details of these discrete phases are given in the third section. The fourth section discusses an intake and compression sub-model used to obtain the

initial conditions in the cylinder prior to diesel injection. The sub-model used for nitric oxide kinetics, and the assumptions involved are described in the fifth section. The sixth section summarizes the contents of this chapter.

3.2 Thermodynamic Calculations

In the present multizone model, the cylinder is divided into a number of small zones, as shown in Figure 3.1. The overall shape of the zones follows the geometry of the fuel spray jet. Each zone can be considered as a separate control volume with homogeneous properties. Figure 3.1 does not represent the true zone division process used in the present work. The zone geometry, process of zone division and the formation of additional zones is discussed in Section 3.3. This section deals with the development of the thermodynamic equations and the solution procedure required to obtain the cylinder pressure, zone temperatures, and zone volumes, during the valve-closed portion of the cycle.

In a typical combustion process the kinetic energy of the injected fuel is not significant when compared with the heat transfer, work, and enthalpy terms of the energy equation. In general, the rate form of the first law energy equation for a control volume, neglecting kinetic and potential energy effects, is,

$$\frac{dU}{dt} = Q' - W' + \sum m'_{in} h_{in} - \sum m'_{out} h_{out} \tag{3.1}$$

where

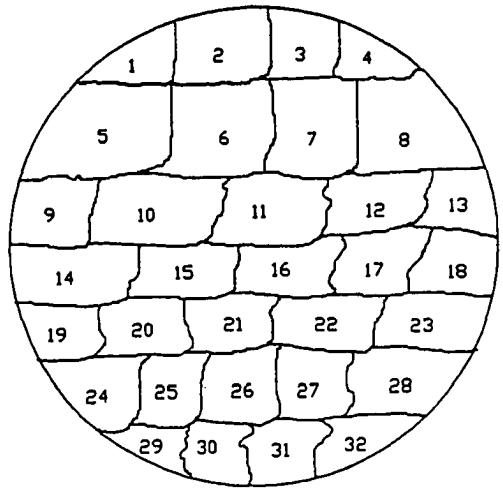

Figure 3.1: General Description of Zone Division in the Cylinder (Top View)

U' = total internal energy of the contents in the the control volume

Q' = the net rate of heat transfer into the control volume

W' = the rate at which work is done by the contents of the control volume on the surroundings

m'_{in} = the rate at which mass enters the control volume

h_{in} = the specific enthalpy of the contents entering the control volume

m'_{out} = the rate at which mass exits the control volume

h_{out} = the specific enthalpy of the contents exiting the control volume.

For constant speed operation of the engine, the time derivatives in Equation 3.1 can be written in terms of the change in crank angle θ as

$$\frac{dU}{d\theta} = \dot{Q} - \dot{W} + \dot{m}_{in}h_{in} - \dot{m}_{out}h_{out} \tag{3.2}$$

where $\dot{Q}$, $\dot{W}$, and $\dot{m}$ denote rates of heat transfer, work, and mass flow respectively, each on a crank angle basis.

The total amount of mass in the control volume, changes with θ according to the mass conservation equation

$$\frac{dm}{d\theta} = \dot{m}_{in} - \dot{m}_{out} \tag{3.3}$$

Assuming that the pressure is uniform throughout the control volume of interest, the work term $\dot{W}$ in Equation 3.2 can be expressed as the product of the instantaneous cylinder pressure p and the rate of change in cylinder volume $\frac{dV}{d\theta}$. The change in cylinder volume is obtained by differentiating the volume equation for the slider-crank equation in [30]. By noting that U can be expressed as the product of specific internal energy u and mass m and substituting for $\frac{dm}{d\theta}$ from Equation 3.3 into Equation 3.2:

$$m\frac{du}{d\theta} + \dot{m}_{in}u - \dot{m}_{out}u = \dot{Q} - p\frac{dV}{d\theta} + \sum \dot{m}_{in}h_{in} - \sum \dot{m}_{out}h_{out} \tag{3.4}$$

The contents of each individual zone or control volume are considered to behave as a mixture of ideal gases. The general ideal gas equation for each control volume is

$$pV = mRT \tag{3.5}$$

The derivative of the ideal gas equation in terms of the changing crank angle is.

$$p\frac{dV}{d\theta} + V\frac{dp}{d\theta} = \frac{dm}{d\theta}RT + mT\frac{dR}{d\theta} + mR\frac{dT}{d\theta} \tag{3.6}$$

When the engine operates with alcohol fumigation, the individual zones contain a mixture of diesel fuel, alcohol, water, and air. Hence, the specific gas constant R and the specific internal energy u for each zone are dependent on the composition of the mass contained in it. The procedure followed to obtain the values of R and u for the individual zones, based on their composition is described next.

Assuming the fumigated alcohol to be ethanol, the chemical reaction for the combustion of diesel fuel, ethanol, water vapor, and dry air on the basis of one mole of dry air can be expressed as:

$$\bar{\gamma}C_{13.78}H_{24.26} + \bar{\alpha}C_2H_5OH + \bar{\beta}H_2O + (0.2096O_2 + 0.7811N_2 + 0.0093Ar)$$
$$\text{—— (Equilibrium products of combustion)} \qquad (3.7)$$

where $\bar{\alpha}$, $\bar{\beta}$, and $\bar{\gamma}$ are the moles of ethanol, water, and the diesel fuel involved in the reaction per mole of dry air, respectively. For the case of methanol fumigation, the chemical reaction can be represented by an equation similar to Equation 3.7, by replacing C_2H_5OH with CH_3OH. The diesel fuel used for the engine tests has been analyzed as equivalent to $C_{13.78}H_{24.26}$ (Appendix G). The moisture contained in the laboratory air used by the engine is evaluated using the measured dry bulb and wet bulb temperatures and combined with the water in the alcohol-water mixture fumigated into the engine. The moles of diesel fuel, alcohol, water vapor, and dry air involved in the reaction are calculated from the measured flow rates of diesel fuel, alcohol-water mixture, and laboratory air supplied to the engine, and the measured concentration of pure alcohol in the alcohol-water mixture. The measurement procedures are described in Chapter 4, on Experimental Apparatus and Test Procedure.

The mass ratios α, β, and γ are defined as:

$$\alpha = \frac{m_{alc}}{m_{air}} \tag{3.8}$$

$$\beta = \frac{m_{wat}}{m_{air}} \tag{3.9}$$

$$\gamma = \frac{m_{dsl}}{m_{air}} \tag{3.10}$$

The corresponding mole ratios are given by,

$$\bar{\alpha} = \alpha \frac{M_{air}}{M_{alc}} \tag{3.11}$$

$$\bar{\beta} = \beta \frac{M_{air}}{M_{wat}} \tag{3.12}$$

$$\bar{\gamma} = \gamma \frac{M_{air}}{M_{dsl}} \tag{3.13}$$

where M_{dsl}, M_{alc}, M_{wat}, and M_{air} are the molecular weights of diesel fuel, alcohol, water, and dry air respectively.

The cylinder is assumed to contain two types of zones: unburned zones that are too rich or too lean to burn, and burned zones which contain equilibrium products of combustion. The unburned zones are composed of a gaseous mixture of diesel fuel, alcohol, water, and dry air. The thermodynamic properties such as the specific gas constant R and the specific internal energy u, are dependent on the temperature, pressure, and the mole fractions of the individual constituents present in each control volume. Hence, for both unburned and burned zones:

$$R = R(p, T, \alpha, \beta, \gamma) \tag{3.14}$$

$$u = u(p, T, \alpha, \beta, \gamma) \tag{3.15}$$

where p is the cylinder pressure which is assumed uniform throughout the cylinder and T is the individual zone temperature. Differentiating Equation 3.14 and Equation 3.15

with respect to the crank position θ gives:

$$\frac{dR}{d\theta} = \frac{\partial R}{\partial p}\frac{dp}{d\theta} + \frac{\partial R}{\partial T}\frac{dT}{d\theta} + \frac{\partial R}{\partial \alpha}\frac{d\alpha}{d\theta} + \frac{\partial R}{\partial \beta}\frac{d\beta}{d\theta} + \frac{\partial R}{\partial \gamma}\frac{d\gamma}{d\theta} \tag{3.16}$$

$$\frac{du}{d\theta} = \frac{\partial u}{\partial p}\frac{dp}{d\theta} + \frac{\partial u}{\partial T}\frac{dT}{d\theta} + \frac{\partial u}{\partial \alpha}\frac{d\alpha}{d\theta} + \frac{\partial u}{\partial \beta}\frac{d\beta}{d\theta} + \frac{\partial u}{\partial \gamma}\frac{d\gamma}{d\theta} \tag{3.17}$$

For a specified engine operating condition, the composition of the alcohol and water mixture injected into the intake manifold of the engine is fixed. Also, the vaporized alcohol and water is assumed to be distributed uniformly throughout the engine cylinder. Hence, the values of the mass ratios of alcohol to air and water to air are constant at any spatial location in the cylinder throughout the engine cycle. Since α and β are held constant over the entire cycle, the derivatives $\frac{d\alpha}{d\theta}$ and $\frac{d\beta}{d\theta}$ are zero. The terms containing $\frac{d\alpha}{d\theta}$ and $\frac{d\beta}{d\theta}$ in Equation 3.16 and Equation 3.17 will not be included in the further development of the governing equations.

Substituting Equation 3.6, Equation 3.16, and Equation 3.17 into Equation 3.4 to replace $\frac{dT}{d\theta}$, $\frac{dR}{d\theta}$, and $\frac{du}{d\theta}$ respectively, and grouping together the terms containing $\frac{dV}{d\theta}$ and $\frac{dp}{d\theta}$ gives the following differential equation.

$$\begin{aligned}\frac{dV}{d\theta}(\Phi p + p) &= \dot{Q} + \dot{m}_{in}(h_{in} - u + \Phi RT) - \dot{m}_{out}(h_{out} - u + \Phi RT) \\ &- \frac{dp}{d\theta}\left(m\frac{\partial u}{\partial p} + \Phi V - \Phi mT\frac{\partial R}{\partial p}\right) + \Phi mT\frac{\partial R}{\partial \gamma}\frac{\partial \gamma}{\partial \theta} \\ &- m\frac{\partial u}{\partial \gamma}\frac{\partial \gamma}{\partial \theta}\end{aligned} \tag{3.18}$$

where

$$\Phi = m\frac{\partial u}{\partial T}\left(\frac{1}{mR + mT\frac{\partial R}{\partial T}}\right)$$

Equation 3.18 gives the differential rate of change of volume for the control volume undergoing compression or expansion. The pressure in the cylinder is assumed

uniform. This assumption is valid except under conditions of rapid pressure rise, where large amplitude pressure waves exist. Hence, the pressure in each zone will equal the instantaneous cylinder pressure. Equation 3.18 is applicable to any specific control volume. If the cylinder is divided into n control volumes, and if subscript i, is used to denote an individual control volume, an equation analogous to Equation 3.18, can be written for each individual control volume. For a cylinder containing n zones, n such equations can be written for the valve-closed portion of the cycle. By summing up the corresponding terms of the n separate equations written for the n zones, the following equation can be obtained for the cylinder as a whole.

$$\begin{aligned}
\sum_{i=1}^{n} \frac{dV_i}{d\theta}(\Phi_i p_{cyl} + p_{cyl}) &= \sum_{i=1}^{n} \dot{Q}_i + \sum_{i=1}^{n} \dot{m}_{i,in}(h_{i,in} - u_i + \Phi_i R_i T_i) \\
&- \sum_{i=1}^{n} \dot{m}_{i,out}(h_{i,out} - u_i + \Phi_i R_i T_i) \\
&- \frac{dp_{cyl}}{d\theta} \sum_{i=1}^{n} \left(m_i \frac{\partial u_i}{\partial p_{cyl}} + \Phi_i V_i - \Phi_i m_i T_i \frac{\partial R_i}{\partial p_{cyl}} \right) \\
&+ \sum_{i=1}^{n} \Phi_i m_i T_i \frac{\partial R_i}{\partial \gamma_i} \frac{d\gamma_i}{d\theta} \\
&- \sum_{i=1}^{n} m_i \frac{\partial u_i}{\partial \gamma_i} \frac{d\gamma_i}{d\theta}
\end{aligned} \tag{3.19}$$

where p_{cyl} refers to the instantaneous cylinder pressure at the current crank position θ. For a cylinder containing n zones, an additional equation is obtained by noting that the sum of the individual zone volumes must equal the total cylinder volume.

$$\sum_{i=1}^{n} \frac{dV_i}{d\theta} = \frac{dV_{cyl}}{d\theta} \tag{3.20}$$

Substituting the volume constraint condition from Equation 3.20 into Equa-

tion 3.19, and rearranging Equation 3.19 to obtain $\frac{dp_{cyl}}{d\theta}$:

$$\begin{aligned}\frac{dp_{cyl}}{d\theta} &= \left[\sum_{i=1}^{n}\Psi_i\dot{Q}_i + \sum_{i=1}^{n}\Psi_i\dot{m}_{i,in}(h_{i,in} - u_i + \Phi R_i T_i)\right. \\ &- \sum_{i=1}^{n}\Psi_i\dot{m}_{i,out}(h_{i,out} - u_i + \Phi R_i T_i) \\ &+ \sum_{i=1}^{n}\Psi_i\Phi_i m_i T_i\frac{\partial R_i}{\partial\gamma_i}\frac{d\gamma_i}{d\theta} \\ &- \left.\sum_{i=1}^{n}\Psi_i m_i\frac{\partial u_i}{\partial\gamma_i}\frac{d\gamma_i}{d\theta} - \sum_{i=1}^{n}\frac{dV_i}{d\theta}\right] \\ &/ \left[\sum_{i=1}^{n}\Psi_i m_i\frac{\partial u_i}{\partial p_{cyl}} + \sum_{i=1}^{n}\Psi_i\Phi_i V_i - \sum_{i=1}^{n}\Psi_i\Phi_i m_i T_i\frac{\partial R_i}{\partial p_{cyl}}\right] \qquad (3.21)\end{aligned}$$

where

$$\begin{aligned}\Psi_i &= \frac{1}{\Phi_i p_{cyl} + p_{cyl}} \\ \Phi_i &= m_i\frac{\partial u_i}{\partial T_i}\left(\frac{1}{m_i R_i + m_i T_i\frac{\partial R_i}{\partial T_i}}\right)\end{aligned}$$

The volume change in any individual zone is given by solving Equation 3.18 for $\frac{dV_i}{d\theta}$.

As mentioned in Chapter 2, Annand's correlation [34] was used with appropriate steady-state temperature values for the walls, and a bulk cylinder gas temperature to calculate the heat transfer rate. Annand's correlation [34] is of the form

$$\dot{Q}_{cyl} = 0.49\frac{K_{cyl}}{B}(Re)^{0.7}(T_{cyl} - T_w) + b_A({T_{cyl}}^4 - {T_w}^4) \qquad (3.22)$$

where

B = cylinder bore

K_{cyl} = thermal conductivity of cylinder gas

Re = Reynolds number based on piston speed and cylinder bore

T_{cyl} = bulk cylinder gas temperature

T_w = cylinder wall temperature

b_A = $3.267 \times 10^{-03}\ Watts/m^2 - K^4$.

The surface area of the combustion chamber was divided into three regions, the head surface, the piston surface, and the sleeve surface. A characteristic temperature was assigned to each region. The surface areas of the head and piston are constant, but the sleeve area depends on the piston position. The characteristic cylinder temperature used for the heat transfer calculations is given by

$$T_{cyl} = \frac{\sum_{i=1}^{n} m_i R_i T_i}{\sum_{i=1}^{n} m_i R_i} \tag{3.23}$$

where

n = total number of zones in the cylinder

m_i = mass of zone i

R_i = specific gas constant of zone i

T_i = temperature of zone i.

$\dot{Q}_{cyl}$ gives the instantaneous total heat transfer rate out of the cylinder. This total heat transfer rate is apportioned to each individual zone, on a mass and temperature weighted basis:

$$\dot{Q}_i = \dot{Q}_{cyl} \left(\frac{m_i T_i}{\sum_{i=1}^{n} m_i T_i} \right) \tag{3.24}$$

where $\dot{Q}_i$ is the instantaneous heat transfer rate per unit surface area, out of zone i

to the coolant. In this analysis it is assumed that there is no heat transfer between the individual zones [15].

The instantaneous temperature of each zone is obtained from the ideal gas equation using the overall cylinder pressure and the individual zone volume. The instantaneous values of p_{cyl} and V_i are obtained by solving the set of coupled differential equations described above using the integrating subroutine IVPRK from the IMSL utility software package.

The thermodynamic properties such as R_i, u_i, h_i, and their partial derivatives $\frac{\partial R_i}{\partial p_{cyl}}$, $\frac{\partial R_i}{\partial T_i}$, $\frac{\partial R_i}{\partial \gamma_i}$, $\frac{\partial u_i}{\partial p_{cyl}}$, $\frac{\partial u_i}{\partial T_i}$, $\frac{\partial u_i}{\partial \gamma_i}$ are obtained from the thermodynamic property routines for unburned mixture (Appendix B) and for burned equilibrium combustion products (Appendix C) depending on the state of the zone.

The instantaneous total mass of each zone, m_i, and the instantaneous rates of mass transfer into the zone $\dot{m}_{i,in}$ and out of the zone $\dot{m}_{i,out}$ are required to solve the set of differential equations developed. Also, the specific enthalpy of the mass entering a zone $h_{i,in}$ and the specific enthalpy of the mass leaving a zone $h_{i,out}$ are to be evaluated for solving the above set of equations. A separate sub-program has been developed to provide the instantaneous mass, instantaneous rate of mass transfer, and the physical composition of the instantaneous contents in a zone, and the composition of the contents transferred into or out of a zone. Based on the physical make-up of the mass entering or leaving a particular zone, the values of the specific enthalpies h_{in} and h_{out} are obtained from the property routines for unburned mixture and equilibrium combustion products, as the case may be.

The sub-program for mass calculations is based on the mathematical modeling

of a transient spray, including wall impingement effects, and is discussed in the next section.

3.3 Transient Spray Calculations

The zone mass information required by the thermodynamic equations discussed in the previous section are obtained by modeling the development of the fuel spray and the resulting mixing between diesel fuel and the mixture of alcohol, water, and air surrounding the injected diesel fuel. This section justifies the assumption of a gas jet to describe the diesel spray and proceeds to discuss the correlations used to obtain the spray geometry, the fuel-air distribution in the spray plume the zone division process, the evolution of additional burning zones, and the calculation of initial conditions required by the multizone model.

Fuel injected into the compressed mixture of alcohol, water, and air in the engine cylinder develops into a spray plume. The shape of this spray, in the absence of a swirling cross-flow, is characterized by its penetration X_t, and the cone angle φ, as shown in Figure 3.2. The spray geometry in a swirling flow is shown in Figure 3.3. The injector characteristics such as nozzle hole size, nozzle L/D ratio, and injection pressure, and the cylinder properties such as pressure, viscosity, swirl velocity, and density influence the shape of the spray. A shearing action at the boundary of the spray plume results in the entrainment of the alcohol, water, and air mixture into the spray. When fuel injection ends, the spray detaches from the nozzle tip, but the entrainment of the surrounding alcohol, water, and air mixture into the spray continues until all the fresh mixture of alcohol, water, and air is completely entrained

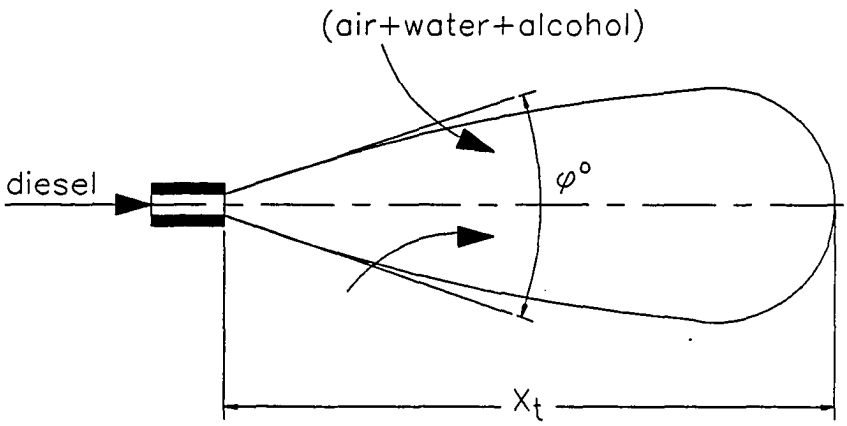

Figure 3.2: Spray Geometry in a Non-swirling Medium

into the spray. The process of mixing resulting from entrainment dilutes the fuel-rich locations within the spray plume, and creates pockets of fuel-air mixture which are capable of spontaneous combustion.

This section on transient spray calculations deals with the process of spray development, spray structure, modeling the process of mixing of fuel with the surrounding mixture of alcohol, water, and air, and the mathematical correlations used to determine the composition of the mixture at any geometric location within the cylinder. The division of the spray plume into a number of well-defined smaller zones, which are axisymmetric and characterized by a fixed mass of diesel fuel, is necessary to account for variations in properties within the plume. The procedure followed to carry out zone divisions is explained in Sections 3.3.4 and 3.3.5. In small direct-injection diesel engines the cylinder diameter and the combustion bowl diameter are quite small. This results in the spray plume impinging on the bowl wall. When this occurs, the fuel

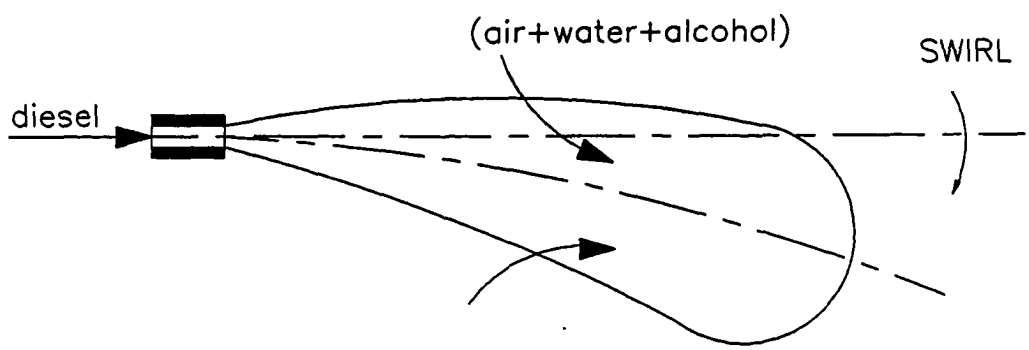

Figure 3.3: Spray Geometry in a Swirling Medium

jet ceases to be a free jet and a wall zone evolves. To account for this, the portion of the engine cycle between the start of diesel fuel injection and opening of the exhaust valve is divided into five discrete phases, and each phase is modeled separately. These different phases of combustion are described later in Section 3.4.

Before proceeding to discuss the details of the various aspects of the transient spray model, a brief discussion of the general spray structure used in the present model is appropriate. In the present spray analysis, the medium surrounding the diesel spray plume contains either no diesel fuel or very little diesel fuel, and is too lean to ignite. Hence, the medium surrounding the spray plume can be referred to as the lean zone. Entrainment of mass from the lean zone into the spray plume continues during and after the injection period until the lean zone is completely depleted. This entrainment process results in preparing additional fresh fuel for combustion and also provides fresh air to the already burned locations in the spray plume allowing for more

complete combustion. The fuel-air distribution in the spray plume is not uniform, and hence the entire spray plume cannot be considered to possess uniform properties. To model the spray in a more realistic manner the spray is divided into a number of smaller sections or zones. Within each of these smaller zones the properties can be assumed to be uniform. The procedure used for dividing the spray plume into zones and obtaining the local masses of fuel and air in each of these zones will be discussed next.

In the present model, the spray plume is divided into a number of smaller zones, as shown in Figures 3.4, 3.5, and 3.6. The zone boundaries correspond to lines of constant equivalence ratio, refered to as iso-phi lines. Phi is the common symbol for equivalence ratio. At incipient ignition the outermost boundary of the spray plume is prescribed to equal the lean limit of combustion. The mass of diesel fuel contained in the cylinder outside this lean iso-phi boundary is very small and does not participate in combustion until the entire mass in the lean zone is mixed with the spray plume, close to the end of the expansion stroke. Less than 1% of the total diesel fuel injected is contained in the lean zone, and ignoring this fuel for the initial part of combustion does not introduce significant errors in the results of the cycle simulation. The flammability limits of various hydrocarbon fuels listed in Appendix E of Glassman [42] was used to verify the allowable ranges of lean and rich limits for diesel fuel. Chiu et al. [15] used a rich limit of 3.0 for an engine operating only on diesel fuel. In a related publication, Shahed et al. [22] varied the lean limit of combustion from 0.3 to 0.7 for diesel operation, and observed that this had very little effect on the initial pressure rise and no effect on the subsequent pressure data.

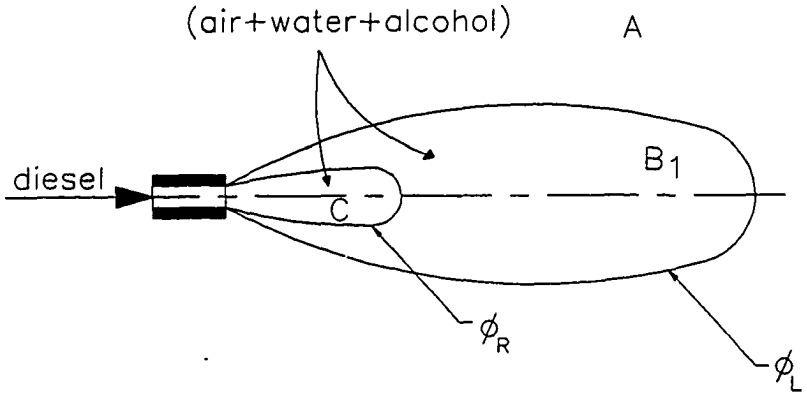

Figure 3.4: Zone Division at Incipient Ignition (θ_{ign})

Gupta et al. [26] used a lean limit of 0.5 and a rich limit of 3.0 for a single fuel diesel combustion model. It is assumed in the present model that ignition is initiated in the mixture due to autoignition of the diesel fuel, hence on the basis of the previous studies, a lean limit of 0.6 and a rich limit of 3.0 were used.

Under the high pressure and temperature prevailing in the cylinder, the fuel-air mixture contained within the iso-phi lines corresponding to the lean limit and the rich limit is capable of spontaneous combustion. This combustible fuel-air mixture is further divided into several zones. The division of zones is based on a fixed mass of diesel fuel in each of these burning zones. As explained earlier, the entrainment of alcohol, water and air mixture from the lean zone into the rich core zone results in the formation of new zones. The new zones are assumed to evolve at the interface between the rich core zone and the adjacent burned gas zone. When the mass of

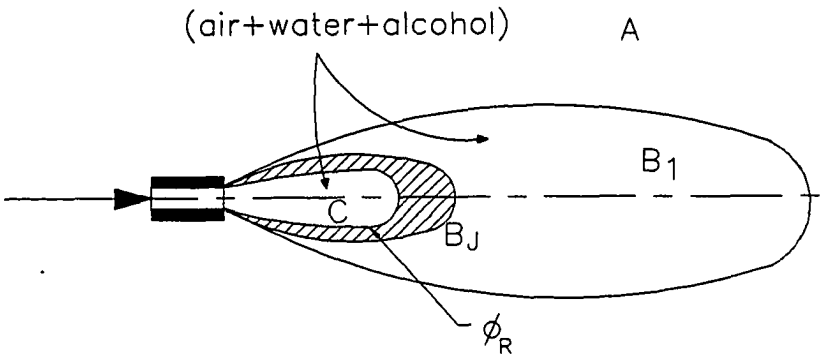

Figure 3.5: Zone Division at $\theta_{ign} + \Delta\theta$

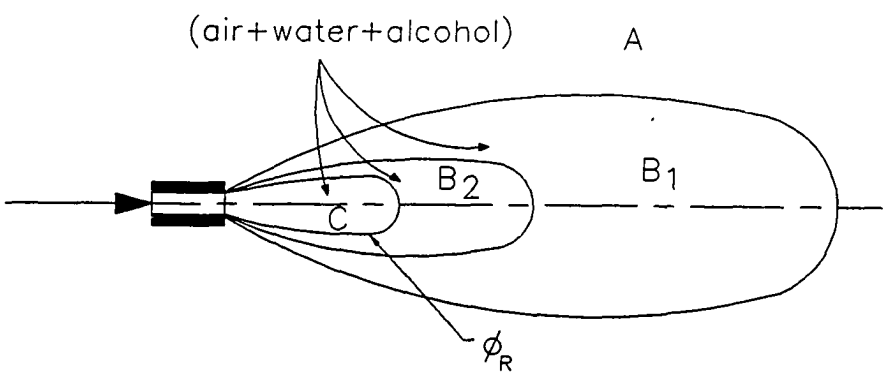

Figure 3.6: Zone Division at $\theta_{ign} + K_\theta(\Delta\theta)$. New Zone B_2 is Evolved

diesel fuel in this interface zone is greater than or equal to the diesel mass required to form a combustible zone, the newly evolved zone is separated from the core zone, and a new zone is created.

Figures 3.4, 3.5, and 3.6 illustrate the process of new zone formation. Figure 3.4 shows a lean zone, zone A, a rich core zone, zone C, and a burning zone, zone B_1, at incipient ignition, corresponding to the crank position θ_{ign}. Figure 3.5 shows the zone division at the crank position, $\theta_{ign} + K_\theta(\Delta\theta)$, where $\Delta\theta$ is a small increment in the crank position, and K_θ is an integer corresponding to the number of $\Delta\theta$ steps required to form the new zone, zone B_2. During the crank step $\Delta\theta$, the injection of diesel fuel continues, and the alcohol, water, and air mixture from zone A is entrained into zone C and zone B_1. The boundary of the rich core zone, zone C, is still maintained at the rich limit, and the new boundaries of the previously formed zones, zone A and zone B_1, are identified by keeping the mass of diesel fuel fixed in these zones. The mass of diesel fuel in each zone is obtained by the procedure detailed below in Section 3.3.5. The newly forming zone, zone B_j, is formed along the skin of the core zone, zone C. For the present model, the mass of diesel fuel required in zone B_j to evolve into a new burning zone, is set at one-third of the mass of diesel fuel in zone B_1. The mass of diesel fuel in zone B_j is evaluated at the new crank position $\theta + \Delta\theta$. If the diesel mass in zone B_j is less than one-third of the diesel mass in zone B_1, the crank position is again incremented by $\Delta\theta$, and the updated masses are calculated. The B_j zone is evolved into the new B_i zone, zone B_2, when the diesel mass in zone B_j is equal to or greater than that required to form a new B_i zone. Figure 3.6 shows the formation of zone B_2 at the crank position $\theta_{ign} + K_\theta(\Delta\theta)$.

The spray penetration and cone angle at any crank position determine the entrainment rate of the lean mixture from zone A into the spray plume and the formation of new zones. A brief description of the available correlations for spray geometry and those used in the present model are discussed in Section 3.3.2. The spray analysis used in the model treats the liquid diesel fuel spray as a gas jet. The justification for this approach is discussed in Section 3.3.1.

3.3.1 Justification of gas jet assumption

In the present multizone model, the fuel spray injected into the cylinder is assumed to be a turbulent gas jet. Several studies [43, 44, 45] suggest that the gas jet approximation is representative of actual engines. Chigier [43] has reviewed recent experimental studies on spray combustion and concluded that the structure of a flame is similar to a gas diffusion flame, and there is no evidence of flames around individual drops. Chigier [43] emphasized that the droplets in a typical diesel spray have a mean diameter of about 15 microns, and the largest droplets are around 70 microns in diameter. As the air temperature in the combustion chamber approaches the critical temperature of diesel fuel, the droplets evaporate rapidly and a large portion of the spray is in gaseous form. Chigier [43] suggested that under the high pressure and temperature conditions existing in diesel engines the fuel droplets in the spray would evaporate completely within 10 mm of the nozzle tip.

Wallace and Horner [44] modeled the droplet trajectory and subsequent evaporation of the diesel fuel droplets using equations for momentum, heat, and mass transfer. Their results indicate that for an engine operating at 2000 rev/min with

a swirl ratio of 3. droplets of 20 micron evaporate almost instantaneously within a period of about 0.25 degrees of crank rotation. Droplets of 50 micron and 100 micron size were found to evaporate in 1 degree and 3 degrees of crank rotation, respectively. Based on their model predictions, Wallace and Horner [44] conclude that for small droplets with less than 50 micron diameter, evaporation follows injection very rapidly and the fuel jet entering the swirling air in the engine can be modeled as a vapor jet.

In related research, Packer et al. [45] carried out experimental and theoretical work to study fuel jet mixing under high swirl conditions. Experimental work included tests on single shot injection of diesel fuel into a high swirl combustion chamber. Based on their experimental observations and theoretical calculations, the authors confirm that even at a very early stage of the injection process, evaporation can be considered to be complete.

Expressions for the distribution of fuel droplet size and mean droplet diameter are often used to characterize the spray. A commonly used mean diameter is the Sauter Mean Diameter (SMD). SMD is the diameter of the fuel droplet that has the same surface to volume ratio as that of the total spray. To estimate the size of diesel fuel droplets in the diesel engine, used for the experiments discussed later in this dissertation, the SMD of the droplets was calculated using the empirical correlation of Hiroyasu and Kadota [46].

$$SMD = A_D(\Delta p)^{-0.135}(\rho_{cyl})^{0.121}(Q_{dsl})^{0.131} \tag{3.25}$$

where

A_D = empirical constant for the nozzle

Δp = difference between injection pressure and cylinder pressure at the start of injection, in MPa

ρ_{cyl} = density of cylinder contents at the start of injection, in kg/m^3

Q_{dsl} = diesel fuel delivery rate, in $mm^3/stroke$.

The empirical constant A_D for a hole-type nozzle is equal to 23.9. For a typical engine test run corresponding to full load operation at an engine speed of 1500 rev/min with diesel fuel, and an injection pressure of 25 MPa, the SMD is 25 microns. This mean droplet size is in close agreement with the values suggested by Chigier [43] and Wallace and Horner [44]. Hence, for the injector used in the present engine, the droplets can be assumed to vaporize within 1 to 2 degrees of crank rotation. This justifies the use of a gas jet to represent the diesel fuel spray in the present model.

3.3.2 Spray geometry

The spray penetration and cone angle at any crank position determine the entrainment rate of the lean mixture from zone A into the spray plume, and the formation of new zones. Brief descriptions of the available correlations for spray geometry, and those used in the present model are provided in this subsection.

For a jet injected into a non-swirling medium the spray shape is shown in Figure 3.2. In the presence of a swirling medium the spray is bent over, as shown in Figure 3.3.

Several correlations are available in the literature for obtaining the spray penetration and cone angle in a non-swirling flow. Hay and Jones [47] carried out a compara-

tive study on the spray penetration correlations provided by several researchers. They presented and compared the experimental techniques used to obtain the correlations, the proposed correlations, and their limitations. Hay and Jones [47] noted that all the twelve correlations compared were based on three main parameters: nozzle diameter, injection pressure, and cylinder air density. The authors used actual test data for these three main parameters from a Sulzer LVA 24 medium speed diesel engine, under full load, medium load, and light load operations. The penetration values predicted by each of the twelve correlations were studied by varying the load in the engine, the injection pressure, the density of cylinder air, and the nozzle diameter. Based on their comparisons, the authors recommend Dent's correlation [18]. Dent's correlation [18] is suitable under all engine operating conditions except for very high air densities, corresponding to cylinder pressures exceeding 100 atmospheres. At cylinder pressures below 100 atmospheres, the experimental data points obtained from the engine lie very close to the penetration correlation line of Dent [18].

Dent [18] developed a spray penetration correlation for fuel injected into a non-swirling medium from experimental information on gas jet mixing published by other researchers. The penetration values predicted by his correlation were found to compare well with experimental data obtained from various sources in diesel engine, cold bomb, hot bomb, and liquid injection tests. For an engine environment, Dent's spray penetration equation is

$$X_t = 13.6 \left[\left(\frac{\Delta p}{\rho_{cyl}} \right)^{1/2} tdo \right]^{1/2} \left(\frac{530}{T_{cyl}} \right)^{1/4} \tag{3.26}$$

where

X_t = penetration distance, in inches

Δp = difference between injection pressure and cylinder gas pressure at the start of injection, in psi

ρ_{cyl} = density of cylinder contents at the start of injection, in $lb/in.^3$

t = injection time, in seconds

do = injector orifice diameter, in inches

T_{cyl} = cylinder gas temperature, in degrees Rankine.

The values of cylinder gas pressure, temperature, and density are those corresponding to the start of fuel injection. The spray penetration values calculated from Dent's correlation Dent [18] were very close to penetration data measured on an engine, confirming the accuracy of the correlation. Dent's paper does not provide any information on the spray cone angle.

Wakuri et al. [23] studied the spray characteristics using momentum theory. They proposed that the air entrained into the fuel jet stream results in a gaseous mixture. The authors confirmed their theory with experimental results in a constant volume chamber charged with high pressure, high temperature nitrogen into which the fuel was injected. The chamber pressure was varied from atmospheric to 24 atm., and the temperature was varied from ambient to 600°C. Injector orifice diameters of 0.31, 0.34, and 0.38 mm were used. The injection pressure ranged from 400 to 750 atmospheres. The spray was photographed with a high-speed camera at the rate of 7000 frames per second. Based on a large set of experimental data, the proposed penetration correlation is

$$X_t = K_w\sqrt{t} \tag{3.27}$$

where K_w is a constant determined from given design data, and is a function of jet velocity, orifice diameter, dynamic viscosity of chamber contents, the density of chamber medium, and fuel density. An exact relationship for K_w is not supplied by the authors in their paper. The spray cone angle is given by

$$\varphi = \frac{tan^{-1}\sqrt{C_w \rho_f \rho_c}}{(\frac{K_w}{\sqrt{V_o d_o}})^2} \tag{3.28}$$

where, C_w is the coefficient of contraction of the fuel flowing through the orifice, Vo is the fuel jet velocity, do is the orifice diameter, ρ_f is the fuel density, and ρ_c is the density of the cylinder medium. Over the entire range of pressure and temperatures used for their tests, described earlier, Wakuri et al. [23] found that the chamber air viscosity had very little effect on spray penetration and cone angle. The spray cone angle was expressed as a strong function of the ratio of fuel density to chamber air density.

$$\varphi = G_w \left(\frac{\rho_f}{\rho_c}\right) \tag{3.29}$$

Where G_w is a parameter based on jet velocity, nozzle orifice diameter, and fuel density. Figure 15 in their paper [23], reproduced in Figure 3.7, is a plot of spray cone angle as a function of the density ratio. For density ratios ($\frac{\rho_f}{\rho_c}$) below 200, the cone angle data predicted by Wakuri's correlation is within $\pm 17\%$ of the measured values. The error between the cone angles predicted by Wakuri's correlation and the measured values is within $\pm 30\%$, at higher density ratios exceeding 200.

For the wide range of alcohol fumigation tests carried out on the engine for the present study, the density of the cylinder contents ranged from 15 to 25 kg/m^3, depending on the engine speed, load, and the amount of water and alcohol fumigated

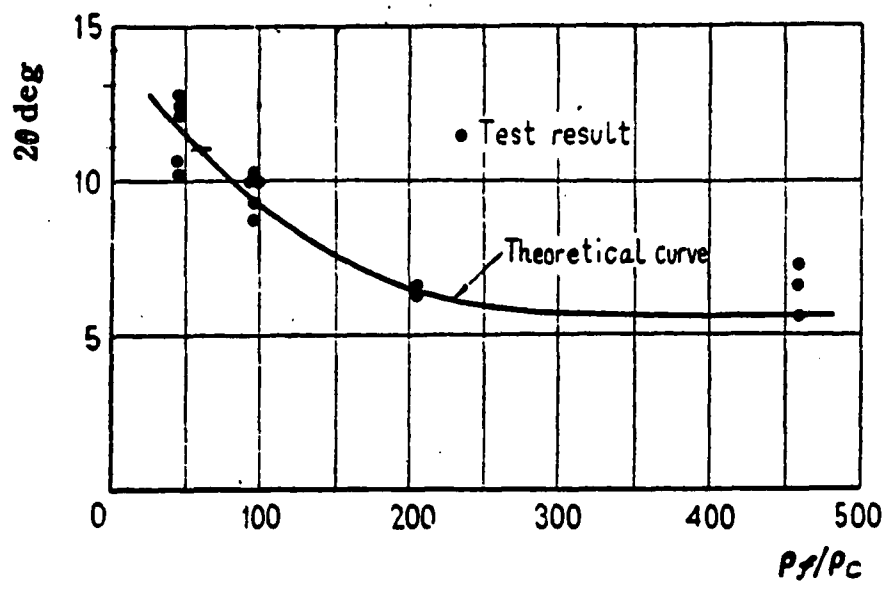

Figure 3.7: Plot of Spray Cone Angle (Reproduced from Wakuri et al. [23])

into the engine. The average API gravity at 60°F, of the two diesel samples used for the engine tests was 32.9 (see Appendix G). The corresponding density of diesel fuel given by the API handbook [48], Table 3 is 860.3 kg/m^3. Hence, the density ratio ranged from 57 to 34. For this range of the density ratio, the cone angle in Figure 15 of Reference [23] ranges from 11.0 to 12.0 degrees. An average cone angle of 11.5 degrees was used in the present modeling effort. In the present work, the spray penetration correlation of Dent [18], and the cone angle specification of Wakuri et al. [23] for fuel injected into a non-swirling medium, are used.

The actual fumigation tests were conducted on a medium swirl engine, with a swirl ratio of about five. Swirl ratio is defined as the angular velocity of the in-cylinder air rotation, which has equal angular momentum to the actual flow, divided by the angular rotational speed of the engine. Hiroyasu et al. [19] studied the effect of swirl on spray geometry. For injection into non-swirling flow, the spray penetration after spray break-up is expressed by

$$X_t = 2.95 \left(\frac{\Delta p}{\rho_{cyl}} \right)^{1/4} \sqrt{do\ t} \tag{3.30}$$

where

X_t = the spray penetration, in meters

Δp = the difference between the injection pressure and the cylinder pressure, in Pa

ρ_{cyl} = the density of the cylinder medium, in kg/m^3

do = the injector orifice diameter, in inches

t = the injection duration, in seconds

Under typical operating conditions, spray break-up occurs within one crank de-

gree after the start of injection. The cone angle is given by

$$\varphi = 0.05 \left(\frac{do^2 \rho_{cyl} \Delta p}{\mu_{cyl}} \right)^{1/4} \tag{3.31}$$

where, μ_{cyl} is the dynamic viscosity of the cylinder medium, in Pascal-seconds, and φ is the cone angle in degrees. The correlations of Hiroyasu et al. [19] for both X_t and φ were reported to predict values within $\pm 10\%$ of the corresponding data measured on a constant-volume chamber.

Dent [18] compared his penetration correlation with the engine measurements of Taylor [49], over a wide range of cylinder pressures, cylinder temperatures, cylinder density, and injector hole sizes. The penetration values calculated from Dent's correlation [18] matched closely with those measured by Taylor [49] in the engine. Hiroyasu et al.'s [19] spray penetration equation for a diesel spray in a non-swirling flow resulted in about 25 to 30% over-penetration, and the spray impinged on the bowl wall prior to ignition. Hiroyasu et al. [19] used a constant volume combustion chamber for their experiments, and not an actual engine. Hence, it is possible that their correlation may not be suitable for all engine operating conditions. Based on these conclusions, the penetration correlation of Dent [18] was chosen for the present study. The use of Hiroyasu's cone angle equation [19] resulted in a wider spray cone and over-entrainment. The alcohol, water, and air mixture from the lean zone was entrained into the spray plume too rapidly. This caused an unrealistic burning pattern in the cylinder. It is worth noting that, due to lack of dependable spray correlations, Chiu et al. [15] resorted to their own apparatus to measure spray penetration and cone angle, for the range of engine operating conditions used in their multizone modeling effort. The design and development of such test rigs is tedious and was not

considered for the present work.

Dent's correlation [18] indicated that the spray penetrated about 70 to 75% of the bowl radius at the time of ignition, and the average cone angle of 11.5 degrees given by Wakuri's correlation [23] did not result in over-entrainment. Other cone angle correlations were not easy to find in published literature. Hence, Wakuri's correlation [23] was used in this research.

Hiroyasu et al. [19] provide expressions for the effect of swirl on penetration and cone angle, such that

$$X_{t,s} = C'_X X_t \tag{3.32}$$

$$\varphi_s = C'_\varphi \varphi \tag{3.33}$$

where

X_t = spray penetration in the absence of swirl, in meters

$X_{t,s}$ = spray penetration in a swirling medium, in meters

φ = spray cone angle in the absence of swirl, in degrees

φ_s = spray cone angle in a swirling medium, in degrees

C'_x = swirl factor for penetration

C'_φ = swirl factor for cone angle

In the present modeling effort, X_t is given by Dent's correlation [18] and φ is assigned an average value of 11.5 degrees based on the work of Wakuri et al. [23].

In the presence of swirling air motion, the spray is swept over in the direction of the swirl, as shown in Figure 3.3. Hiroyasu et al. [19] represented this bent over spray with increased air entrainment as a straight spray with reduced penetration $X_{t,s}$ and proportionally increased cone angle φ_s as shown in Figure 3.8.

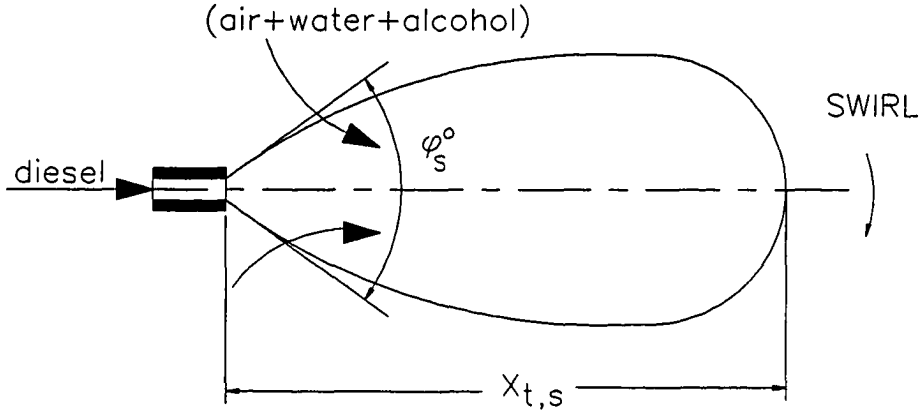

Figure 3.8: Modified Spray Geometry in a Swirling Medium

The value of C_X is less than unity, and the value of C_φ is greater than unity. The swirl factors are given by

$$C_x = \left(1 + \frac{\pi r_s n X_t}{30 Vo}\right)^{-1} \tag{3.34}$$

$$C_\varphi = \left(1 + \frac{\pi r_s n X_t}{30 Vo}\right)^{2} \tag{3.35}$$

where

r_s = swirl ratio

n = engine speed, in rev./min.

Vo = fuel jet velocity, in m/sec.

The jet velocity Vo is given by

$$Vo = C_d \sqrt{\frac{2\Delta_p}{\rho_f}} \tag{3.36}$$

where C_d is the discharge coefficient of the orifice, and is assigned a value of 0.8 [19].

for the orifice used in the present injector with an L/D ratio of 2.0.

The values of Δp, ρ_f, Vo, ρ_{cyl}, μ_{cyl}, etc. are assigned values corresponding to those at the start of injection. Also, the value of μ_{cyl} is assumed to equal the value of dynamic viscosity of air, and the effect of water and alcohol in the cylinder is ignored. This should not result in a significant error since the dynamic viscosity is not involved in calculating the penetration, and Wakuri et al. [23] clearly stated that the viscosity of the medium has very little effect on the spray cone angle.

In the present model, the spray penetration and cone angle in the swirling engine medium is calculated using the swirl factors of Hiroyasu et al. [19].

At the end of injection, the spray detaches from the nozzle and moves towards the bowl wall. The present model assumes that the tail velocity is one-half the tip velocity following the suggestion of Chiu et al. [15].

This section described the procedure used to obtain the penetration and cone angle for a fuel jet sprayed into a swirling medium in the cylinder. As discussed earlier, the momentum of the spray causes entrainment of the alcohol, water, and air mixture in the cylinder into the spray plume. The spatial distribution of the diesel fuel in the spray plume due to this mixing process is required to calculate the instantaneous mass of diesel fuel, and alcohol, water, and air mixture in each zone. The procedure used in the present multizone model to determine the fuel-air distribution in the spray plume is explained in the next subsection.

3.3.3 Fuel-air distribution correlations

The shear layer between the injected fuel spray and the surrounding medium results in entrainment of the alcohol, water, and air mixture into the spray plume. In the present modeling work, the concentration of diesel fuel along the spray centerline, $C'm$, is assumed to decrease hyperbolically downstream of the nozzle based on the work of Chiu et al. [15] of the Cummins Engine Company. Hence,

$$at \quad x = 0, \qquad C'm = 1 \tag{3.37}$$

$$for \quad X_l < x < X_t, \qquad C'm = \frac{1}{\xi(\theta)x + 1} \tag{3.38}$$

$$for \quad x < X_l, \qquad C'm = 0 \tag{3.39}$$

where $\xi(\theta)$ is the overall time varying concentration of diesel fuel in the cylinder, for a transient spray. $\xi(\theta)$ is a function of the crank position only and is evaluated based on the principle of conservation of diesel mass in the cylinder. X_l is the distance of the spray tail from the fuel nozzle. During the injection period the spray is attached to the nozzle, and X_l is zero. After the end of injection the spray detaches from the nozzle and moves away from the nozzle into the cylinder. The value of X_l after end of injection is calculated by assuming the tail velocity to be one-half of the tip velocity, as suggested by Chiu et al. [15]. The distribution of injected diesel fuel in the spray plume, across the spray centerline is assumed to be the same as that of a steady jet, using the similarity profile given by Abramovich [27].

$$\frac{C'(x,y,\theta)}{C'm(x,\theta)} = 1 - \left(\frac{y}{b}\right)^{1.5} \tag{3.40}$$

where

C' = local mass ratio of diesel fuel to total mass of diesel, alcohol, water, and air

$C'm$ = the concentration along the spray axis

y = vertical distance form the spray centerline

b = half-width of the spray at any axial location. x.

Figures 3.9 and 3.10 show the diesel concentration profiles along and across the spray axis.

The spray half-width at any locations along the spray axis is given by

$$b = x \tan\left(\frac{\varphi_s}{2}\right) \tag{3.41}$$

where φ_s is the spray cone angle in a swirling flow.

At any crank position, the mass of diesel fuel injected should equal the mass of diesel fuel contained within the spray plume. If $\frac{dm_f}{d\theta}$ is the diesel injection rate obtained from the primary diesel injection diagram, then,

$$\int_0^\theta \frac{dm_f}{d\theta} d\theta = 2\pi \int_{X_l}^{X_t} \int_0^b C' \rho \, y \, dy \, dx \tag{3.42}$$

where ρ is the local density of the diesel, alcohol, water, and air mixture. The local mixture density ρ is given by

$$\rho = \frac{\rho_{awa}}{1 - (1 - \frac{R_f}{R_{awa}})C'} \tag{3.43}$$

ρ_{awa} is the density of the uniform mixture of alcohol, water, and air in the cylinder. R_f and R_{awa} are the gas constants of the diesel fuel, and the alcohol, water, and air mixture fumigated into the engine. Combining Equation 3.38 and Equation 3.40,

$$C' = \frac{1}{\xi(\theta)x + 1}\left(1 - \left(\frac{y}{b}\right)^{1.5}\right) \tag{3.44}$$

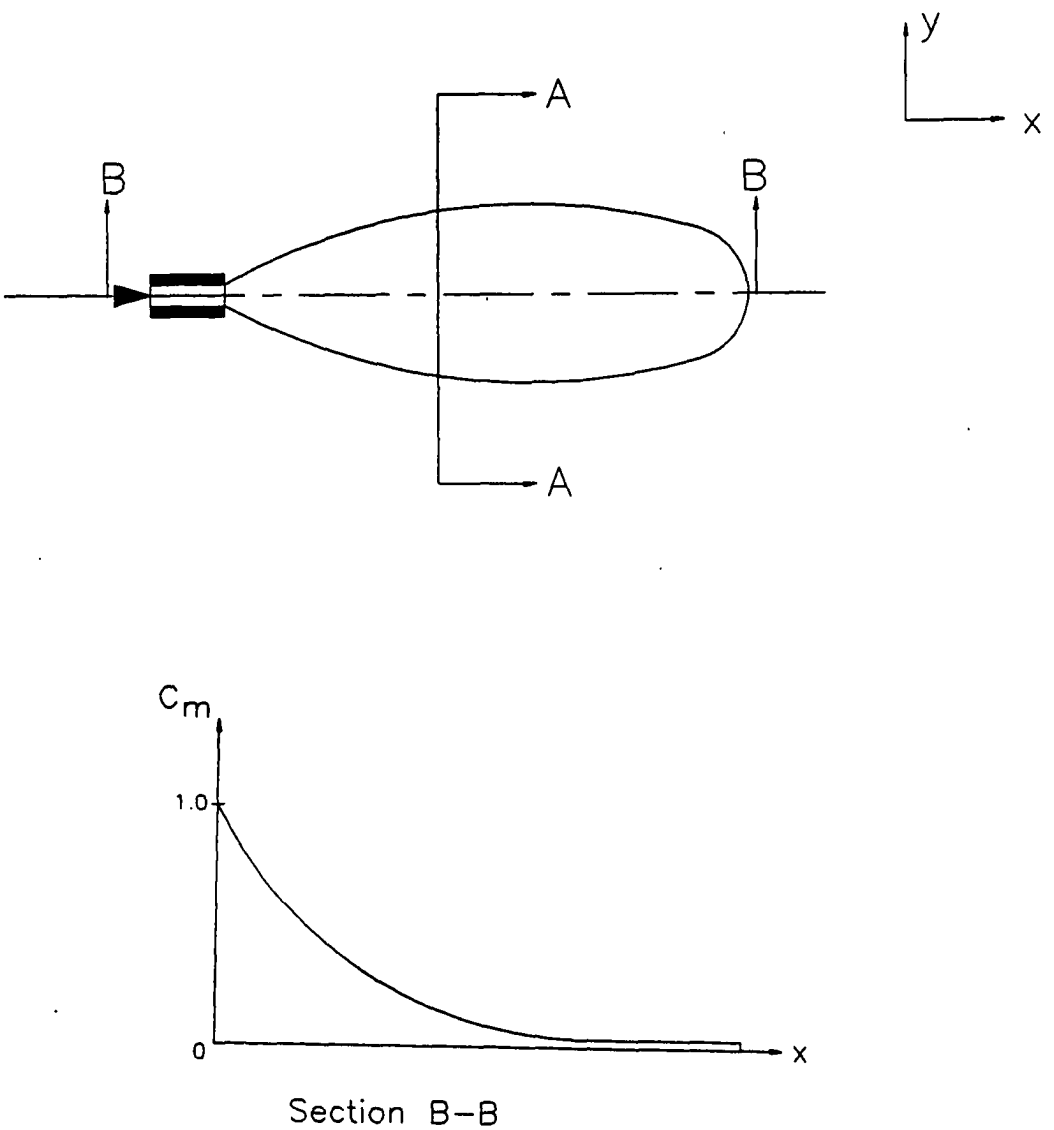

Figure 3.9: Diesel Concentration Profile Along the Spray Axis

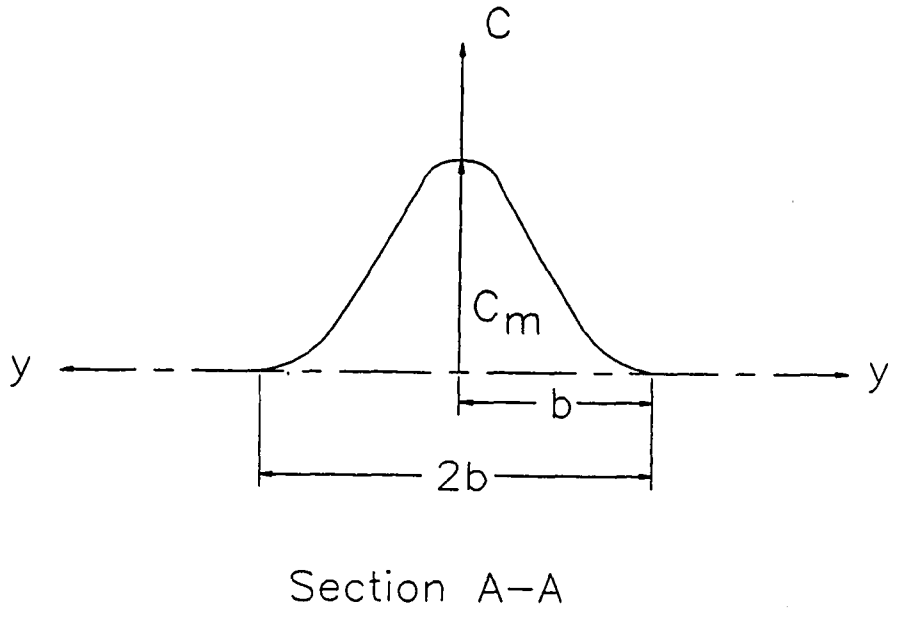

Figure 3.10: Diesel Concentration Profile Across the Spray Axis

Substituting Equation 3.44 into Equation 3.43,

$$\rho = \frac{\rho_{awa}}{1-(1-\frac{R_f}{R_{awa}})\frac{1}{\xi(\theta)x+1}(1-(\frac{y}{b})^{1.5})} \tag{3.45}$$

Equation 3.42 can be expressed as

$$\int_0^\theta \frac{dm_f}{d\theta}d\theta = 2\pi \int_{X_l}^{X_t}\int_0^b \frac{1}{\xi(\theta)x+1}(1-(\frac{y}{b})^{1.5})\frac{\rho_{awa}\ y\ dy\ dx}{1-(1-\frac{R_f}{R_{awa}})\frac{1}{\xi(\theta)x+1}(1-(\frac{y}{b})^{1.5})} \tag{3.46}$$

This double integral expression can be simplified into the following single integral by performing one integration and several algebraic manipulations

$$\int_0^\theta \frac{dm_f}{d\theta}d\theta = 2\pi \int_{X_l}^{X_t}\left[\begin{matrix}(y=b)\\(y=0)\end{matrix}\right.\frac{2\rho_{awa}}{\beta_5}(\frac{1}{\beta_4}+a^3)$$

$$\left\{ y^{1/2} - a^3 \left[\frac{1}{6a^2} log \frac{(a + y^{1/2})^3}{a^3 + y^{3/2}} \frac{1}{\sqrt{3}a^2} tan^{-1} \frac{2y^{1/2} - a}{\sqrt{3}a} \right] \right\}$$
$$+ \frac{\rho_{awa} y^2}{2\beta_5} \Bigg] d_x \tag{3.47}$$

where

$$\begin{aligned} \beta_4 &= \frac{1}{b^{1.5}} \\ \beta_5 &= 1 - (\frac{R_f}{R_{awa}}) \\ a &= (\frac{1-\beta_5 C'm}{C'm\beta_4\beta_5})^{1/3} \\ C'm &= \frac{1}{\xi(\theta)x+1} \end{aligned}$$

In the above equation, $\xi(\theta)$ is the only unknown, and the equation is solved iteratively by Newton's method.

At 1/2 degree after the start of injection an initial value of 0.005 is chosen for $\xi(\theta)$, and the initial value of the integral is evaluated and compared with the actual mass of diesel fuel injected. If the relative difference in the diesel fuel mass is over 0.01%. the value of $\xi(\theta)$ is updated using Newton's method [50], and the calculation repeated until convergence is achieved. This value of $\xi(\theta)$ characterizes the overall concentration of diesel fuel in the cylinder, and is used for all future spray calculations at that crank position. Also, this value of $\xi(\theta)$ is used as the initial value of $\xi(\theta)$ for the next incremented crank position. With the value of $\xi(\theta)$ at which diesel fuel mass convergence is achieved, the distribution of diesel fuel, and the alcohol, water, and air mixture in the entire spray plume can be obtained. The local concentration of diesel fuel in the spray can be obtained from Equation 3.37 through Equation 3.40.

3.3.4 Definition of zone boundaries

The division of the spray plume into a number of zones is based on a nearly constant mass of diesel fuel in each burning zone. The inner and outer boundaries of each of these zones is specified by lines of constant equivalence ratio. Along the spray, the limits of integration in Equation 3.42 are the tail location X_l for the lower limit, and the tip penetration X_t for the upper limit. For the entire spray the limits of integration across the spray are from 0 to the half-width. b. For an individual burned zone, zone B_i, in the spray, the mass of diesel fuel is

$$m_{dsl,B_i} = 2\pi \int_{X_l}^{X_t} \int_{y(\phi_{i+1})}^{y(\phi_i)} C' \rho \, y \, dy \, dx \tag{3.48}$$

Equations for obtaining the diesel mass in each of the burning zones requires the limits of integration across the spray to be expressed as a function of the equivalence ratio ϕ. ϕ_{i+1} corresponds to the inner boundary of the zone or that closer to the core, and ϕ_i corresponds to the outer boundary of the zone. The procedure used to express the physical location of the zone boundary y as a function of the equivalence ratio ϕ is outlined below.

In the double integral expression for diesel fuel mass in the burning zone, zone B_i, the lower and upper limits for integration with respect to y are to be input as functions of the values of the equivalence ratios corresponding to the inner and outer boundaries of the zone, zone B_i. In the actual engine tests, a mixture of alcohol and water was fumigated into the engine. Hence, the cylinder and the spray plume contain a mixture of diesel fuel, alcohol fuel, water, and air. The equivalence ratio for a single fuel operation is defined as the actual fuel-air ratio, on a mass basis, divided by the stoichiometric or theoretical fuel-air ratio. For the presence of two fuels such

as diesel and alcohol in the cylinder, the equivalence ratio is calculated on the basis of excess oxygen:

$$\phi = \frac{\text{moles of oxygen consumed}}{\text{moles of oxygen supplied}} \tag{3.49}$$

The moles of oxygen supplied and consumed, can be obtained from the chemical reaction involved. Consider a sample test case in which ethanol is used as the secondary fuel. The chemical equation representing the combustion process is expressed as

$$X_1' C_{13.78} H_{24.26} - X_2' C_2 H_5 OH + X_3' H_2 O + 1(O_2 + 3.7274 N_2 + 0.0444 Ar)$$
$$\longrightarrow X_4' CO_2 + X_5' H_2 O + X_6' O_2 + 3.7274 N_2 - 0.0444 Ar \tag{3.50}$$

Low concentration product species such as carbon monoxide, oxides of nitrogen, and unburned hydrocarbons are ignored in the above reaction. $X1'$, $X2'$, and $X3'$ are the moles of diesel fuel, ethanol, and water reacting with 4.7718 moles of air in zone B_i. Thus $X1'$, $X2'$, and $X3'$ are given by

$$X_1' = 4.7718\gamma \left(\frac{M_{air}}{M_{dsl}}\right) \tag{3.51}$$

$$X_2' = 4.7718\alpha \left(\frac{M_{air}}{M_{ethanol}}\right) \tag{3.52}$$

$$X_3' = 4.7718\beta \left(\frac{M_{air}}{M_{wat}}\right) \tag{3.53}$$

where M_{eth}, M_{wat}, M_{dsl}, and M_{air} are the molecular weights of ethanol, water, diesel fuel, and air respectively. α, β, and γ are the mass ratios of ethanol to air, water to air, and diesel to air, respectively. The mass ratios can be calculated from the measured mass flow rates of ethanol, water, diesel fuel, and air. For a specific

operating condition of the engine, α and β are uniform throughout the cylinder for the entire cycle.

From the definition of equivalence ratio given in Equation 3.49, the equivalence ratio for the chemical reaction in Equation 3.50 becomes

$$\phi = 1 - \frac{X_6'}{1} \tag{3.54}$$

Performing atom balances between the reactants and products for carbon, hydrogen, and oxygen, the values of $X4'$, $X5'$, and $X6'$ can be expressed as simple functions of the known values of $X1'$, $X2'$, and $X3'$. By simple mathematical manipulations, the moles of excess oxygen in the products of combustion can be expressed in terms of $X1'$ and $X2'$. Substituting for $X1'$ in terms of γ from Equation 3.51 in the expression for $X6'$ gives:

$$X_6' = \frac{1}{2}\left[-(2 \times 13.78 + \frac{24.26}{2})\gamma(\frac{M_{air}}{M_{dsl}}) - 6X_2' + 2\right] \tag{3.55}$$

where γ is the instantaneous local mass fraction of diesel to air, and can be represented as a function of the crank position θ. Substituting (1-ϕ) for $X6'$ from Equation 3.54 into Equation 3.55, and rearranging gives:

$$\gamma(\theta) = \frac{\left[2(1-\theta) + 6X_2' - 2\right]}{\left[-(2 \times 13.78 + \frac{24.26}{2})\frac{M_{air}}{M_{dsl}}\right]} \tag{3.56}$$

The local diesel concentration C can be expressed as

$$C = \frac{m_{dsl}}{m_{dsl} + m_{alc} + m_{wat} + m_{air}} \tag{3.57}$$

Dividing the numerator and denominator of this expression by the local mass of air gives

$$C = \frac{\gamma(\theta)}{\gamma(\theta) + \alpha + \beta + 1} \tag{3.58}$$

Substituting for $\gamma(\theta)$ from Equation 3.56

$$C = \frac{\frac{1}{A_2}[2(1-\phi) + 6X_2^{'} - 2]}{\frac{1}{A_2}[2(1-\phi) + 6X_2^{'} - 2] + \alpha + \beta + 1} \tag{3.59}$$

where

$$A_2 = -(2\text{x}13.78+24.26/2)\frac{M_{air}}{M_{dsl}}$$

A_2 has a numerical value of -6.05.

Equating the expressions in Equation 3.44 and Equation 3.59:

$$\frac{1}{\xi(\theta)x+1}\left(1-(\frac{y}{b})^{1.5}\right) = \frac{2(1-\phi) + 6X_2{}' - 2}{2(1-\phi) + 6X_2{}' - 2 + A_2\alpha + A_2\beta + A_2} \tag{3.60}$$

By suitable simplifications, for ethanol as the secondary fuel, y can be expressed in terms of the equivalence ratio ϕ as

$$y = b\left\{1-(\xi(\theta)x+1)\left(\frac{6X_2{}' - 2\phi}{6X_2{}' - 2\phi + A_2\alpha + A_2\beta + A_2}\right)\right\}^{\frac{1}{1.5}} \tag{3.61}$$

The above expressions for y as a function of θ can be used in the diesel mass Equation 3.48 for the individual zones, and the iso-equivalence ratio boundaries of each burning zone can be evaluated. The process of zone division at incipient ignition and the progressive evolution of additional B_i zones is described in the next section.

3.3.5 Evolution of zones

When the primary diesel fuel is injected into the compressed high pressure, high temperature cylinder charge in the form of a finely atomized spray, the diesel droplets

vaporize rapidly and undergo the pre-combustion chemical reactions with air. Soon after the start of injection, the diesel fuel vapor is mixed with the cylinder charge and spontaneous ignition occurs at several locations in the cylinder. The time required to prepare the diesel fuel to initiate spontaneous combustion in the cylinder is referred to as the ignition delay. As discussed in Chapter 2, several correlations are available in the published literature to estimate the ignition delay. The work of Hardenberg and Hase [29] has been widely used for modeling work. Hardenberg and Hase show that their ignition delay correlation [29] gives good agreement with a wide variety of experimental data obtained on direct injection diesel engines. Hence, this correlation was chosen for the present work. The ignition delay is given by

$$\theta_{id} = (0.36 + 0.22 S_p) exp \left[Ea \left(\frac{1}{Ru T_{cyl}} - \frac{1}{17,190} \right) \left(\frac{21.2}{p_{cyl} - 12.4} \right)^{0.63} \right] \quad (3.62)$$

where

Sp = mean piston speed, in m/sec

Ru = universal gas constant, in kJ/kmole/K

p_{cyl} = cylinder pressure at the start of injection, in bars

T_{cyl} = cylinder temperature at the start of injection, in Kelvin

Ea = activation energy, in kJ/kmole.

The activation energy Ea is given by Ea = 618,840/($C.N-25$)
where $C.N$ is the cetane number of the fuel. The average cetane number for the No.2 diesel fuel used for actual engine tests is specified to be 45 [30].

The crank position corresponding to incipient ignition is given by

$$\theta_{ign} = \theta_{inj} + \theta_{id} \quad (3.63)$$

where θ_{inj} is the crank angle corresponding to the start of injection, θ_{id} is the ignition delay in degrees, and θ_{ign} is the crank position corresponding to incipient ignition. In the model, the crank position is incremented by 0.5 degrees from the start of injection, until ignition. At each updated crank position the value of the diesel fuel distribution factor $\xi(\theta)$ is calculated. At incipient ignition, the cylinder volume apportioned to each spray is divided into a number of zones. In the engine being modeled for this study, the injector has four holes, and hence each spray is assigned one-fourth of the cylinder. The cylinder is divided into three zones at incipient ignition. The iso-equivalence ratio, or iso-phi lines, corresponding to the lean limit (ϕ_L=0.6), and the rich limit (ϕ_R=3.0), are superimposed on the spray plume. The zone containing mixture leaner than the lean limit is zone A, the rich core is zone C, and the zone containing the combustible part of the mixture is zone B_1. The diesel fuel injection diagram specifies the actual mass of diesel fuel injected during the ignition delay period. The value of a new $\xi(\theta)$ is calculated based on this actual diesel mass. The mass of diesel fuel, and the mass of alcohol, water, and air mixture in each zone are obtained from the double integral expressions for each zone, given below.

Zone A:

The lower limit of integration along the y-direction corresponds to the lean limit iso-equivalence ratio line, ϕ_L=0.6. The upper limit of integration along y, corresponds to the outer boundary of the radial concentration profile, where ϕ=0. The diesel mass in zone A is given by

$$m_{dsl,A} = 2\pi \int_{X_l}^{X_t} \int_{y(\phi_L)}^{y(\phi=0)} C' \rho \, y \, dy \, dx \qquad (3.64)$$

The mass of alcohol, water, and air mixture in zone A is obtained from

$$m_{awa,A} = 2\pi \int_{X_l}^{X_t} \int_{y(\phi_2)}^{y(\phi=0)} (1 - C')\rho \; y \; dy \; dx \tag{3.65}$$

Zone C:

The lower limit of y integration corresponds to the nozzle tip, y=0, and the upper limit corresponds to the rich limit of combustion, ϕ_R(=3.0). The mass of diesel fuel, and alcohol, water, and air mixture are given by

$$m_{dsl,C'} = 2\pi \int_{X_l}^{X_t} \int_{y=0}^{y(\phi_R)} C' \; \rho \; y \; dy \; dx \tag{3.66}$$

$$m_{awa,C'} = 2\pi \int_{X_l}^{X_t} \int_{y=0}^{y(\phi_R)} (1 - C') \; \rho \; y \; dy \; dx \tag{3.67}$$

Zone B_1:

At incipient ignition, only one burning B_i zone is assumed to exist in the cylinder, and is bounded by the rich and lean limits of combustion. The masses of diesel fuel, and air, water, and alcohol mixture in zone B_1 are given by

$$m_{dsl,B_1} = 2\pi \int_{X_l}^{X_t} \int_{y(\phi_R)}^{y(\phi_2)} C' \; \rho \; y \; dy \; dx \tag{3.68}$$

$$m_{awa,B_1} = 2\pi \int_{X_l}^{X_t} \int_{y(\phi_R)}^{y(\phi_2)} (1 - C') \; \rho \; y \; dy \; dx \tag{3.69}$$

Zone B_1 is assumed to burn instantaneously to equilibrium combustion products at the end of the ignition delay period. Hence, the mass of diesel fuel that can be associated with the premixed phase of diesel combustion will equal the mass of diesel fuel in zone B_1.

Evolution of new B_i zones are based on a fixed mass of diesel fuel required to form the additional B_i zones. In the present model, the diesel mass required to form

new B_i zones is set at one-third of the diesel mass in zone B_1, to divide the cylinder into a reasonable number of zones. The B_1 zone is capable of sustaining spontaneous combustion, and is assumed to burn instantaneously. The crank position is then incremented in small steps of $\Delta\theta$. The numerical value of $\Delta\theta$ used is in the range of 0.1 to 0.4 degrees, to obtain faster convergence while solving the set of differential equations. The crank position at which a new B_i zone is formed is determined by using the following procedure.

At each incremented crank position, an updated value of the overall distribution factor $\xi(\theta)$ is evaluated. The mass of diesel fuel in the rich core zone, zone C, is obtained at each new crank position by fixing the equivalence ratio of the outer boundary of the zone at the rich limit. The diesel mass contained in the remaining portion of the spray, $m_{dsl,r}$ is calculated using

$$m_{dsl,r} = m_{dsl,inj} - m_{dsl,C} \tag{3.70}$$

Also the diesel mass contained in zone A plus zone B_1 at incipient ignition is subtracted from $m_{dsl,r}$ to obtain the diesel mass in the transient B_j zone being formed on the outer skin of the core zone, zone C.

$$m_{dsl,B_j} = m_{dsl,r} - (m_{dsl,A} + m_{dsl,B_1}) \tag{3.71}$$

If the value of m_{dsl,B_j} is greater than 99% of the mass of diesel fuel required to form a new B_i zone, the B_j zone is evolved into zone B_2. If m_{dsl,B_j} is less than 99% of the diesel mass required for new zone formation, the crank position is again incremented and the process of calculating new values for $\xi(\theta)$, $m_{dsl,r}$, and m_{dsl,B_j} is repeated, until the new B_2 zone is evolved. The crank position at which a new B_2

zone is formed is θ_2, and the crank angle corresponding to ignition is θ_1, such that

$$\theta_2 = \theta_1 + K_\theta(\Delta\theta) \tag{3.72}$$

where K_θ is an integer which refers to the finite number of steps required to form the new B_i zone, zone B_2. The cylinder pressure, zone temperatures, and zone volumes just prior to ignition are obtained from the air intake and compression processes. A brief description of these processes is given in Section 3.5. At incipient ignition, zone B_1 is burned instantaneously, and the cylinder pressure, zone temperatures, and zone volumes after B_1 is burned are obtained by using the subroutine BURNBZ. A description of the instantaneous burning process, the equations involved and the solution procedure is given in Appendix D. After the instantaneous burning of B_1 at θ_1, the piston moves until the new B_2 zone is evolved at θ_2. The thermodynamic properties such as the cylinder pressure, zone temperatures, and zone volumes at θ_2 are obtained by solving the derivative form of the thermodynamic equations, along with mass conservation and volume constraint equations. In the present model, the THERMOZ subroutine solves the relevant equations and provides the necessary thermodynamic properties. The details of setting up the equations, and the solution procedure are given in the section on thermodynamic calculations, Section 3.2.

Between the two zone formation crank positions θ_1 and θ_2, the mixture of alcohol, water, and air from the lean zone, zone A, is entrained into all the other zones. Although, the diesel mass is kept fixed in zones A and B_1, the new iso-phi boundaries must be superimposed on the spray to define the updated mass of alcohol, water, and air mixture in each of these zones.

For zone A, equivalence ratio of the outer boundary is fixed at zero, and Equa-

tion 3.64 is used to find the inner boundary. The left side of Equation 3.64 is the mass of diesel fuel in zone A at incipient ignition. The initial value for the iso-equivalence ratio of the inner boundary of zone A is assumed to equal the lean limit, and Newton's method [50] is used to obtain the exact value of equivalence ratio for the inner boundary of zone A at θ_2. The solution procedure is iterated until the diesel fuel mass in zone A is within 0.01% of the diesel mass required for convergence. For zone C, the equivalence ratio of the inner boundary is infinity (pure diesel) and the outer boundary is set at the rich limit, ϕ_R. For zone B_1, adjacent to zone A, the outer boundary $\phi_{B_1,2}$ is given by the equivalence ratio line corresponding to the inner boundary of zone A. The inner boundary of zone B_1, $\phi_{B_1,1}$ is obtained by solving an equation of the form of Equation 3.73, by prescribing a value of 1 to i.

$$m_{dsl,B_1} = 2\pi \int_{X_l}^{X_t} \int_{y(\phi_{B_i,1})}^{y(\phi_{B_i,2})} C\ \rho\ y\ dy\ dx \tag{3.73}$$

$$m_{awa,B_1} = 2\pi \int_{X_l}^{X_t} \int_{y(\phi_{B_i,1})}^{y(\phi_{B_i,2})} (1-C)\ \rho\ y\ dy\ dx \tag{3.74}$$

For zone B_1, at the new crank position θ_2, the left side of Equation 3.73 is set equal to the diesel mass in zone B_1 at incipient ignition. Again Newton's method [50] is used to obtain the value of the iso-equivalence ratio corresponding to the inner boundary of zone B_1. For the newly evolved zone, zone B_2, the inner boundary equals the outer boundary of zone C, and the outer boundary is fixed by the inner boundary of the last previously formed zone, zone B_1. Once the new zone, zone B_2 is evolved at θ_2 and the mass of diesel and the mass of alcohol, water, and air mixture in all the zones are obtained, the new zone, zone B_2, is burned instantaneously. The crank position is again incremented in small crank steps, $\Delta\theta$, until the formation of another

B_i zone is confirmed. The crank angle at which the new B_i zone is evolved is θ_2, and the crank angle at which the previous B_i zone was evolved is θ_1.

The entrainment rate of alcohol, water, and air from the lean zone, zone A, to the other zones is required by the THERMOZ subroutine to evaluate the thermodynamic properties at the new zone formation crank position, θ_2, immediately after the new B_i zone is formed. The entrainment rate of alcohol, water, and air mixture for the zones is obtained from expressions similar to those used by Chiu et al. [15] to determine the air entrainment rates in their multizone model for a diesel engine, without fumigation.

$$\frac{dm_{e,awa,A}}{d\theta} = \frac{m_{awa,A}(\theta_2) - m_{awa,A}(\theta_1)}{(\theta_2 - \theta_1)} \tag{3.75}$$

$$\frac{dm_{e,awa,C}}{d\theta} = \frac{m_{awa,C}(\theta_2) - m_{awa,C}(\theta_1)}{(\theta_2 - \theta_1)} \tag{3.76}$$

$$\frac{dm_{e,awa,B_i}}{d\theta} = \frac{m_{awa,B_i}(\theta_2) - m_{awa,B_i}(\theta_1)}{(\theta_2 - \theta_1)} \tag{3.77}$$

and the injection rate of diesel fuel into zone C is given by

$$\frac{dm_{e,dsl,C}}{d\theta} = \frac{m_{dsl,C}(\theta_2) - m_{dsl,C}(\theta_1)}{(\theta_2 - \theta_1)} \tag{3.78}$$

Before the new B_i zone is separated from zone C, the value of $\frac{dm_{e,dsl,C}}{d\theta}$ should equal the injection rate of diesel fuel. The diesel mass in all the zones, except zone C is fixed. Hence, the entrainment rate of diesel fuel for zone A, and the previously formed B_i zones is zero.

With the procedure explained in this section, the instantaneous mass of diesel fuel, and the mass of alcohol, water, and air mixture in each zone can be calculated. Also, the mathematical expressions for obtaining the entrainment rate of diesel fuel into the rich core zone, and the entrainment rates of the mixture of alcohol, water,

and air from the lean zone to the remaining zones in the cylinder, developed in this section were used in the model.

The general procedure discussed in this section is for a free jet in the absence of wall impingement. This procedure needs to be slightly modified to model wall impingement of the jet. The different phases of the present multizone model and their features are explained in Section 3.4.

3.4 Phases of the Combustion Process

During the initial period of fuel injection, the spray is a free jet. However, the combustion bowl diameter for the engine is 60.2 mm, with a swirl ratio of 5.0. hence about 7 to 8 degrees after the start of injection, the spray reaches the bowl wall. A free jet is no longer an accurate description of the spray. A method of modeling the spray after it impinges on the wall is proposed below. To simplify and better understand the process of modeling combustion and expansion, five discrete phases are considered.

Phase 1:

This phase extends from the start of injection to the crank position at which the spray tip reaches the wall. In this phase, the spray is modeled as a free jet. The procedure to model this free jet has been discussed in Section 3.3. Figure 3.11 represents this phase.

Phase 2:

The second phase starts when the spray impinges on the wall, and extends until the end of fuel injection. A new wall zone, zone D, is formed at the beginning of this

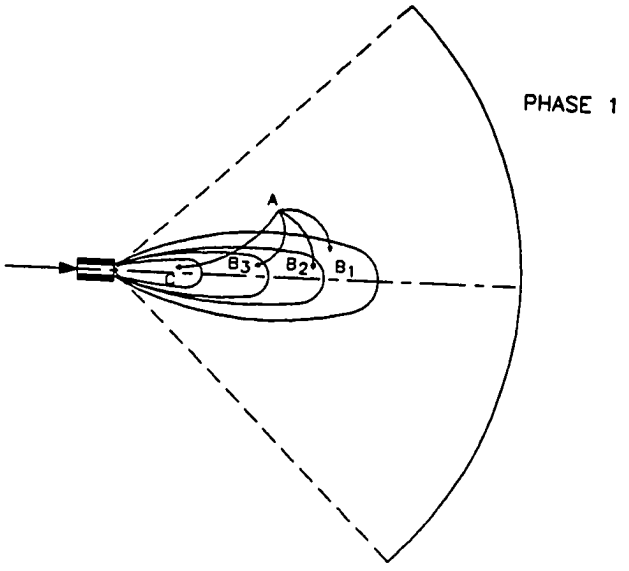

Figure 3.11: Phase 1: Free Jet

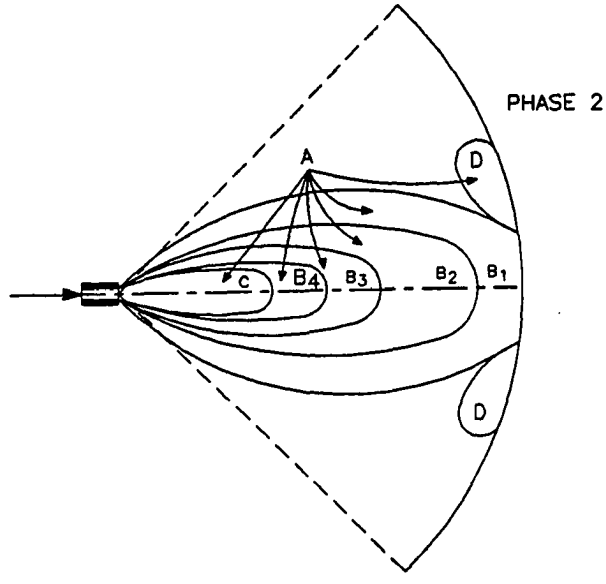

Figure 3.12: Phase 2: Wall Jet with Fuel Injection

phase. The contents of the spray plume impinging on the wall are transferred to the wall zone. The rate at which diesel fuel from the spray plume is transferred to zone D is set equal to the diesel injection rate. Hence, the mass of diesel fuel in the spray plume is kept constant, throughout this phase. Figure 3.12 shows Phase 2.

With increasing crank angle, zone A continues to become smaller, and zone D begins to grow, and the entrainment of alcohol, water, and air mixture from zone A to zone D is given by the expression

$$\dot{m}_{e,awa,A-D,\theta_1-\theta_2} = \frac{m_{dsl,A}(\theta_1) + m_{awa,A}(\theta_1)}{K_{AD}} \tag{3.79}$$

where K_{AD} is a constant which fixes the transfer rate of the mixture of alcohol, water

and air from zone A to zone D. A numerical value of 30 is used for K_{AD}. K_{AD} was varied from 10 to 100, but for values exceeding 30, the transfer is too slow and zone A is not completely transferred to zone D, even by the end of the expansion stroke. For values of K_{AD} below 15, the transfer rate is too rapid, resulting in over-entrainment, and zone A is emptied close to the end of the injection process. A number of cycle simulations were carried out with the values of 15, 20, 25 and 30 for K_{AD}. Of these the best match between experimental data and model predictions for indicated mean effective pressure, indicated thermal efficiency, and exhaust temperature was observed when K_{AD} was equal to 30. Hence, K_{AD} was assigned a value of 30 for all the cycle simulations carried out in the present work.

The process of formation of new B_i zones, instantaneous burning of the new B_i zone, and the calculation of thermodynamic properties of the zones, is identical to that used in Phase 1. The spray plume contains burned products in the zones which are physically located close to the bowl wall. Hence, the transfer of diesel mass from the spray plume to the wall zone, results in a proportional transfer of alcohol, water, and air mixture. The transfer process is assumed to occur instantaneously. The details of this process are given in Appendix E.

Phase 3:

Phase three begins when injection stops, and the spray tail begins to move downstream. The transfer of contents of the spray plume to the wall zone, zone D, continues. Diesel fuel is transferred from the spray plume into zone D at a constant rate corresponding to the rate of injection just prior to the end of injection. Although no additional diesel fuel is injected, the rich core zone, zone C, continues to entrain a

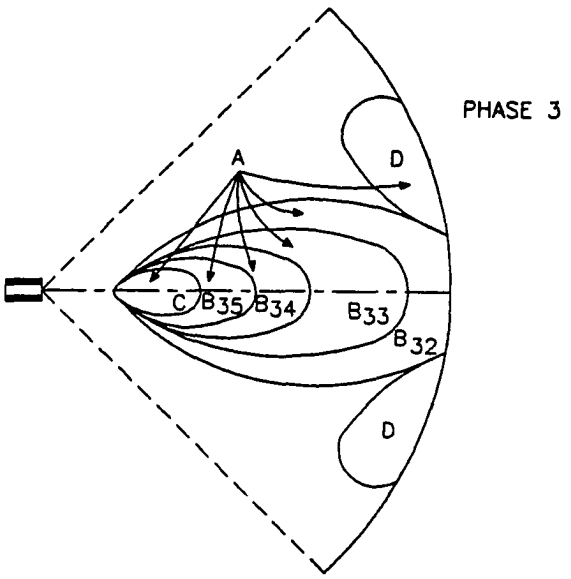

Figure 3.13: Phase 3: Wall Jet following End of Injection

mixture of alcohol, water and air from zone A and evolve new B_i zones. Figure 3.13 shows Phase 3.

The newly evolved B_i zones are burned instantaneously as detailed in Section 3.3. The B_i zones closer to the bowl wall are transferred into zone D, and are mixed instantaneously with the contents of zone D. The processes of instantaneous transfer of previously burned B_i zones into zone D, and instantaneous mixing are detailed in Appendix E. The entrainment of alcohol, water, and air mixture from zone A to zone D is given by the expression in Equation 3.79. As mentioned earlier, a numerical value of 30 is used for K_{AD}. When zone C does not contain sufficient diesel fuel to form additional B_i zones, a mixture of alcohol, water and air is entrained into it from

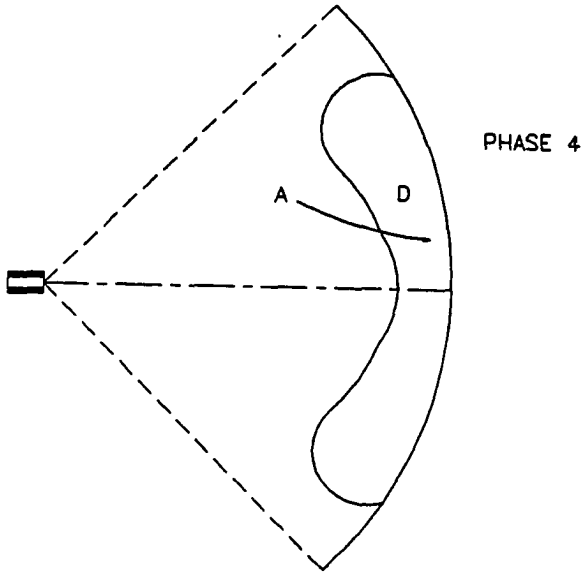

Figure 3.14: Phase 4: Wall Jet, Spray Plume Completely Transferred to Zone D

zone A until the overall equivalence ratio of zone C is below the rich limit, o_R. Zone C is then treated as a B_i zone, and burned instantaneously. Phase 3 continues until all the B_i zones, and zone C are completely transferred to zone D.

Phase 4:

This phase begins when only zone A and zone D remain in the cylinder. Figure 3.14 represents this phase.

The only mass transfer to be considered is the transfer of the mixture of alcohol, water, and air from zone A to zone D, following the mass tranfer rate expression given in Equation 3.79. No more new zones can be formed and hence there is no need for instantaneous burning. All B_i zones have been emptied into zone D. hence

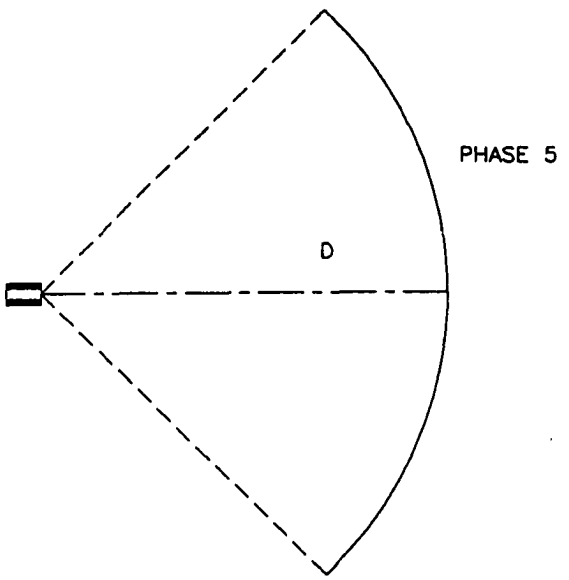

Figure 3.15: Phase 5: Cylinder Contents are Homogeneous

the instantaneous mixing process is not relevant. The transfer of alcohol, water, and air from zone A to zone D and the resulting burning in zone D are modeled in the subroutine, THERMOZ, along with the expansion of the cylinder contents due to piston movement from θ_1 to θ_2. In this phase, the crank position is stepped up in increments of 2 degrees, until all of zone A is completely transferred to zone D.

Phase 5:

This phase essentially expands the cylinder containing a single, homogeneous zone, zone D, from the end of Phase 4 to the BDC position of the expansion stroke. Figure 3.15 shows Phase 5.

The crank position is incremented in 5 degree steps, and at each new position,

the thermodynamics sub-model, THERMOZ, is used to obtain cylinder pressure and the bulk cylinder temperature. The cycle simulation is complete at the end of this phase.

The present multizone model, divided into five phases as detailed above, is only capable of modeling the injection, combustion, and expansion phases of the cycle. The initial conditions in the cylinder at the beginning of the injection process are to be supplied as inputs to the model. The intake and compression model developed for a fumigated diesel engine has been used in the present work to obtain the initial conditions.

3.5 Initial Conditions for the Model

The intake and compression process model included in the present multizone model to obtain the initial conditions, is described in this subsection. The present multizone model attempts to simulate a fumigated diesel engine. A mixture of alcohol and water is fumigated along with the intake air stream. The mixture of alcohol and water injected into the intake air stream downstream of the turbo-compressor, influences the conditions in the cylinder at the end of the intake stroke. Jiang and Van Gerpen [17] modeled the mixing of alcohol, water, and air in the intake manifold, the intake process into the cylinder, and the compression of the fumigated mixture in the cylinder. For mixing in the intake manifold, the intake pipe was assumed to be an open control volume, as shown in Figure 3.16. Equilibrium between the liquid and vapor states of alcohol and water was assumed at all times. The mixture was modeled as an ideal gas, at a constant pressure equal to the boost pressure. The temperature

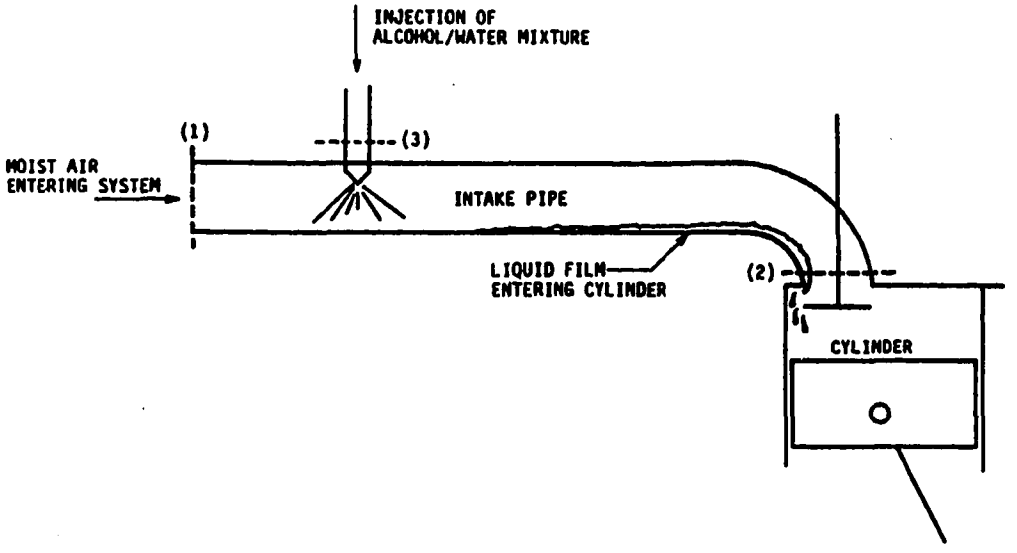

Figure 3.16: Control Volumes for Intake Pipe and Engine Cylinder

of the mixture was evaluated iteratively by solving the first law energy equation and the mass conservation equation. The possibility of a fraction of the fumigated water exiting in liquid state was also included in the model. The high volatility of both methanol and ethanol indicate that all of the alcohol will vaporize before the mixture enters the engine cylinder. The temperature at the end of the intake process was obtained by a second iterative process. The mass of alcohol, water, and air trapped in the cylinder was input from the measured flow rates. Using the ideal gas equation, an assumed cylinder temperature, and the total cylinder volume at bottom dead center, the cylinder pressure was evaluated. The actual cylinder temperature at the end of the intake process was obtained by iterating an assumed temperature until the cylinder pressure equaled the measured boost pressure in the intake manifold. The instantaneous cylinder pressure and temperature during compression were obtained by modeling the cylinder as a closed control volume containing air, alcohol vapor, and water in both liquid and vapor state. The mixture of air, alcohol vapor, and water vapor was assumed to behave as an ideal gas. Liquid water, if present in the cylinder, was assumed to be in equilibrium with water in vapor phase. It was assumed that chemical reactions are incapable of occuring during this process. The instantaneous cylinder pressure and temperature are obtained by simultaneously solving the differential form of the first law energy equation, and the mass conservation equation. The instantaneous heat transfer rate was obtained by using Annand's correlation [34], and the instantaneous cylinder volume and rate of change of volume were given by the slider-crank mechanism analysis [30]. An IMSL ordinary differential equation solver routine, DVERK, on the VAX-11/785 computer, was used to integrate the set of

differential equations over the compression process up to the start of diesel injection. The cylinder pressure, and temperature at the start of injection are the initial inputs to the multizone spray model.

3.6 Nitric Oxide Sub-model

A nitric oxide (NO) sub-model has been incorporated in the present multizone model. The NO model is included in the subroutine which solves the set of thermodynamic equations to obtain instantaneous values of cylinder pressure, zone temperatures, zone volumes, work output, and heat transfer. The instantaneous concentration of NO in the individual zones is computed by integrating the NO rate equation for the individual zones. The instantaneous concentration of total NO in the cylinder is obtained by combining the instantaneous NO concentrations in the individual zones.

The NO formation and destruction in the individual zones is based on the assumption of partial equilibrium. The individual species such as O_2, N_2, O, N, H, and OH are assumed to follow equilibrium concentrations corresponding to the instantaneous value of cylinder pressure, zone temperature, and zone composition, but the NO concentration in the zones is kinetically controlled. The equilibrium concentrations of O_2, N_2, O, N, H, and OH are obtained from a computer program that calculates the equilibrium composition of the products of combustion (PER) [51], based on the instantaneous zone conditions.

The kinetic NO reactions are represented by a three reaction Zeldovich mechanism [52]:

$$O + N_2 = NO + N \tag{3.80}$$

$$N + O_2 \rightleftharpoons NO + O \tag{3.81}$$

$$N + OH \rightleftharpoons NO + H \tag{3.82}$$

These three reactions are assumed to follow temperature dependent forward and backward reaction rates. The expressions to calculate the reaction rates, and the procedure used to combine these reactions to evaluate the instantaneous NO concentration are detailed in Appendix F.

The actual plots of NO history in the cylinder, provided by the multizone model, are given in Chapter 5. Exhaust concentrations of NO predicted by the model are compared with experimental data, and discussed in Chapter 5.

3.7 Summary

The procedure used in the present model to obtain the relevant engine parameters such as the cylinder pressure, and bulk cylinder temperature, and NO concentration in the cylinder, as a function of the instantaneous crank position, has been described in this chapter. The initial conditions at the beginning of the primary diesel fuel injection are obtained from a previously developed intake and compression model [17], as described in Section 3.5. In order to obtain the relevant thermodynamic properties in the cylinder, during combustion and expansion, the derivative form of the first law energy equation for an open control volume is used along with the ideal gas assumption for the zone contents, and the cylinder volume constraint. The cylinder is divided into a number of discrete zones, and the thermodynamic equations are written and solved for each of these zones. To provide the necessary mass transfer information for individual zones to the thermodynamic equations, a transient spray

mixing model based on the work of Chiu et al. [15] at the Cummins Engine Company is incorporated, with suitable modifications. Additional sub-models to include the spray impingement on the wall have been developed. The development of a wall model and the assumptions involved have been described. A simple nitric oxide sub-model incorporated in the multizone model to predict the instantaneous concentration of NO in the cylinder and the exhaust NO concentration has also been discussed in this chapter.

The predictions of the multizone model have been validated with experimental data obtained on a fumigated diesel engine. The test set-up, and the procedure used to obtain engine data are discussed in the next chapter.

4. EXPERIMENTAL APPARATUS AND TEST PROCEDURE

The experimental fumigation tests were conducted on a four-stroke, four-cylinder, turbocharged diesel engine. The engine-dynamometer set-up used for the tests and the procedure used to acquire and process the data are described in this chapter. The chapter is divided into four main sections. The first section describes the experimental apparatus. The second section describes the data acquisition system used to record the test results. The experimental procedure is discussed in the third section, and the fourth section outlines the calculation of the performance and emission parameters from the measured data. Figure 4.1 shows a schematic of the experimental apparatus.

4.1 Experimental Apparatus

4.1.1 Engine

The engine used for this work was a John Deere Model 4276T four-cylinder, four-stroke, turbocharged diesel engine. The combustion system was a bowl-in-piston direct-injection, medium swirl type. A brief list of the engine's characteristics is provided in Table 4.1.

The engine was directly coupled to a General Electric DC dynamometer. The dynamometer was used to motor the engine for initial start up and is capable of

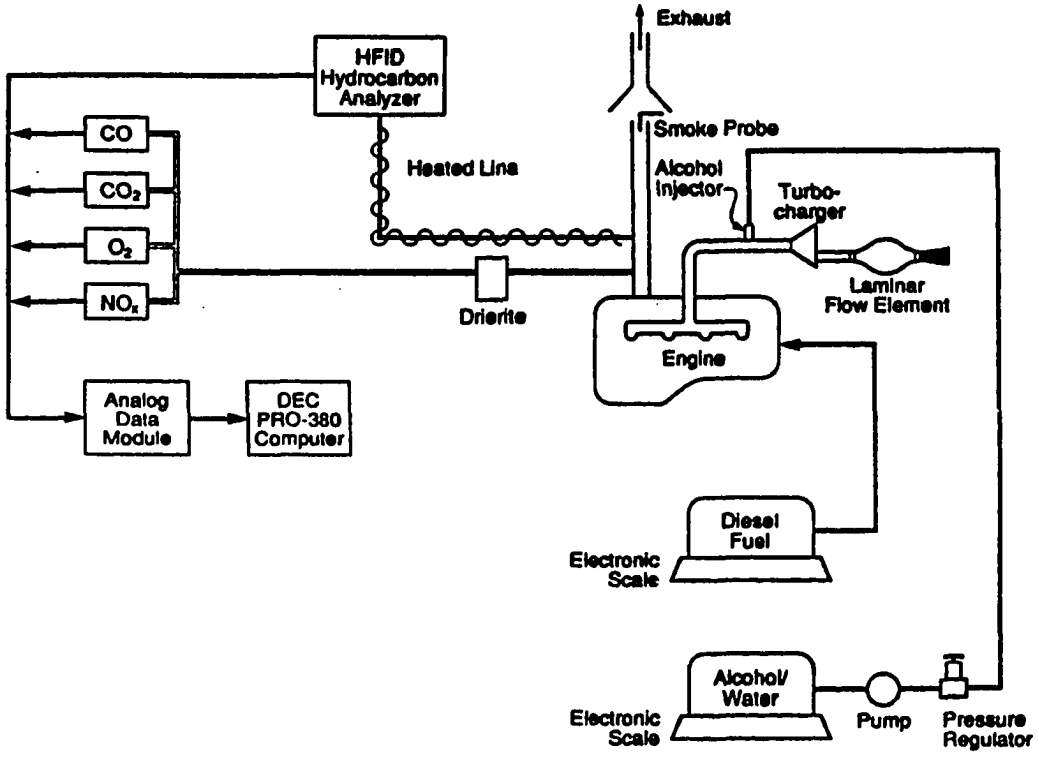

Figure 4.1: Schematic of Experimental Apparatus

Table 4.1: John Deere 4276 T Four Cylinder Engine Specifications

Bore	106.5	mm	(4.19 $in.$)
Stroke	127.0	mm	(5.0 $in.$)
Connecting Rod Length	202.9	mm	(7.99 $in.$)
Displacement Per Cylinder	1131.3	cm^3	(69.0 $in.^3$)
Total Engine Displacement	4525.2	cm^3	(276.0 $in.^3$)
Compression Ratio	16.8	: 1	
Valve Timing			
Intake	opens at 2 deg. bTDC, closes at 80 deg. aTDC		
Exhaust	opens at 56 deg. bTDC, closes at 29 deg. aTDC		
Combustion System	Bowl-in-piston direct-injection. nominal swirl ratio = 5		
Injection System			
	Roosa-Master JDB435 MB 3795 Pump		
	Roosa-Master 4 holes x 0.3 mm diameter injector		
	Nozzle l/d ratio = 2.0		
	3200 psi normal opening pressure		
	Maximum needle lift = 0.34 mm.		

switching to a power absorbing mode when the engine delivers power. The engine was equipped with a speed governor that was left intact. The dynamometer provided speed control of the engine, while the fuel governor lever was adjusted to set the required load on the engine. The torque output of the engine was measured with a Lebow strain gage load cell mounted on the torque arm of the dynamometer.

4.1.2 Fumigation system

The alcohol and water mixture was injected into the intake manifold of the engine after the turbocharger compressor about ten inches before the pipe branches into separate passages for the individual cylinders. A commercially available fumigation system produced by Midwest Power Inc. of Radcliffe, Iowa was used. This included the injector, an electric fuel pump, a bypass pressure regulator and a positive fuel shut-off solenoid for safety.

4.1.3 Measurement of fuel flows, temperatures, pressures, and exhaust emissions

This section briefly describes the instruments used to measure flow rates, temperatures, and pressures during the fumigation tests. The emissions measurement equipment will also be discussed in this section.

The diesel fuel, and alcohol and water mixture flow rates were measured using Toledo and Sartorius electronic scales respectively. A stop watch was used to time the mass of diesel fuel and alcohol and water mixture supplied to the engine. A Meriam laminar flow element was used to measure the air flow rate to the engine. The

differential pressure across the laminar flow element was measured using an inclined manometer.

Thermocouples were located at the air intake, to measure the intake air dry and wet bulb temperatures, and at a number of locations in the exhaust line, close to the exhaust valves for measuring the bulk and the individual cylinder gas temperatures. Boost pressure, exhaust back pressure, and engine lubricating oil line pressure were measured with pressure gages. The temperature of the diesel fuel supplied to the engine was maintained at about 38 to 44°C by a heat exchanger to maintain near constant mass of fuel injected into the engine.

In this investigation, exhaust concentrations of carbon monoxide (CO), carbon dioxide (CO_2), nitric oxide (NO), unburned hydrocarbons (HC), oxygen (O_2), and smoke were measured for each engine operating condition. Figure 4.1 shows a schematic of the exhaust measurement equipment used. Exhaust emissions were sampled directly from the exhaust pipe of the engine, about four feet downstream of the turbocharger. Two separate sample lines were used to obtain sufficient flow rate of the exhaust. One of the sample lines was heated to prevent condensation of the exhaust. This heated sample was supplied to a Beckman Model 402 Heated Flame Ionization Detector (HFID) type hydrocarbon analyzer. The HFID analyzer was calibrated in hexane equivalent units. The second sample line used for the CO, CO_2, NO_X, and O_2 analyzers was not heated. The water vapor in this line was removed by passing the exhaust through a desiccant. A particle filter made of packed fiberglass was used to trap the carbon particles in the exhaust. A Thermoelectron Chemiluminescent NO_X analyzer, and a Beckman Model 955 Chemiluminescent NO_X analyzer

were used to measure nitric oxide. Two separate Beckman Model 864 nondispersive infrared (NDIR) analyzers were used for measuring carbon monoxide and carbon dioxide. A Beckman Model 7003 polarigraphic analyzer was used to measure oxygen. The engine smoke was measured using a Bosch smoke pump and Bosch smoke meter. The probe of the smoke pump was inserted into the exhaust stack about fifty inches downstream of the turbocharger. The Bosch Smoke measurement involves drawing a constant volume of exhaust through a clean paper filter at atmospheric pressure. This paper filter is then rated using a Bosch smoke meter which shines a light on the sooted paper, and measures reflected light with a photocell. The sooted filter paper is measured on a scale from 0 to 10, where 0 corresponds to a clean filter, and 10 to a completely black filter.

4.2 Data Acquisition System

A Digital Equipment Corporation Analog Data Module (ADM) was used with a Digital Equipment PRO-380 computer to acquire data from the emissions equipment. The output signals from the emissions equipment were provided to the ADM which converted the signal into digital form. The converted data were then stored on the PRO-380 computer for analysis. The ADM sampled the data at the rate of 8 channels per second, and the data were displayed on the computer monitor every two seconds. The data sets were averaged every twenty seconds and the averaged data were stored on the computer. The date and time from the computer's clock were also stored for every data set to enable correlation of emissions data with the rest of the data recorded manually.

4.3 Experimental Procedure

This section describes the procedures used to collect the experimental data. The matrix of different operating conditions used for the engine tests is described in the first section. The second section discusses the procedure used for preparing the alcohol and water mixture. The standard procedure followed to run the engine tests and obtain the relevant data is explained in the third section.

4.3.1 Test matrix

The tests were carried out at two different speeds (1500 rpm and 2100 rpm), four different load conditions (25%, 50%, 75%, and 100% of the rated load at the selected speed) and four different levels of torque substitution. The flow rate of the alcohol and water mixture was varied according to the fraction of the engine brake torque derived from it. The percentage torque supplied by the additive was varied from 10% to 40% in increments of 10%. At each torque substitution rate, eight different additive qualities or proofs, ranging from 40 proof to 169.5 proof, were tested.

Additive mixtures prepared from methanol and ethanol were compared at two different engine operating conditions:

1. 1500 rpm, 100% load, 20% torque derived from the alcohol, and
2. 2100 rpm, 100% load, 30% torque derived from the alcohol.

The additive mixture quality was varied from 40 proof to 169.5 proof for these tests.

Preliminary calculations using the data from the methanol-ethanol comparison established that comparable qualities of both mixtures perform identically, so the remaining tests were conducted using ethanol and water mixtures exclusively. Engine

operation at light loads with higher torque replacements from low proofs of the alcohol and water mixture resulted in misfire and unstable behavior. This is attributed to the large flow rates of water in the fumigated mixture supplied to the engine. Test cases resulting in unstable engine operation were abandoned to prevent engine damage.

The effect of distilled water present in the additive mixture was also investigated. Distilled water was fumigated separately into the engine with gradually increasing flow rates. The tests were conducted at 1500 rpm, full load and 1500 rpm, 75% load conditions. For the tests at full load the fueling was set to its maximum value and the water flow rate was gradually increased until the engine began to misfire. At the 75% load condition, the fuel governor control was adjusted to compensate for the loss in engine power with increasing water flow rate and a constant torque output was maintained. At the 75% load setting, after the governor reached its maximum fueling position, additional diesel fuel could not be supplied to the engine. Beyond this point, increasing the water flow rate resulted in misfire. Unstable engine behavior was caused by cylinder bulk gas quenching due to excessive water injection, and further tests at this operating condition were discontinued.

4.3.2 Alcohol and water mixture preparation

The secondary fuel fumigated into the intake manifold of the engine is a mixture of alcohol, water, and a very small quantity of oil. Engine tests were carried out with both methanol and water, and ethanol and water mixtures. To allow comparisons, mixtures of methanol and water containing net energy equal to corresponding mixtures of ethanol and water were fumigated in consecutive tests. In order to obtain

data that can be meaningfully interpreted, the two different alcohol mixtures were always compared in consecutive tests.

The standard used for defining ethanol and water mixture is 'proof'. Pure ethanol is equivalent to 200 proof. Different proofs of ethanol are obtained by mixing distilled water with ethanol in different proportions. The specific gravity for different proofs of ethanol are tabulated in Table No. 6 of the Gauging Manual of the U. S. Bureau of Alcohol, Tobacco and Firearms [53]. This table also provides the volume proportions of ethanol and distilled water required to prepare a mixture with a certain proof value.

For comparing mixtures of ethanol and water with methanol and water, the equivalent amount of methanol in water that matches a certain proof of ethanol, both in terms of lower heating value and enthalpy of vaporization, was prepared. This ensures equal cooling effect caused by the two alcohols. The lower heating value of pure ethanol is higher than that for pure methanol. Hence, the quantity of methanol required to prepare a mixture of equivalent ethanol proof would be larger than that of ethanol. By this method mixtures of ethanol, and methanol which have the same ratio of latent heat of vaporization to lower heating value will result.

Knowing the latent heat of vaporization of a mixture of ethanol and water, the lower heating value of ethanol, and the heat of vaporization and lower heating value of pure methanol, the ratio of methanol to distilled water, either on a volume basis or on a mass basis required to equal the ethanol and water mixture is determined. Such a methanol and water mixture corresponding to a known proof value of ethanol and water mixture is denoted by the unit Pr. EEM (Proof Equivalent Ethanol-Methanol). Based on this definition of equal energy content mixtures, chemically pure methanol

(99.9% Methanol) is equivalent to 169.5 proof ethanol.

Mixtures of ethanol and water are obtained by mixing individual volumes of 180 proof ethanol with distilled water. The specific gravity for the ethanol and water mixture provided in the proof table given in Reference [53] was used as the standard. Volume proportions and specific gravity data of methanol and water mixtures are not readily available in published literature. A table of mass fraction of methanol in water was developed on the basis of equivalent proof definition. Table 4.2 lists the mass fraction of methanol in water for Pr. EEM values ranging from 40 to 169.5. While preparing the first batch of methanol mixtures, pure methanol and distilled water were cooled to 60°F, and were mixed according to the mass proportions specified in Table 4.2. The individual volumes of methanol and water used in the mixtures were recorded. The mixtures were stirred to enable the alcohol and water molecules to rearrange their bonding. Since this rearrangement process is exothermic, the mixtures were allowed to cool to room temperature. Preparation of ethanol and water mixtures also involved stirring and cooling after the exothermic rearrangement of the molecules. The specific gravity of these mixtures was recorded at 60°F, using hydrometers certified by the American Petroleum Institute. The specific gravity values are listed in Table 4.2. The specific gravity values obtained from this preliminary mixtures were used as the standard for mixture preparation during the remaining tests. A few ounces of lubricant were added to every five gallons of the alcohol and water mixtures, by Midwest Power Inc., to prevent excessive wear and damage to the alcohol fumigation system.

Table 4.2: Methanol-Water Mixture Data

Pr. EEM	Mass Fraction of Methanol in Water	Specific Gravity at 60°F.
40	0.216	0.9674
60	0.325	0.9510
80	0.437	0.9315
100	0.552	0.9082
120	0.673	0.8830
140	0.799	0.8355
160	0.934	0.8126
169.5	1.000	0.7958

4.3.3 Test procedure

A consistent procedure was used for collecting the data to insure repeatability. At the start of each engine test, the emission instruments were calibrated with known concentrations of the gas to be analyzed. Before actual data collection, the engine was brought to an equilibrium operating condition (at the required test speed and load) as indicated by stable engine coolant and oil temperatures. This engine warm up was done entirely with diesel fuel operation.

After the engine was stabilized, testing was started with diesel-only operation at a speed and load condition at which a series of operating conditions were to be studied. The governor control lever was adjusted to attain the specified load condition. This torque condition was designated as the baseline torque. After recording data with this diesel operation, the governor control lever was adjusted so that the engine's torque was a designated fraction (90%, 80%, 70% or 60%) of the baseline torque. At

this reduced torque, the diesel operation data were recorded, and alcohol and water mixture (beginning with the lowest proof of 40) was injected to regain the baseline torque. The engine was operated with fumigation of the alcohol mixture, and the data were recorded after steady-state operation of the engine was reached (in three to five minutes). The smoke measurement was performed three times for each operating condition and the average Bosch smoke level was recorded. The exhaust emission levels as indicated by the analog meters on the individual analyzers were recorded at each test condition to verify the data recorded on the computer.

After recording all the relevant data, the additive supply was stopped and the engine was returned to diesel-only operation at the reduced torque level. A new additive mixture (next higher proof) was then injected to obtain the baseline torque and data recording procedure descibed above was repeated. The additive proof was increased from 40 to 169.5. After completing this test set, the engine was operated with the next lower baseline torque by changing the position of the governor control lever (from 90% to 80% of the specified torque), and the test procedure was repeated for this torque level. The baseline torque was lowered from 90% to 60% in steps of 10% to enable increasing levels of torque replacement from the additive from 10% to 40%.

A typical test schedule for one day consisted of a fixed speed (1500 or 2100 rpm) with a fixed specified load (100% or 75% or 50% or 25%), at four different baseline torque levels (90%, 80%, 70%, and 60%), and with eight different additive proof levels (40, 60, 80, 100, 120, 140, 160, and 169.5) at each baseline torque setting. This resulted in a total of nearly forty operating conditions at any specified speed and

load condition. A few of these operating conditions were repeated at random to check the reliability and repeatability of the data recorded during the test and were also compared with available data acquired in the previous tests under identical operating conditions.

After completing a prescribed test schedule, the instruments and emission equipments were recalibrated to insure validity of the data obtained. If large errors were noticed during recalibration, the data were discarded for further analysis and the entire test schedule was repeated the following day, until reliable data were acquired.

4.4 Data Analysis

This section describes the conversion of raw data acquired from the engine tests into parameters that can be compared with predictions of the multizone model. The multizone transient spray model developed in the present work, is capable of predicting cylinder pressure, bulk cylinder temperature, exhaust temperature before the turbocharger, and the concentration of nitric oxide in the exhaust.

During the engine tests, provisions were not made for measuring the cylinder pressure and temperature histories. The exhaust temperature before the turbocharger was measured using two type-K thermocouples. The nitric oxide concentration in the exhaust was measured with a chemiluminescent NO_X analyzer. The engine speed, brake torque output by the engine, and friction torque under hot motoring condition were measured at the dynamometer. The brake power and the friction power were calculated using the measured brake and friction torques.

The indicated power (IHP) for a specified engine operating condition was cal-

culated by adding together the brake and friction powers. The measured indicated thermal efficiency, $\eta_{th,ind}$, for a specified engine operating condition is the ratio of the indicated power output by the engine to the total energy supplied by the fuels:

$$\eta_{th,ind} = \frac{IHP}{m'_{dsl} LHV_{dsl} + m'_{alc} LHV_{alc}} \tag{4.1}$$

where m'_{dsl} and m'_{alc} are the mass flow rates of diesel fuel and pure alcohol, and LHV_{dsl} and LHV_{alc} are the lower heating values of diesel and alcohol.

The measured indicated mean effective pressure ($IMEP$) is given by

$$IMEP = \frac{4\pi(\tau_b + \tau_f)}{V_{displ}} \tag{4.2}$$

where τ_b and τ_f are the measured brake torque and friction torque, and V_{displ} is the displacement volume of the engine.

The particulate emissions were estimated from the Bosch smoke number, using a correlation developed by Alkidas [54].

$$P = 24.7(B_n) + 1.92(B_n)^3 \tag{4.3}$$

where B_n is the measured Bosch smoke number and P is the particulate concentration in gm/m^3 of the exhaust sample.

The measured exhaust temperature and the exhaust nitric oxide level, are in suitable forms for direct comparison with model predictions of corresponding parameters.

The data collected by following the procedure described in this chapter are used for comparison with model predictions. A detailed comparative study and discussions of the model predictions with actual test data are undertaken in the next chapter.

5. RESULTS AND DISCUSSION

In this chapter predictions of the multizone model are compared with experimental data. The engine behavior under various operating conditions and the predictions of the multizone model are discussed in detail.

This chapter is divided into three main sections. The first section describes the capabilities of the present multizone model, the procedure used to calculate the parameters that were compared against the experimental data, and the details on how one particular parameter, the exhaust temperature, was calculated from the model results. Details of the test data and comparison of the model predictions with the actual test data are described in the second section. The third section is a discussion of the positive and negative aspects of the present multizone model.

5.1 Capabilites of the Multizone Model

The present multizone model is capable of predicting the in-cylinder pressure, bulk temperature, and nitric oxide concentration over the combustion and expansion phases of the engine cycle. The intake and compression phases of the cycle are modeled using a single zone consisting of air, alcohol and water vapor. The exhaust process is modeled as a sudden expansion of the cylinder contents to the measured back pressure when the exhaust valve opens. The sub-models for intake and compres-

sion phases, and the exhaust phase are combined with the present multizone model to simulate the complete engine cycle.

The cylinder pressure data predicted by the model at a typical engine operating condition of 1500 rpm, full load, with 30% of the torque supplied by fumigating 140 proof ethanol is shown in Figure 5.1. The model-predicted peak pressure for this operating condition is 13.54 MPa, at 7.5 degrees after top-dead- center (TDC). The engine was not instrumented for cylinder pressure measurements, hence the model-predicted pressure curves could not be directly compared with the experimental values. However, a pressure-volume curve was obtained from the predicted pressure-crank angle data and is shown in Figure 5.2. The area enclosed by this pressure-volume curve divided by the displacement volume of the cylinder represents the indicated mean effective pressure (IMEP). For the specified operating condition, the experimentally determined IMEP based on measured brake torque and friction torque is 1041 kPa, and the model predicted value is 1082 kPa.

The indicated thermal efficiency ($\eta_{th,ind}$) is a second parameter used for comparing model predictions with actual test data. As detailed in Chapter 4, the experimental value of the indicated thermal efficiency is given by the ratio of the sum of the brake power and friction power, to the net rate at which energy is supplied to the engine by both diesel fuel and alcohol. The IMEP value predicted by the model is used to calculate the model-predicted value of the indicated thermal efficiency. For the test case under consideration, the $\eta_{th,ind}$ calculated from measured data is 45.4%, and the corresponding model-predicted value is 47.2%.

The model prediction of exhaust temperature is calculated using a two-step pro-

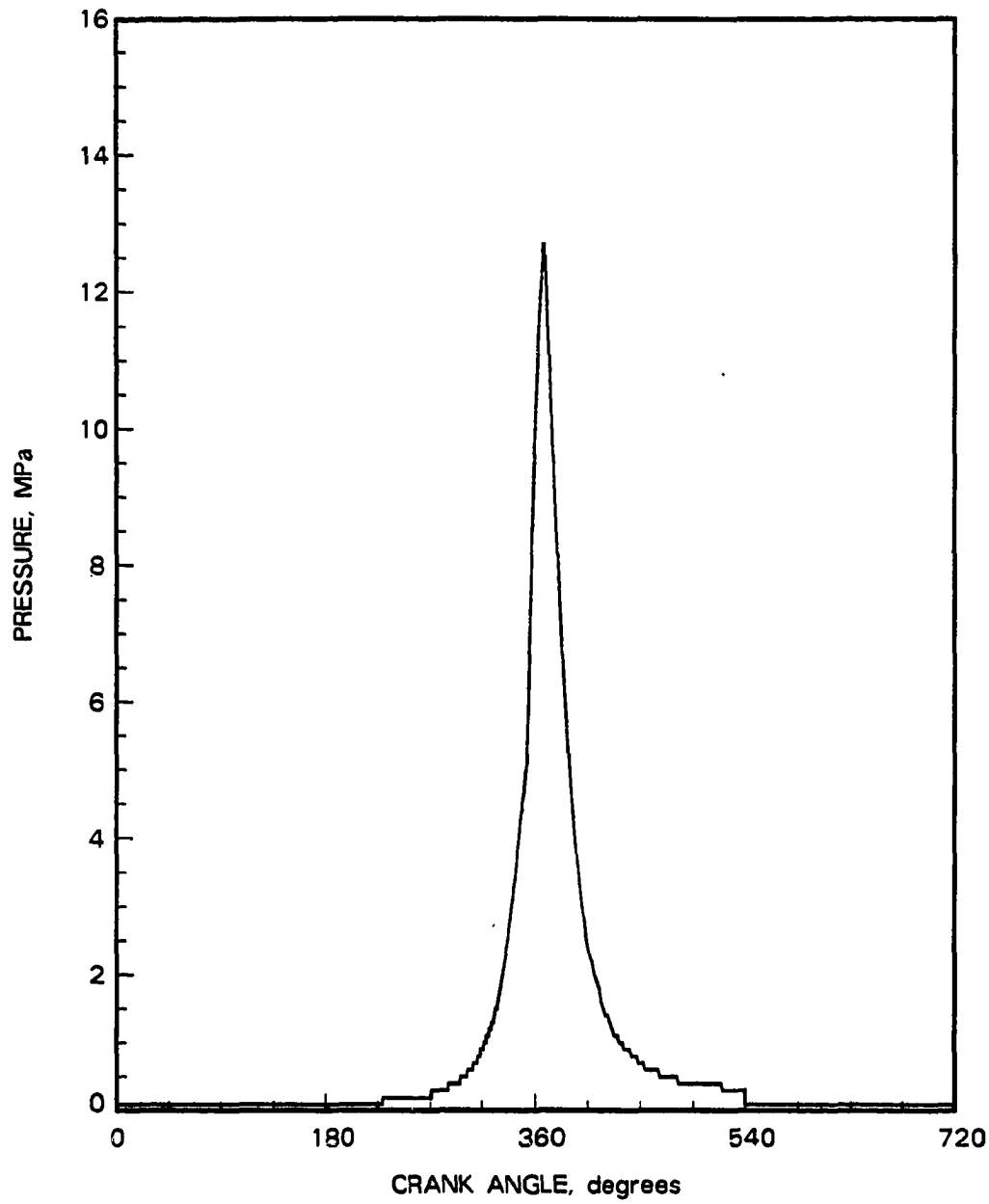

Figure 5.1: Model-predicted Pressure versus Crank Angle, at 1500 rpm, 100% Load, 30% Torque supplied by 140 Proof Ethanol

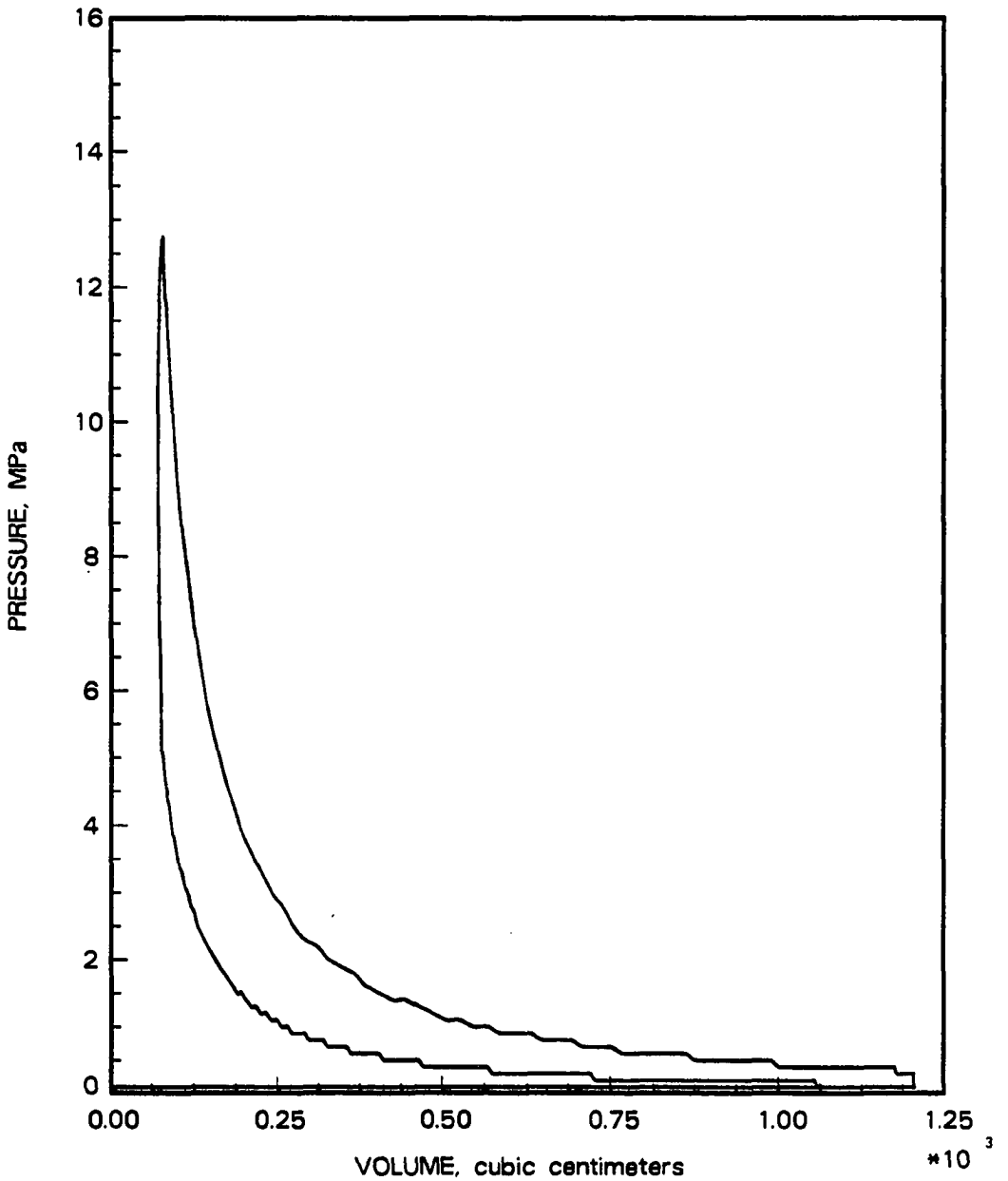

Figure 5.2: Model-predicted Pressure versus Volume, at 1500 rpm, 100% Load, 30% Torque supplied by 140 Proof Ethanol

cedure discussed in Section 5.1.1. For the case described above, the measured exhaust temperature was 737 K and the model-predicted exhaust temperature is 756 K.

The variation of in-cylinder nitric oxide concentration with crank position for the specified engine operating condition is shown in Figure 5.3. The engine test was not designed to record the in-cylinder NO concentration, hence, only measured exhaust concentrations of NO can be used to validate the model. The measured exhaust nitric oxide for this test was 2048 ppm, and the corresponding model-predicted value is 1737 ppm.

The capabilites of the present multizone model, and the procedure used to compare the model predictions with actual test data have been discussed in this section using the results from a typical case. The calculation procedure used to determine the bulk exhaust temperature from the model data is described in the following subsection.

5.1.1 Model-predicted exhaust temperature

In the engine tests, the exhaust temperature before the turbocharger was measured using two thermocouples. The exhaust gas from the first two cylinders was measured using one thermocouple, and a second thermocouple was used to measure the temperature of exhaust gas from cylinders three and four. The arithmetic average of these two temperatures was used as the bulk exhaust temperature.

Although the combustion and expansion strokes are simulated in the present multizone model, the exhaust phase is not modeled in detail. The valve lift profile supplied by the engine manufacturer indicates that the exhaust valve begins to open

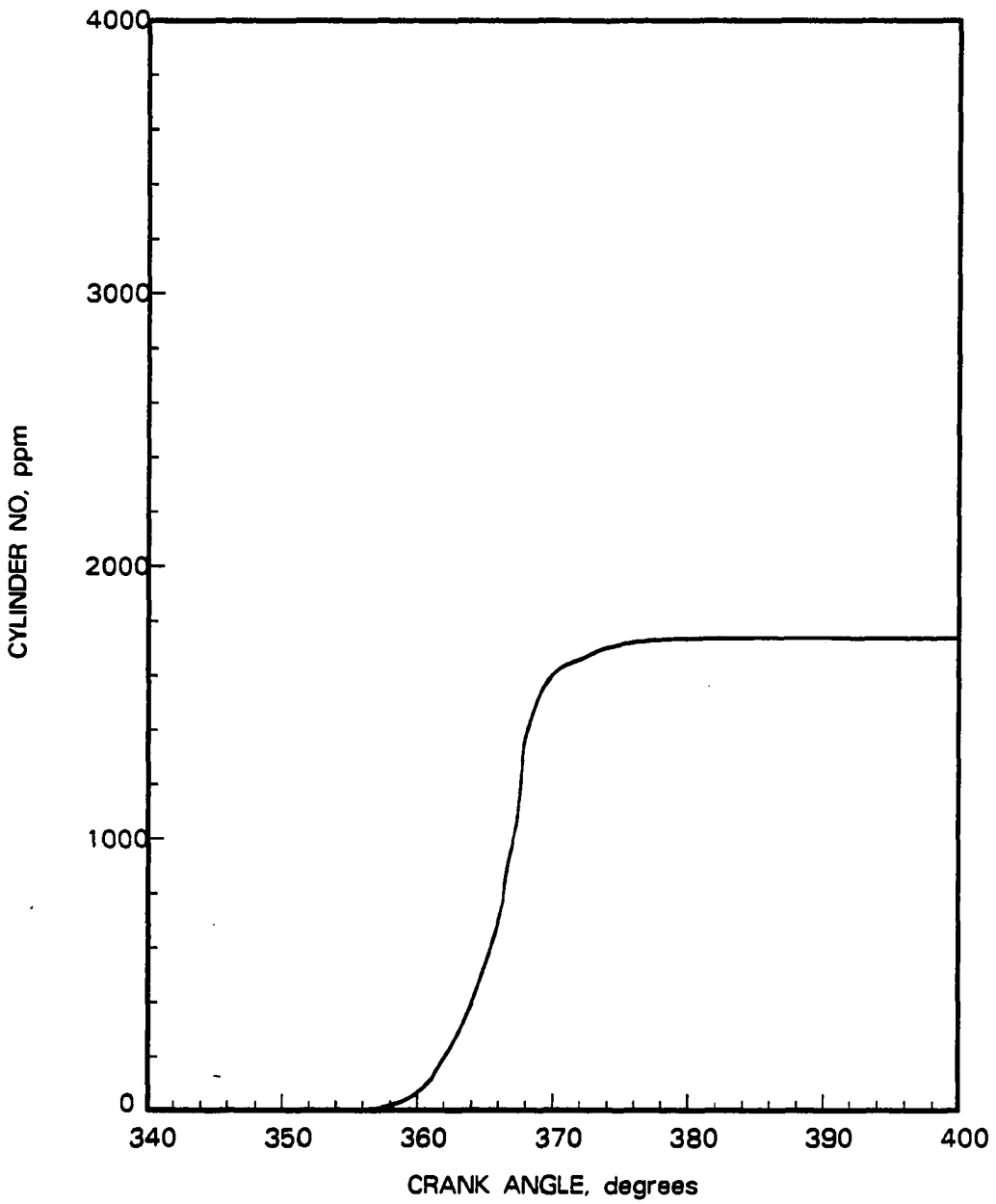

Figure 5.3: Model-predicted Nitric Oxide versus Crank Angle, at 1500 rpm, 100% Load, 30% Torque supplied by 140 Proof Ethanol

at 56 degrees before bottom dead center on the expansion stroke.

In the model, at the crank position corresponding to exhaust valve opening, the cylinder typically contains two zones, zone A and zone D. The bulk cylinder temperature at this crank position is calculated by combining the cylinder volume constraint and the ideal gas equation for the two zones.

$$T_{1,cyl} = \frac{m_{1,A}{}^{C'}v_{1,A}T_{1,A} + m_{1,C'}{}^{C'}v_{1,C'}T_{1,C'}}{m_{1,A}{}^{C'}v_{1,A} + m_{1,C'}{}^{C'}v_{1,C'}} \tag{5.1}$$

where

$T_{1,cyl}$ = bulk cylinder temperature at exhaust valve opening

$m_{1,A}$ = mass of contents in zone A, at exhaust valve opening

$R_{1,A}$ = specific gas constant of the contents in zone A, at exhaust valve opening

$T_{1,A}$ = temperature of zone A, at exhaust valve opening

$m_{1,C'}$ = mass of contents in zone C, at exhaust valve opening

$R_{1,C'}$ = specific gas constant of the contents in zone C, at exhaust valve opening

$T_{1,C'}$ = temperature of zone C, at exhaust valve opening

The exhaust temperature is estimated using a two-step process, comprised of a blowdown process and an exhaust process. The blowdown process assumes instantaneous mass transfer through the valve until the cylinder pressure is reduced to the measured back pressure. The process is assumed to be isentropic for the gases in the cylinder, since it is instantaneous and there is no time for heat transfer. The gases leaving the cylinder are assumed to undergo a constant enthalpy throttling process. The exhaust process models the piston movement forcing the gases from the cylinder

into the exhaust manifold at constant pressure. The gases entering the manifold are assumed to push any previously existing gases ahead, without mixing, as if a flexible diaphragm existed separating the exhaust from successive cycles.

Knowing the initial cylinder pressure at exhaust valve opening, $p_{1,cyl}$, the initial bulk cylinder temperature, $T_{1,cyl}$, and the back pressure, p_{back}, the intermediate temperature of the cylinder contents at the end of blowdown, $T_{2,cyl}$, is given by

$$T_{2,cyl} = T_{1,cyl}\left(\frac{p_{back}}{p_{1,cyl}}\right)^{\frac{k-1}{k}} \tag{5.2}$$

where k is the ratio of specific heats at the crank position corresponding to exhaust valve opening. The specific heats for the bulk cylinder contents are obtained using a mass weighted average of the specific heats for zone D and zone A. The intermediate mass of the cylinder contents, $m_{2,cyl}$, at the end of blowdown is calculated using p_{back} and $T_{2,cyl}$ in the ideal gas equation. The intermediate mass of the gases in the exhaust manifold, $m_{2,man}$, is given by

$$m_{2,man} = m_{1,cyl} - m_{2,cyl} \tag{5.3}$$

The intermediate temperature of the contents in the manifold is calculated by applying the first law energy equation for the control volume comprised of the cylinder and the manifold. The heat transfer term in the energy equation is dropped, since the blowdown process is considered isentropic, and the work term is the product of the back pressure and the change in the volume occupied by the cylinder gases in the manifold.

$$\left[m_{2,cyl}u_{2,cyl} + m_{2,man}u_{2,man}\right] \quad - \quad m_{1,cyl}u_{1,cyl}$$

$$= -W_{cyl}$$

$$= p_{back}(V_{2,man} - V_{1,man}) \qquad (5.4)$$

where

$m_{2,cyl}$ = mass of cylinder contents at the end of blowdown

$u_{2,cyl}$ = specific internal energy of the cylinder contents at the end of blow down

$m_{2,man}$ = mass of gases in the manifold at the end of blowdown

$u_{2,man}$ = specific internal energy of gases in the manifold at the end of blowdown

$m_{1,cyl}$ = mass of cylinder contents at the beginning of blowdown

$u_{1,cyl}$ = specific internal energy of cylinder contents at the beginning of blowdown

W_{cyl} = work done by the cylinder in moving the exhaust gases into the manifold

p_{back} = measured back pressure, before the turbocharger turbine

$V_{2,man}$ = volume of gases contained in the manifold at the end of blowdown

$V_{1,man}$ = volume of gases contained in the manifold at the beginning of blowdown

Noting that the volume occupied by the incoming cylinder gases in the manifold prior to exhaust valve opening $V_{1,man}$ is zero, and that the product of pressure and volume, $p_{back}V_{2,man}$ can be replaced with the product $m_{2,man}R_{2,man}T_{2,man}$ from

the ideal gas equation, Equation 5.4 takes the form

$$m_{2,cyl}Cv_{2,cyl}(T_{2,cyl} - T_{1,cyl}) + m_{2,man}Cv_{2,man}(T_{2,man} - T_{1,man}) = -m_{2,man}R_{2,man}T_{2,man} \quad (5.5)$$

where

$T_{1,cyl}$ = temperature of cylinder gases at exhaust valve opening

$T_{2,cyl}$ = temperature of cylinder gases at the end of blowdown

$T_{2,man}$ = temperature of the gases in the exhaust manifold, at the end of blowdown

$Cv_{2,man}$ = specific heat at constant volume, for the gases in the exhaust manifold, at the end of blowdown

$R_{2,man}$ = specific gas constant, for the gases in the exhaust manifold, at the end of blowdown

The value of $R_{2,man}$ and $Cv_{2,man}$ are functions of manifold pressure, manifold temperature, and the overall composition of the cylinder contents. The value of $T_{2,man}$ is determined by an iterative process.

In the second step, the remaining cylinder contents are transfered to the exhaust manifold at a constant pressure corresponding to the measured back pressure. These incoming gases are assumed to mix perfectly with the gases exhausted during step one. The first law energy equation is used to solve for the final temperature of the gases in the exhaust manifold. The process is assumed adiabatic, so the heat transfer term is set equal to zero.

$$m_{3,man}u_{3,man} - \left[m_{2,cyl}u_{2,cyl} + m_{2,man}u_{2,man}\right]$$

$$= -\left[p_{back}(V_{3,cyl} - V_{2,cyl}) + p_{back}(V_{3,man} - V_{2,man})\right] \qquad (5.6)$$

where

$m_{3,man}$ = mass of gases in the manifold at the end of exhaust

$u_{3,man}$ = specific internal energy of gases in the manifold at the end of exhaust

$m_{2,cyl}$ = mass of cylinder contents at the end of blowdown

$u_{2,cyl}$ = specific internal energy of the cylinder contents at the end of blow down

$m_{2,man}$ = mass of gases in the manifold at the end of blowdown

$u_{2,man}$ = specific internal energy of gases in the manifold at the end of blowdown

p_{back} = measured back pressure, before the turbocharger turbine

$V_{3,cyl}$ = volume of gases contained in the cylinder at the end of exhaust

$V_{2,cyl}$ = volume of gases contained in the cylinder at the end of blowdown

$V_{3,man}$ = volume of gases contained in the manifold at the end of exhaust

$V_{2,man}$ = volume of gases contained in the manifold at the end of blowdown

Combining Equation 5.6 with the law of mass conservation and the ideal gas equation.

and eliminating $C'p$ using, $C'p = C'v + R$, the following equation results

$$\begin{aligned} m_{2,cyl}T_{3,man} &- m_{2,cyl}T_{2,cyl} + m_{2,man}T_{3,man} \\ &- m_{2,man}T_{2,man} = 0 \end{aligned} \tag{5.7}$$

The final manifold temperature, $T_{3,man}$ is the only unknown in the above equation and can be solved for explicitly. This temperature is assumed to be the exhaust temperature before the turbocharger. A subroutine named TEXH is used to calculate the exhaust temperature for each test case.

The measured test data are presented in the next section and compared to the predictions of the multizone model.

5.2 Comparison of Experimental Results and Model Predictions

This section describes the data obtained from fumigation experiments and the corresponding model predictions. Possible reasons for specific engine behavior are stated. This section is divided into five subsections: the effect of speed and load, the effect of torque replacement with fumigated alcohol, the effect of alcohol proof, comparison of ethanol and methanol, and the effect of water injection. In this study, data on the indicated mean effective pressure, indicated thermal efficiency, exhaust temperature, and the concentration of exhaust nitric oxide are of prime concern. Although the concentration of other pollutants such as carbon monoxide (CO), unburned hydrocarbons (HC), and the exhaust smoke level were measured during the tests, the present multizone model is not capable of predicting these quantities. Detailed discussions of the effect of alcohol fumigation on the exhaust concentrations

of CO, HC, and smoke are published elsewhere [55]. General observations on these pollutants are presented in the appropriate subsections.

The present multizone model was used to simulate the performance and emission characteristics of the engine with both diesel-only and fumigated operation. Indicated mean effective pressure, indicated thermal efficiency, exhaust temperature, and exhaust nitric oxide emission were used as the parameters for comparing the model-predicted and measured values with experimental data.

The IMEP given by the model is used to determine the model predicted indicated thermal efficiency, $\eta_{th,ind}$. The IMEP is multiplied by the swept volume of the cylinder to obtain the indicated work done per cycle. The indicated work divided by the total energy supplied by both fuels, based on the measured flow rates of the fuels, gives the indicated thermal efficiency. The same value of the total energy supplied by the two fuels, is used to calculate the experimental indicated thermal efficiency. Since the model-predicted $\eta_{th,ind}$ is based on the corresponding IMEP value given by the model, the relative errors between the model-predicted values of IMEP and $\eta_{th,ind}$, have the same numerical value. Hence, in the tables showing comparisons between the model data and measured values of IMEP and $\eta_{th,ind}$, only one error value is given for each test condition.

For the engine simulations using the present multizone model, the diesel injection pressures were set at 25 MPa at 1500 rpm and 49 MPa at 2100 rpm. The start of injection was set at 15° before TDC, and the injection duration was assumed to be 15° for both 1500 and 2100 rpm. Due to the lack of actual test data from the engine, a constant injection rate was used for all the cases simulated.

5.2.1 Effect of speed and load

As previously mentioned, the engine was operated at two speeds, 1500 rpm and 2100 rpm, and four different loads, 25%, 50%, 75%, and 100% of the rated load at each of the two speeds. The IMEP and $\eta_{th,ind}$ data obtained with diesel-only operation at 1500 rpm and 2100 rpm, for four different load conditions are given in Table 5.1. Table 5.1 also lists the IMEP and $\eta_{th,ind}$ at 1500 rpm for three different loads when 30% of the brake torque was supplied by fumigated ethanol. Two different ethanol proofs, 80 proof and 169.5 proof were used at 100%, 75%, and 50% of full load. Corresponding data for 2100 rpm operation are also given in Table 5.1. The model predicted data and the errors in IMEP between actual test data and model predictions are also given in the table.

For the diesel-only cases listed in Table 5.1, the IMEP decreases with load as expected. The fuel input is decreased at lower loads, resulting in lower cylinder pressure during the combustion and expansion phases of the cycle and hence, lower IMEP. This trend is observed at both 1500 and 2100 rpm. The measured indicated thermal efficiency decreases as the load increases. This is due to an extended duration of combustion at heavier loads as the additional fuel is injected later and takes longer to mix with the air. The late burning fuel has a lower effective expansion ratio that decreases the work output, resulting in lower thermal efficiency.

The model-predicted values of IMEP and $\eta_{th,ind}$ for diesel-only operation were from 1.0% higher to 10.6% lower than the actual test data. General trends in the changes in IMEP with load were well predicted by the model. However, the model-predicted values of indicated thermal efficiency did not show the decrease with in-

Table 5.1: Effect of Speed (1500 rpm and 2100 rpm) and Load (25%, 50%, 75% and 100% of full load) on IMEP and $\eta_{th,ind}$ for Diesel-only and Alcohol Fumigation (30% Torque Replacement from 80 Proof and 169.5 Proof Ethanol)

Speed	Load, %	Ethanol Proof	IMEP, kPa		$\eta_{th,ind}$, %		% Error
			Expt.	Model	Expt.	Model	
1500	100	-	1041	1046	45.6	45.9	0.5
	75	-	835	825	46.3	45.7	-1.2
	50	-	627	592	49.1	46.3	-5.6
	25	-	426	382	50.3	45.1	-10.4
2100	100	-	964	974	46.1	46.6	1.0
	75	-	801	794	47.2	46.8	-0.9
	50	-	622	610	47.5	46.6	-2.0
	25	-	442	395	50.6	45.3	-10.6
1500	100	80	1039	1101	45.8	48.6	6.0
	75	80	839	856	47.3	48.3	2.0
	50	80	620	633	47.5	48.5	2.1
1500	100	169.5	1037	1056	46.0	46.9	1.9
	75	169.5	833	826	46.9	46.5	-0.9
	50	169.5	629	603	48.7	46.7	-4.1
2100	100	80	961	1017	46.4	49.1	5.9
	75	80	803	849	46.2	48.9	5.7
	50	80	619	638	46.9	48.5	3.1
2100	100	169.5	972	977	46.7	47.0	0.6
	75	169.5	800	800	47.1	47.1	0.0
	50	169.5	618	611	47.5	47.0	-1.1

creasing load shown by the experimental data. Reasons for inconsistencies in the model-predicted trends for thermal efficiency are discussed in Section 5.3.2.

The highest discrepancy between model-predicted IMEP and $\eta_{th,ind}$, and the measured data is observed at 25% of full load, for diesel-only operation. The model-predicted values are lower by about 10%. The reason for such poor agreement may be due to inaccurate friction torque measured by the hot motoring test.

No significant change in the measured thermal efficiency was observed with alcohol fumigation. The data tabulated in Table 5.1 for 80 proof and 169.5 proof ethanol at 1500 rpm, show that the thermal efficiency is essentially the same for the two proof levels.

The experimental data for the fumigated 2100 rpm case given in Table 5.1 indicates no significant change in the thermal efficiency with load. The measured thermal efficiency values at the three loads with alcohol fumigation were nearly equal to the corresponding values obtained with diesel fuel only. The variation in the proof of alcohol had no significant effect on the measured indicated thermal efficiencies at all three loads. Theoretically, alcohol fumigation can cause longer ignition delays and delayed combustion, resulting in slightly lower thermal efficiencies. However, the delayed ignition can also result in a larger amount of rapid premixed burning producing a faster average burning rate and a larger fraction of the fuel burning closer to top-dead-center [10]. An increase in engine efficiency with ethanol fumigation has been observed by other researchers [56, 57].

Figure 5.4 shows the effect of load on measured exhaust temperature, at both 1500 rpm and 2100 rpm, for diesel-only operation. The exhaust temperature increases

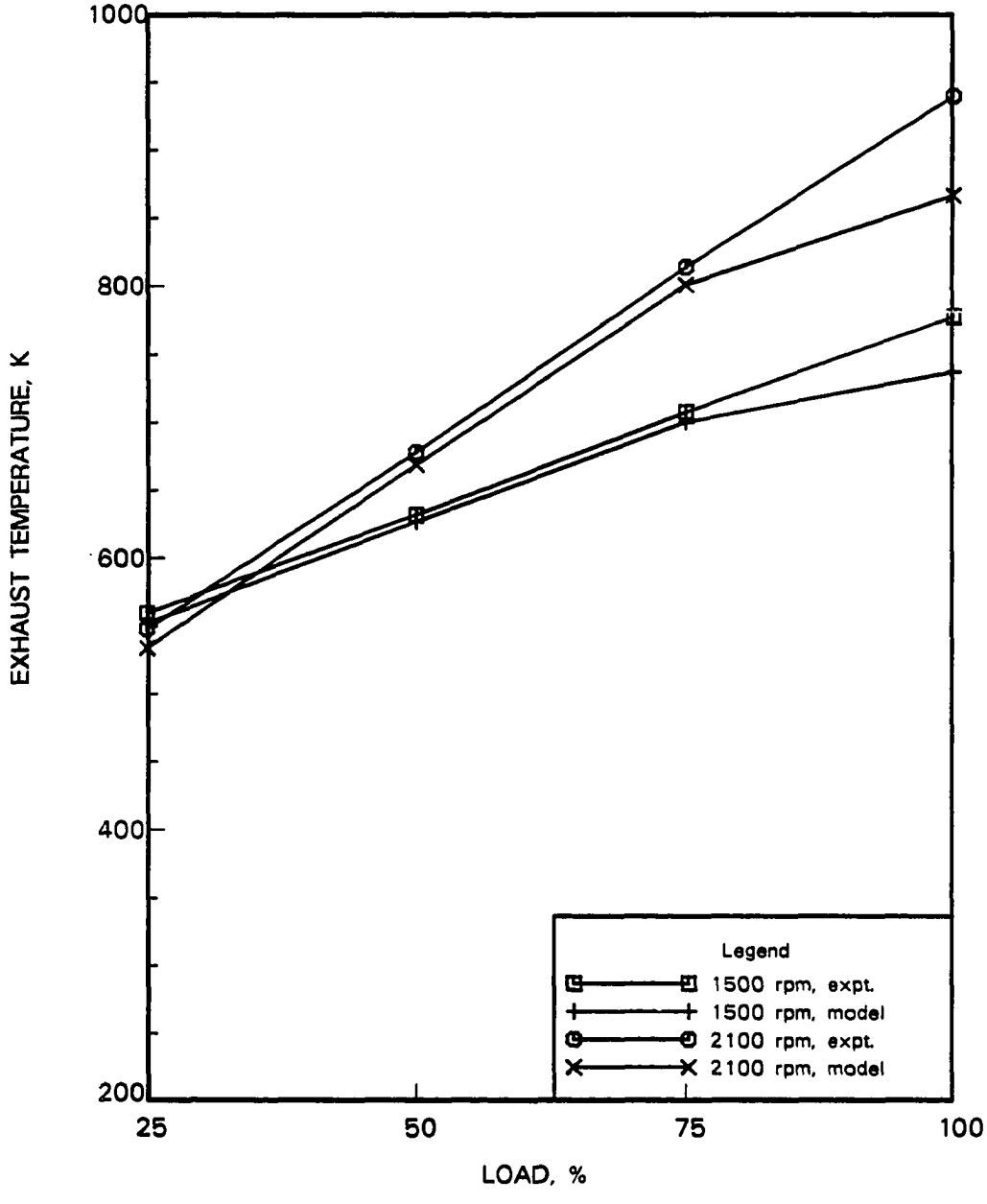

Figure 5.4: Exhaust Temperature versus Load, Diesel-only

with load, due to more fuel being burned at higher loads and the higher equivalence ratio. At 2100 rpm, the exhaust temperature is consistently higher for the four loads shown. At higher speeds, there is less time for heat transfer, and combustion extends later into the expansion stroke, resulting in a higher exhaust temperature.

Figure 5.4 also shows the variation of model-predicted exhaust temperatures with load. The model-predicted exhaust temperature is from 1.1% to 5.8% higher than the measured values. The model predicts lower exhaust temperatures with decreasing load and is in agreement with the trend observed from measured exhaust temperatures. The exhaust temperature variations with load at 2100 rpm are also shown in Figure 5.4. Although the model predicts proper trends, the model-predicted exhaust temperature is from 1.6% to 7.7% lower than the measured values. The reasons for this difference in the model prediction is discussed in Section 5.3.3.

The effect of alcohol fumigation on exhaust temperature at 1500 rpm and 2100 rpm are shown in Figures 5.5 and Figure 5.6, respectively. Data for two different ethanol proofs, 80 proof and 169.5 proof are plotted at three load conditions: 100%, 75% and 50% of full load, with 30% of the torque supplied by the fumigated ethanol.

The exhaust temperatures with alcohol fumigation at both 1500 and 2100 rpm speed are lower than those with diesel-only operation. This trend was expected because of the lower flame temperatures caused by the mixture of alcohol and water entering the cylinder. It can also be seen that the exhaust temperature increased with higher alcohol proof. Higher proof alcohol contains less water, and hence the reduction in flame temperature may not be as pronounced as in the case of lower proof alcohol. These general trends were observed at other operating conditions with

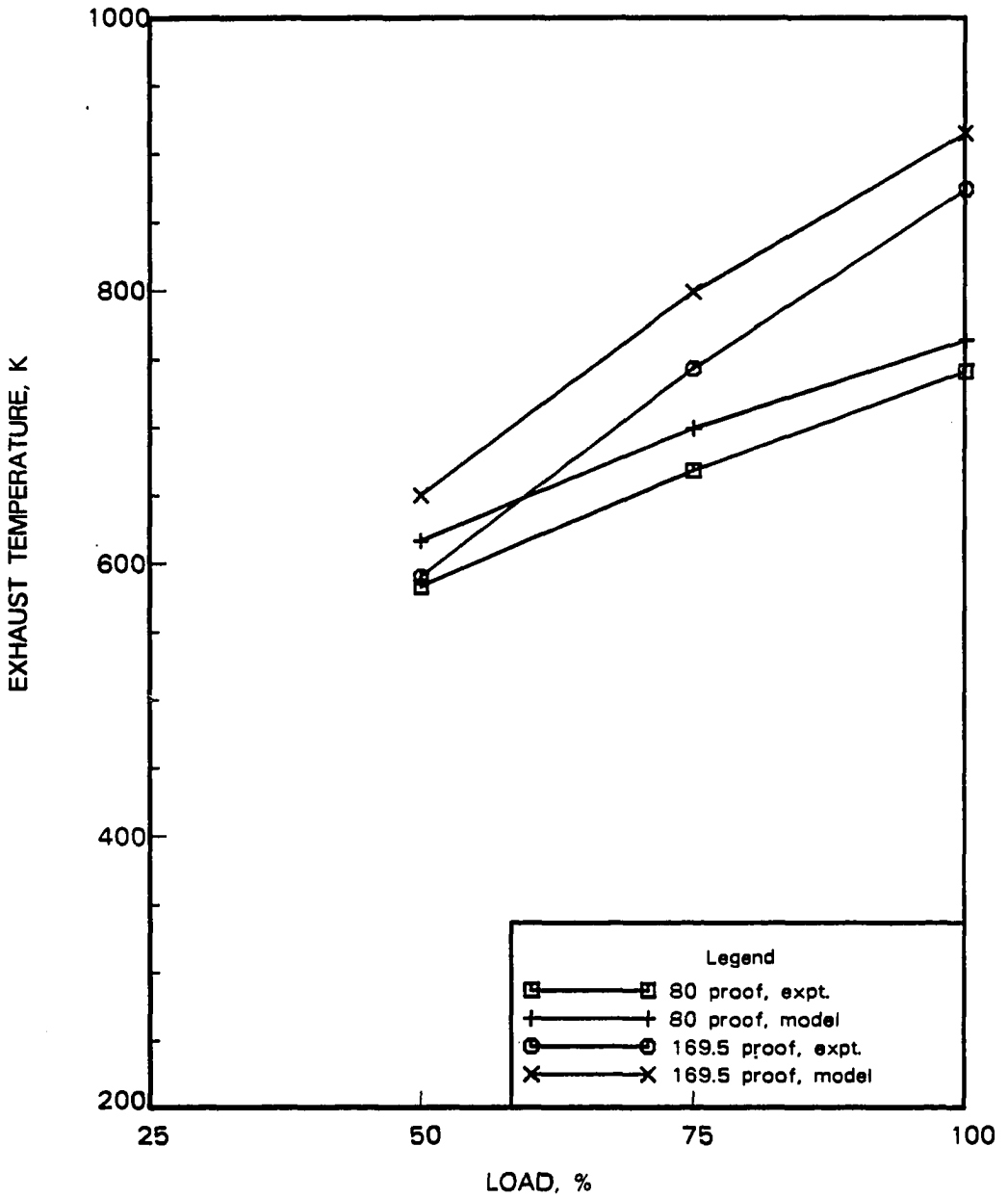

Figure 5.5: Exhaust Temperature versus Load, at 1500 rpm, 30% Torque supplied by Ethanol

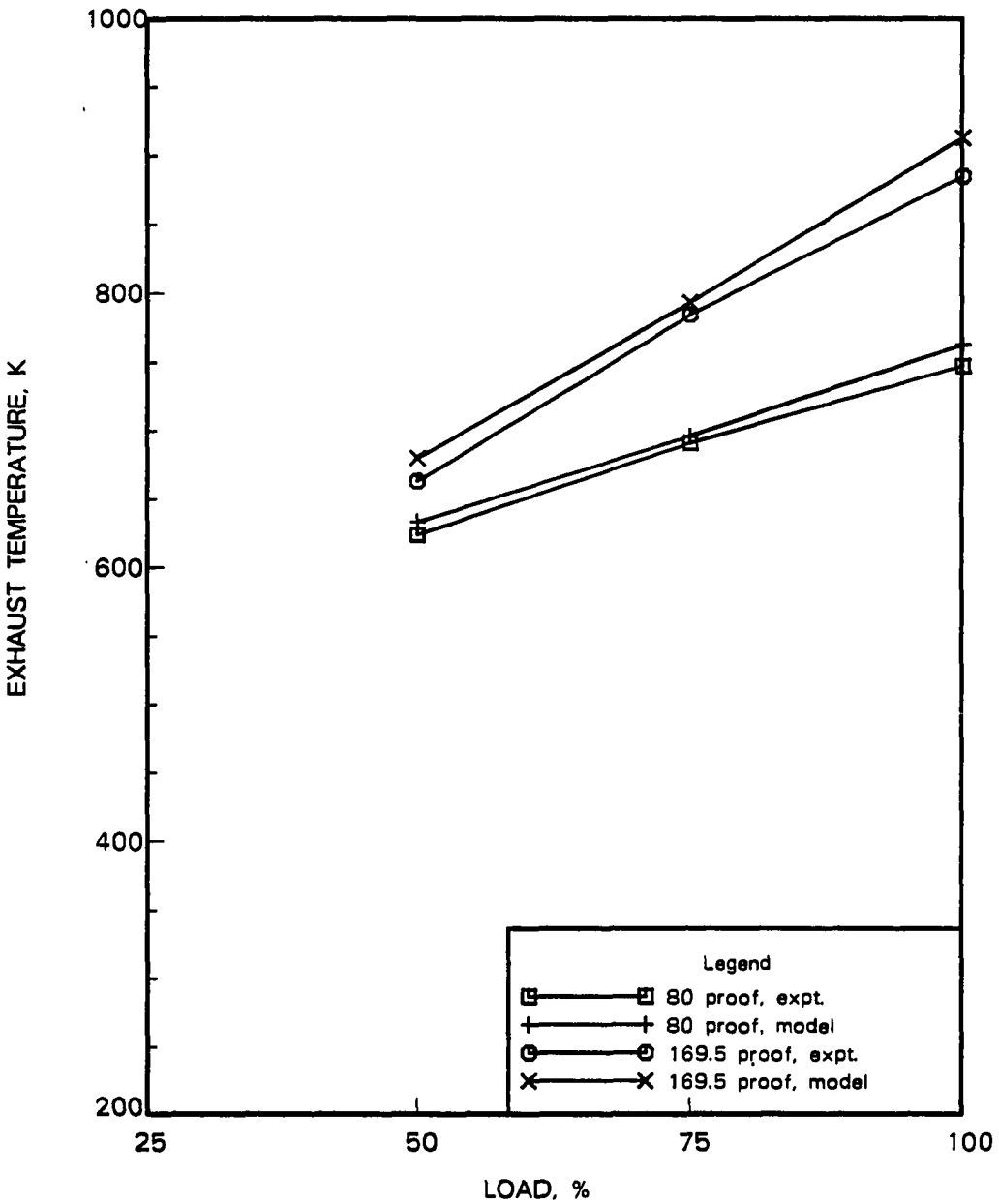

Figure 5.6: Exhaust Temperature versus Load, at 2100 rpm, 30% Torque supplied by Ethanol

alcohol fumigation, as well. The model-predicted exhaust temperature is from 5.7% lower to 10.2% higher for the 1500 rpm case with ethanol fumigation, and 8.2% lower to 3.2% higher for the 2100 rpm case.

Figure 5.7 shows the exhaust nitric oxide concentration at 1500 and 2100 rpm, under four different load conditions, for diesel-only operation. The NO emission increases with increasing load. This is because of lower bulk cylinder temperature at part loads, and the strong dependence of NO formation on temperature.

Figure 5.8 and Figure 5.9 are plots of exhaust NO versus load for 30% torque replacement with fumigated ethanol at 1500 rpm and 2100 rpm. Three different loads: 100%, 75%, and 50% of full load were tested. Data for two different ethanol proofs, 80 proof and 169.5 proof, are plotted in these figures.

As in the case of diesel-only operation, the measured NO concentrations decreased with load for alcohol fumigation. The measured NO concentration increased with proof; the NO level measured at 169.5 proof is higher than that at 80 proof. The higher amount of water in the 80 proof ethanol causes a larger decrease in the flame temperature, resulting in lower exhaust NO concentration. Similar trends of NO emission were observed at both 1500 and 2100 rpm operation.

Exhaust NO emission data predicted by the model for diesel-only operation is also shown in Figure 5.7. Proper trends in NO emission with variations in the load are predicted at both 1500 and 2100 rpm. The model-predicted NO concentrations are from 15% lower to 89% higher than the measured values at 1500 rpm. At 2100 rpm the model predicted NO concentrations are from 5% lower to 117% higher than the measured values. The reason for the large discrepancy in predicting NO is discussed

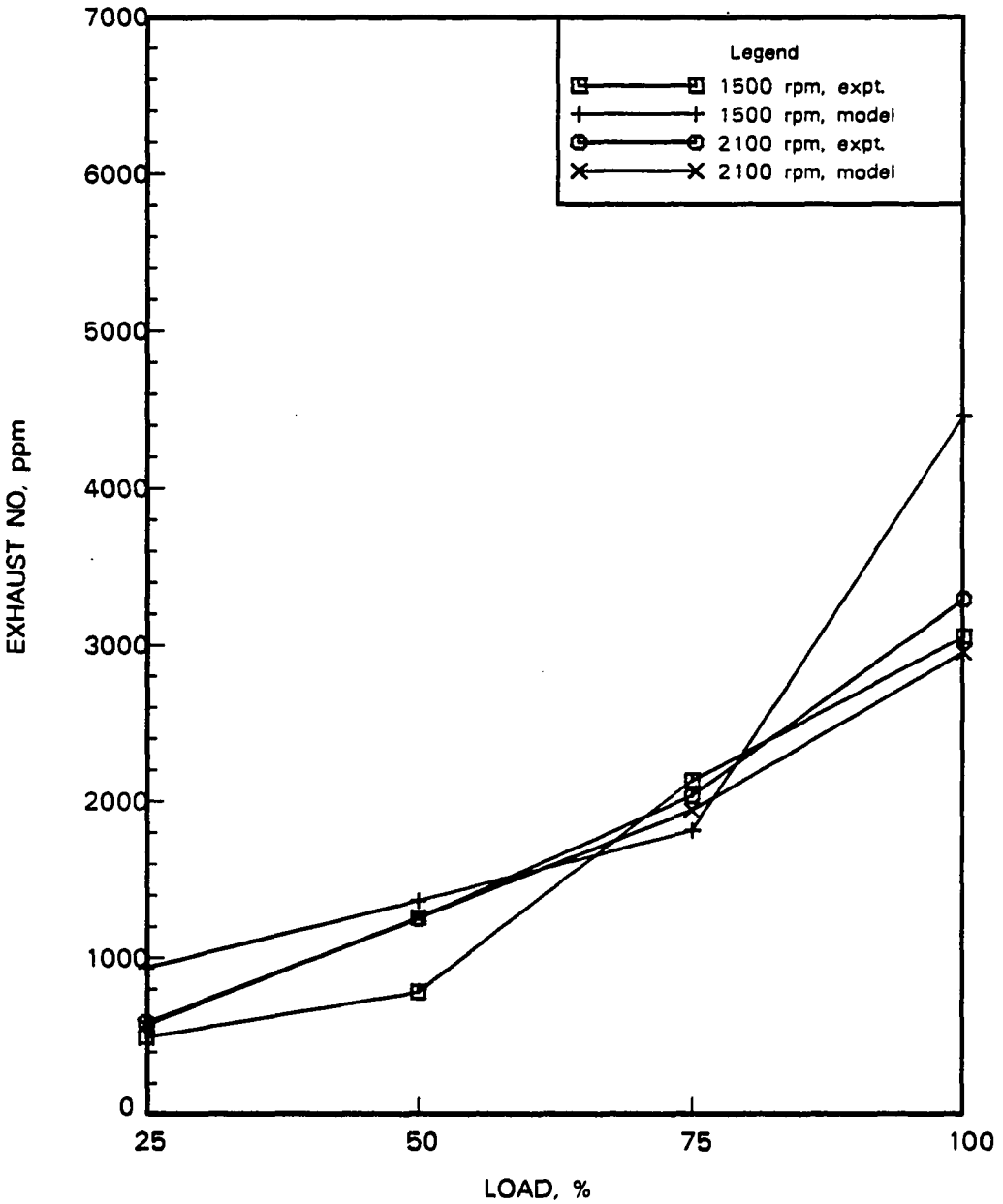

Figure 5.7: Exhaust *NO* Concentration versus Load, Diesel-only at 1500 and 2100 rpm

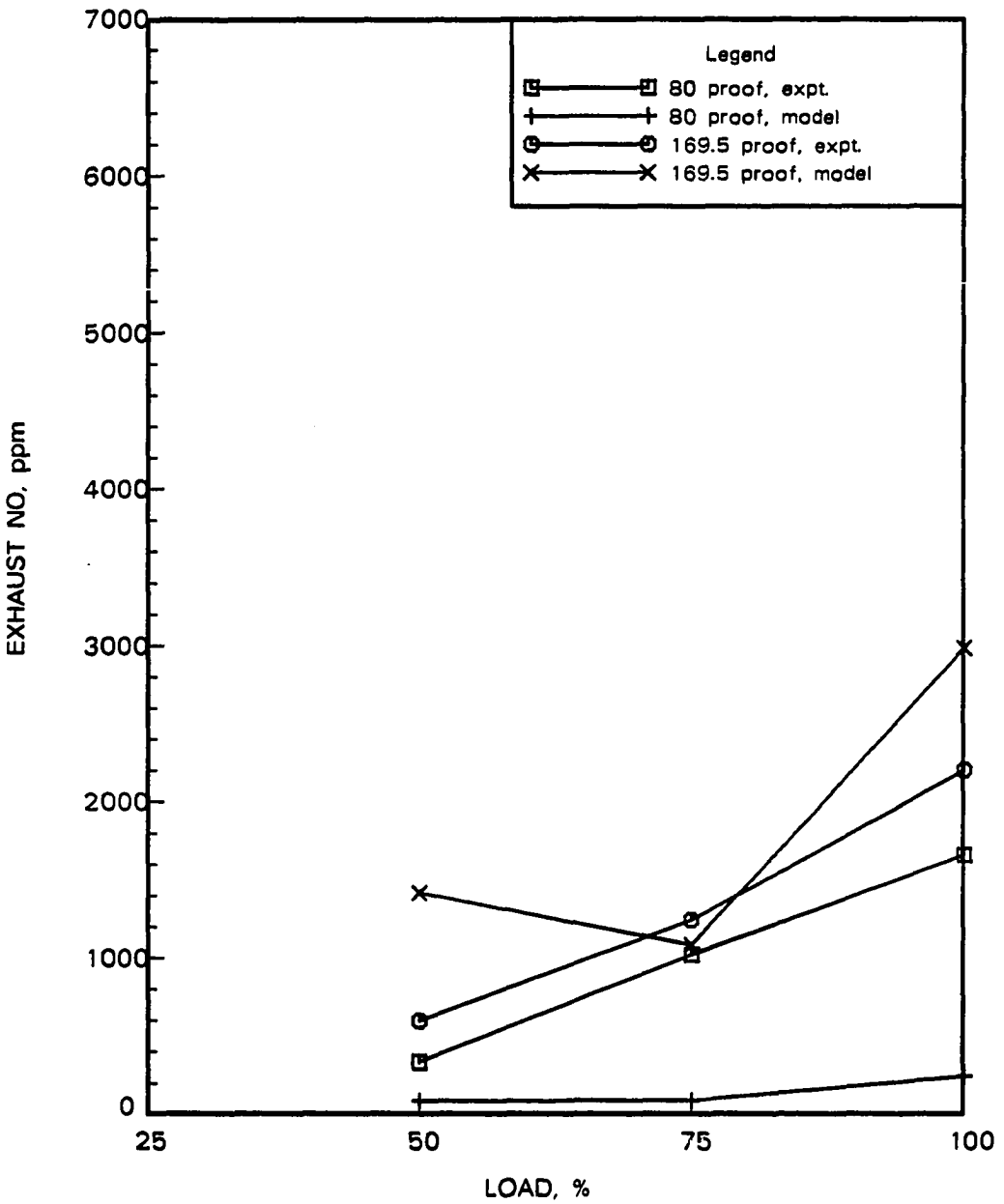

Figure 5.8: Exhaust NO Concentration versus Load, at 1500 rpm, 30% Torque supplied by Ethanol

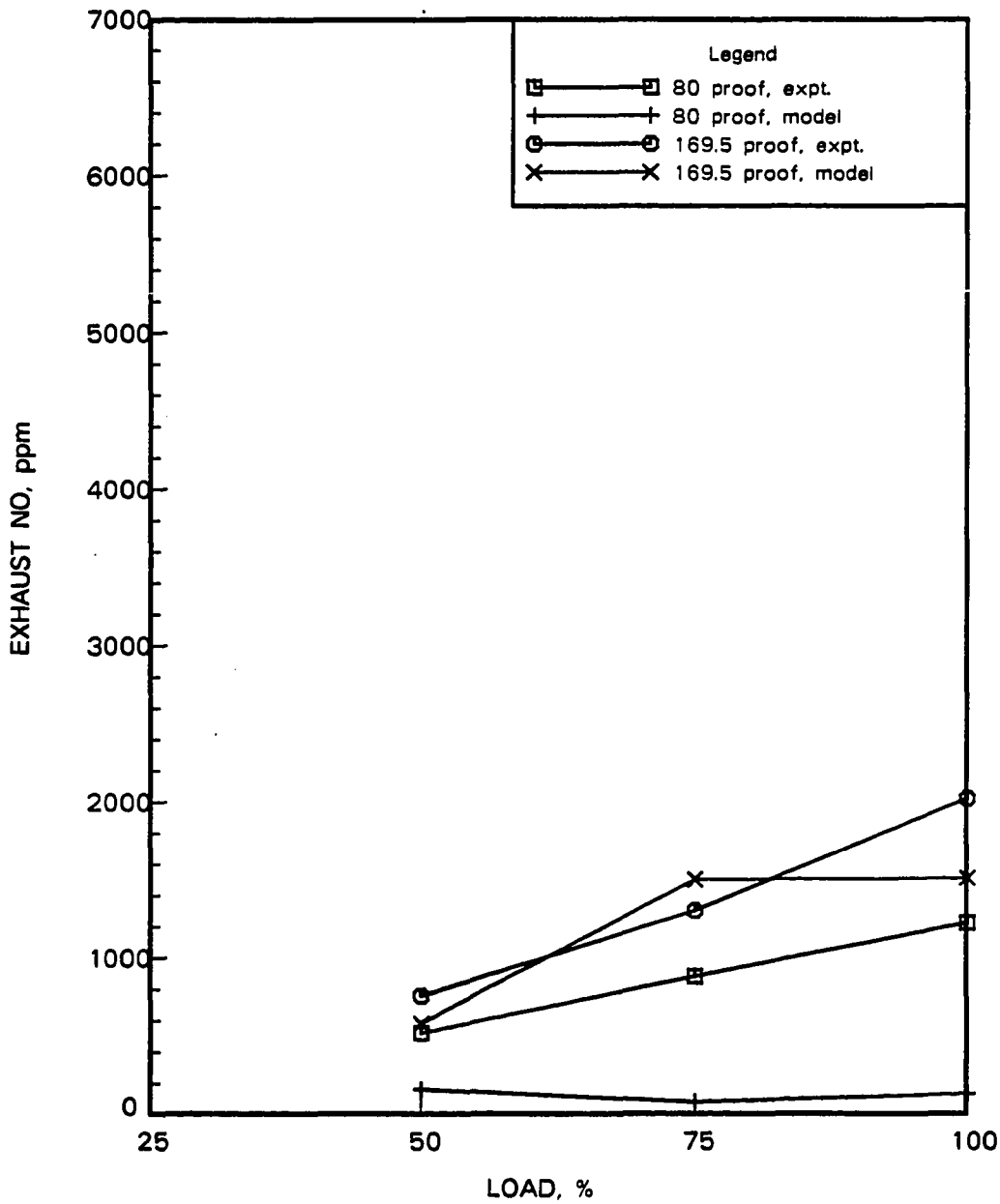

Figure 5.9: Exhaust NO Concentration versus Load, at 2100 rpm, 30% Torque supplied by Ethanol

in detail in Section 5.3.4. This result is not drastically different from that obtained by Chiu et al. [15] with a similar multizone spray model. The transient spray model of Chiu et al. predicted NO from 40% lower to 60% higher than measured values, as shown in Figure 5.10, reproduced from reference [15].

The model-predicted NO concentration is within 91% lower to 138% higher for the 1500 rpm case with ethanol fumigation, and 15% to 91% lower for the 2100 rpm case as shown in Figures 5.8 and 5.9.

The exhaust concentrations of carbon monoxide (CO), unburned hydrocarbons (HC), and exhaust smoke were also measured during the engine tests. With diesel-only operation, CO was nearly constant at 100%, 75%, and 50% of full load. but almost doubled at the 25% load condition, for both 1500 and 2100 rpm. At 1500 rpm. the exhaust HC increased slightly with load decrease, while at 2100 rpm exhaust HC level increased considerably at 50% and 25% of full load. The exhaust HC at 25% load at 2100 rpm was double its value at 100% load. Exhaust smoke decreased with load at 1500 rpm from 1.0 Bosch smoke number (BSN) at 100% load to 0.2 BSN at 25% load. The smoke level at 2100 rpm was 0.1 BSN at all the four different load conditions tested.

With alcohol fumigation CO and HC increased gradually with decreasing load, at both 1500 and 2100 rpm. Tests with both 80 proof and 169.5 proof confirmed this trend. With alcohol fumigation, the smoke level stayed at around 1.0 BSN for 100% load at 1500 rpm. At other operating conditions the smoke was around 0.1 to 0.5 BSN at both 1500 and 2100 rpm, and no significant variation in smoke level was observed with changing the proof of ethanol from 80 to 169.5 proof.

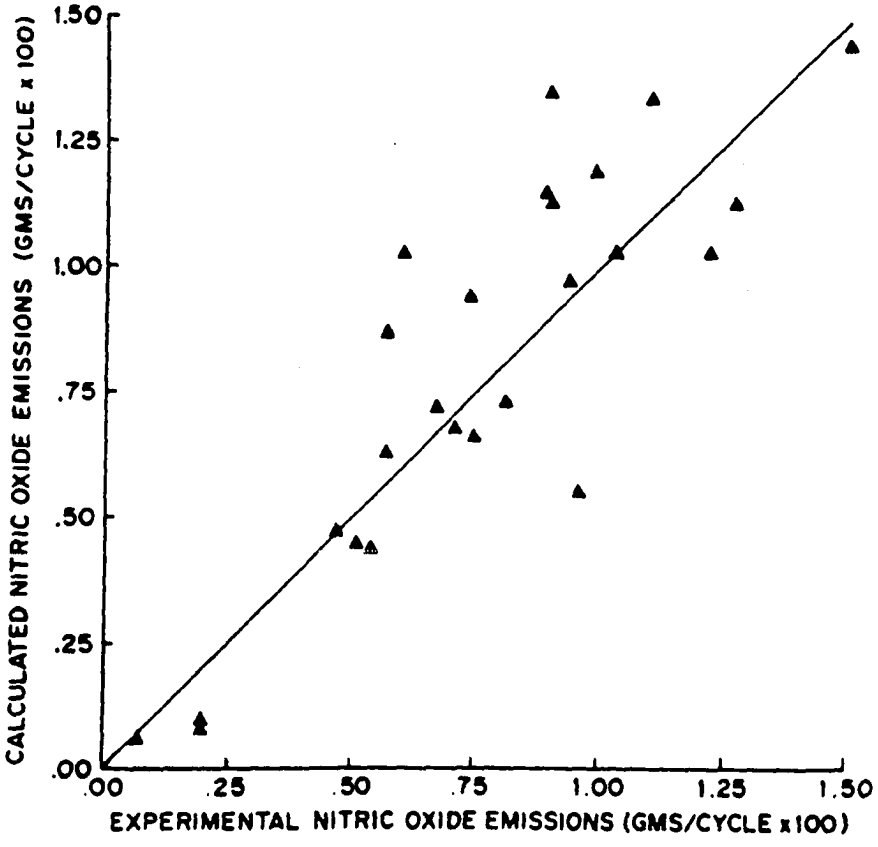

Figure 5.10: Comparison of Model-predicted and Measured Nitric Oxide Emissions (Reproduced from Chiu et al. [15])

5.2.2 Effect of percent torque replacement

The fraction of torque supplied by the mixture of alcohol and water was varied from 10% to 30%, in steps of 10%. To provide a general understanding of the effect of percent torque replacement on engine performance, torque supplied by the alcohol was varied at two different loads: 100% and 50% of full load. The tests were conducted at two speeds: 1500 and 2100 rpm. Test results with 80 and 169.5 proof ethanol will be described below.

The measured and model-predicted values of IMEP and $\eta_{th,ind}$ are given in Table 5.2. As explained earlier, the IMEP decreases with load, and the $\eta_{th,ind}$ decreases with increasing load. No discernible change in both IMEP and $\eta_{th,ind}$ was observed with increasing torque replacement by alcohol. Changes in ethanol proof, and engine speed did not result in significant changes in the trends of IMEP and $\eta_{th,ind}$.

The model data corresponding to a set of twenty one cases, simulated to study the effect of percent torque replacement with 80 proof and 169.5 proof ethanol, are also presented in Table 5.2. The IMEP values predicted by the model are from 5.7% lower to 6.5% higher than the experimental values.

Figure 5.11 is a plot of exhaust temperature versus torque replacement for 80 proof and 169.5 proof ethanol at 1500 rpm, 100% load operation. The exhaust temperature decreased with increased torque replacement. The amount of fumigated mixture of alcohol and water is increased when the percent torque replaced is increased, resulting in a higher water flow rate into the engine. The higher water flow rate reduces the flame temperature and a lower exhaust temperature results. The re-

Table 5.2: Effect of Percent Torque Replacement (10%, 20% and 30%) on IMEP and $\eta_{th,ind}$, at 1500 and 2100 rpm, with 80 Proof and 169.5 Proof Ethanol

Speed	Load %	%Torque From Alcohol	Alcohol Proof	IMEP, kPa		$\eta_{th,ind}$, %		% Error
				Expt.	Model	Expt.	Model	
1500	100	10	80	1041	1059	45.8	46.6	1.8
1500	100	20	80	1046	1091	46.1	48.1	4.3
1500	100	30	80	1039	1101	45.8	48.6	6.0
1500	100	10	169.5	1046	1052	45.8	46.1	0.5
1500	100	20	169.5	1048	1056	45.9	46.3	0.8
1500	100	30	169.5	1037	1056	46.0	46.9	1.8
1500	50	10	80	622	588	49.1	46.5	-5.4
1500	50	20	80	623	608	48.9	47.7	-2.4
1500	50	30	80	620	633	47.5	48.5	2.1
1500	50	10	169.5	622	589	49.0	46.4	-5.3
1500	50	20	169.5	623	588	49.3	46.6	-5.7
1500	50	30	169.5	629	603	48.7	46.7	-4.1
2100	100	10	80	968	1011	45.7	47.8	4.4
2100	100	20	80	968	1031	44.7	47.6	6.5
2100	100	30	80	961	1017	46.4	49.1	5.9
2100	50	10	80	621	610	47.8	47.0	-1.7
2100	50	20	80	622	616	47.6	47.0	-1.0
2100	50	30	80	619	638	46.9	48.5	3.1
2100	50	10	169.5	624	617	47.4	46.9	-1.2
2100	50	20	169.5	621	614	47.5	47.0	-1.1
2100	50	30	169.5	619	611	47.5	47.0	-1.2

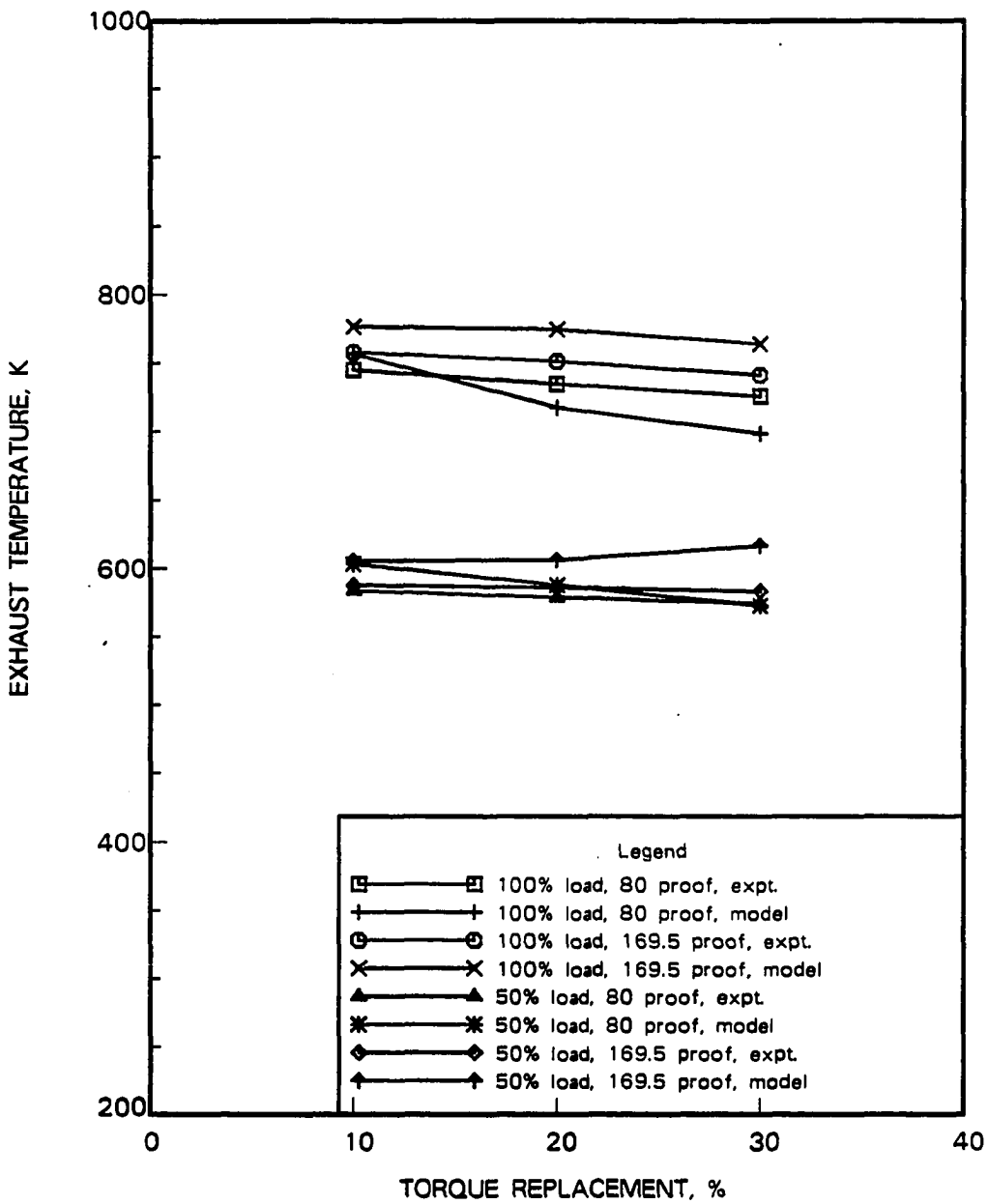

Figure 5.11: Exhaust Temperature versus Percent Torque Replacement from Ethanol at 1500 rpm

duction in measured exhaust temperature at 50% of full load with increasing torque replacement by 169.5 proof ethanol was quite small due to the low fraction of water in the fumigated mixture. Similar behavior was observed at an engine speed of 2100 rpm and the results are shown in Figure 5.12.

Figure 5.11 and Figure 5.12 also show the variation of model predicted exhaust temperature with increasing torque replacement. The model correctly predicts the reduction in exhaust temperature with increased percent torque replacement with alcohol. At 1500 rpm the model-predicted exhaust temperature is from 5.7% lower to 2.4% higher than the measured values. The model predictions of exhaust temperature at 2100 rpm are from 1.5% to 2.6% higher than the experimental values.

The variation of exhaust NO emission with percent torque replacement is plotted in Figures 5.13 and 5.14. The measured NO emission decreases with increasing torque replacement by the fumigated alcohol and water mixture. The increased flow rate of the alcohol and water mixture at higher torque replacement decreases the flame temperature in the cylinder gas, resulting in lower NO formation in the cylinder.

Figure 5.13 also shows the variation of model-predicted exhaust NO emission with increasing torque replacement by 80 proof ethanol at 1500 rpm and 100% load operation. The model predicts a reduction in NO emission with increasing percent torque replacement. However, the model overpredicts the magnitude of the reduction in NO emission, and is from 85% lower to 7% higher than the experimental values. Figure 5.14 shows that the model predictions of NO emission are within 23% lower to 36% higher than the experimental values. Under the conditions described above, the decrease in NO at higher torque replacements is overpredicted by the model, and

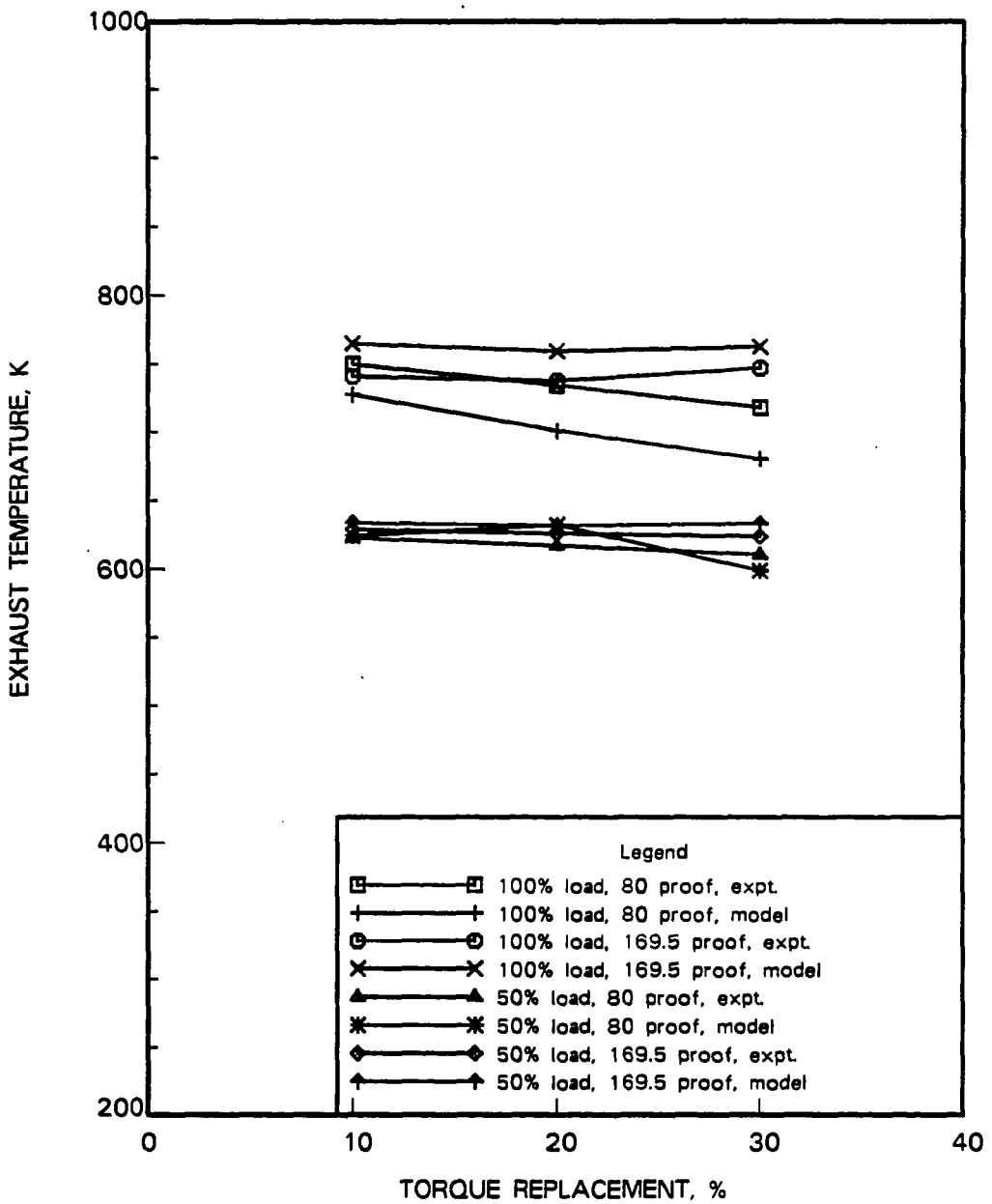

Figure 5.12: Exhaust Temperature versus Percent Torque Replacement from Ethanol at 2100 rpm

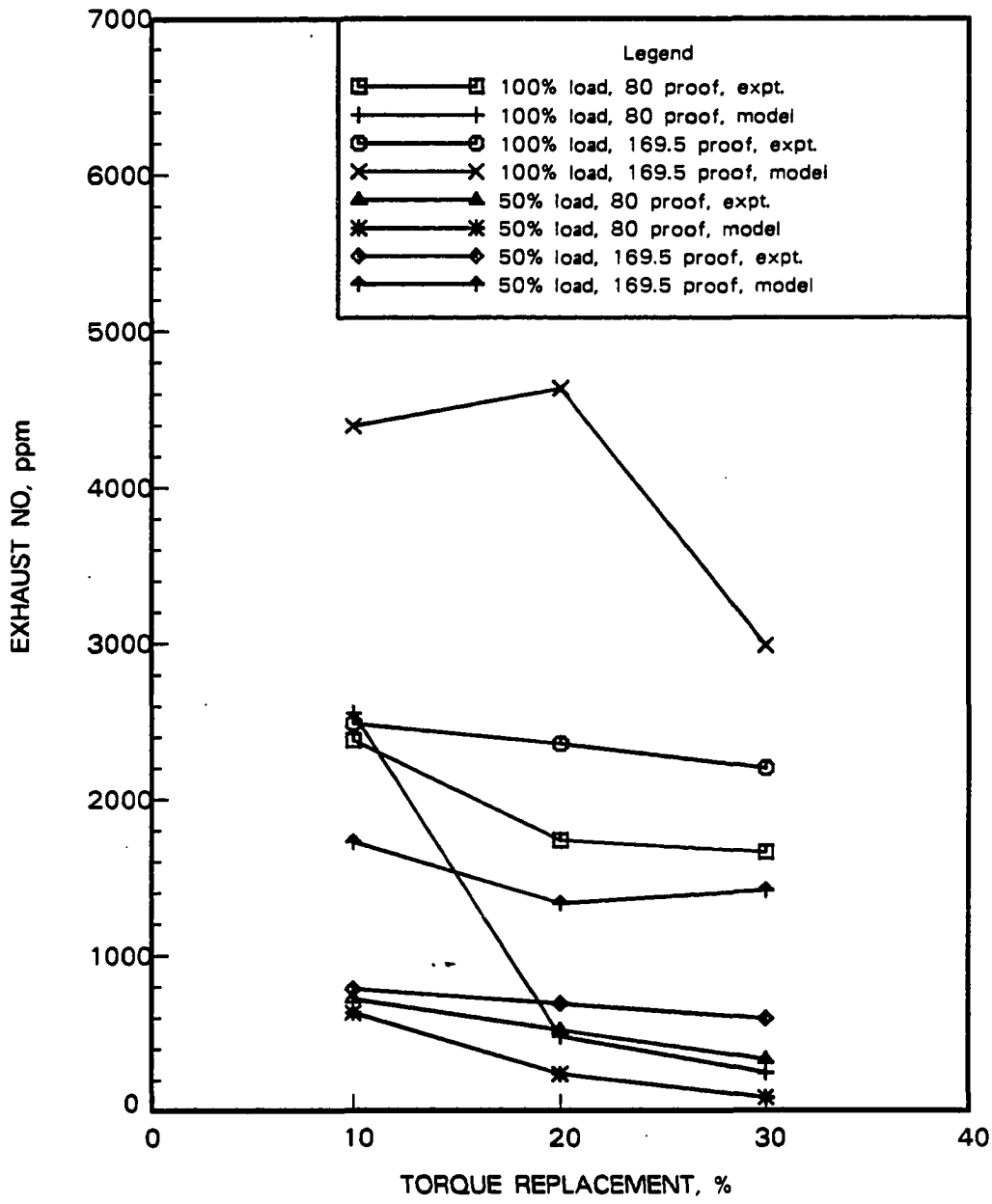

Figure 5.13: Exhaust NO Concentration versus Percent Torque Replacement from Ethanol at 1500 rpm

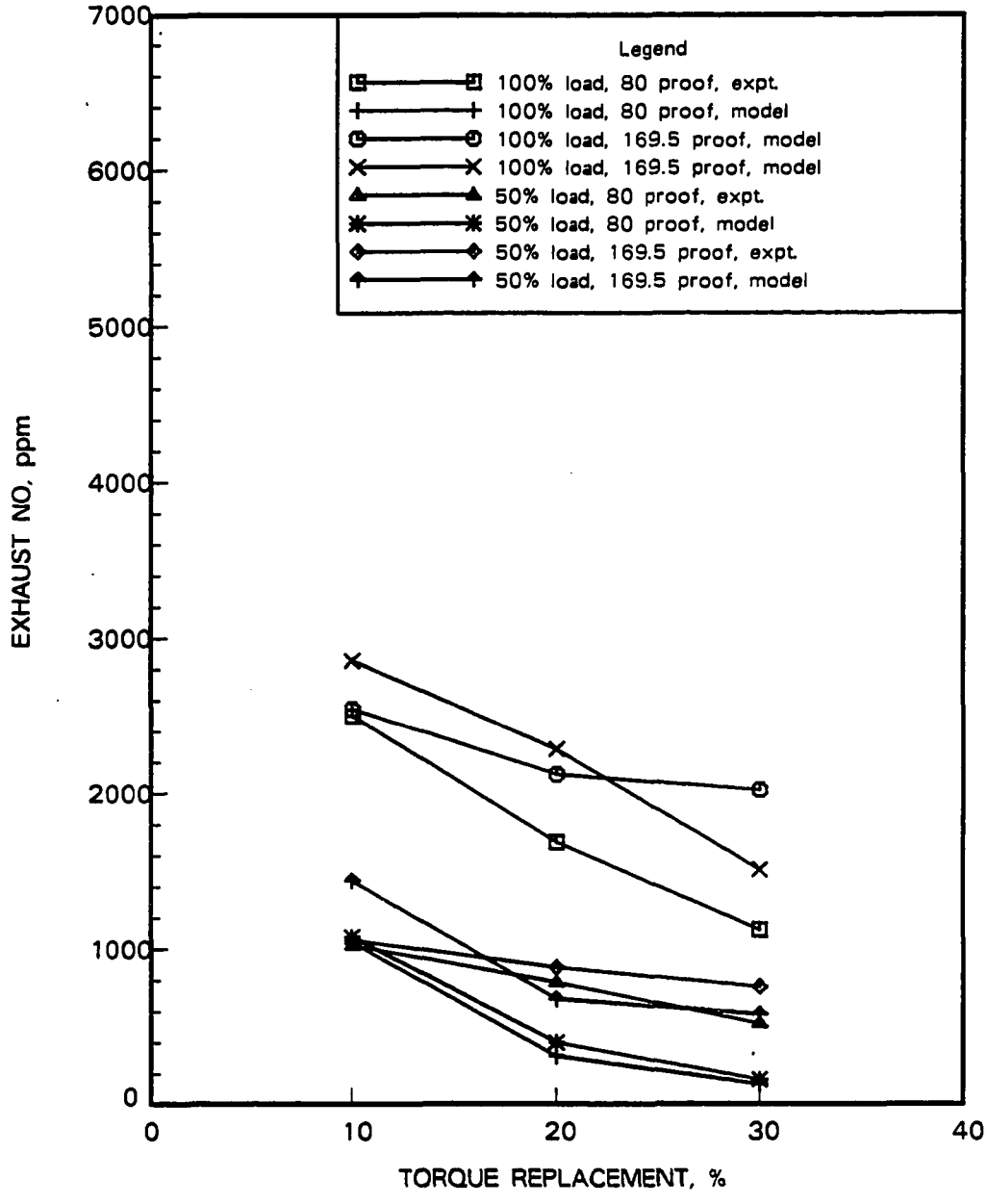

Figure 5.14: Exhaust NO Concentration versus Percent Torque Replacement from Ethanol at 2100 rpm

the reason for this discrepancy is discussed in Section 5.3.4.

Increasing the torque replacement by the fumigated alcohol from 10% to 30% resulted in a substantial increase in the exhaust CO and HC. At 1500 rpm, 100% load operation, 30% torque substitution with 80 proof ethanol, CO increased to nearly five times its diesel-only value, and unburned HC was doubled. At 1500 rpm, 50% load operation, CO increased by nearly eleven times, and unburned HC was tripled. At 2100 rpm, 100% load operation, 30% torque substitution with 80 proof ethanol, CO increased to nearly thirteen times its diesel-only value, and unburned HC increased by nearly four times. At 2100 rpm, 50% load operation, with 80 proof ethanol, CO increased by eighteen times, and unburned HC was doubled. Nearly identical increases in CO and unburned HC levels were observed with 169.5 proof ethanol fumigation. The exhaust smoke levels did not change significantly from their diesel-only values for all the speed, load, percent torque substitution, and ethanol proof values used.

5.2.3 Effect of alcohol proof

The quality of the ethanol and water mixture was varied from 40 proof to 169.5 proof. Eight different mixture proofs: 40, 60 ,80, 100, 120, 140, 160, and 169.5 were tested.

Table 5.3 gives the measured and model-predicted data for IMEP and $\eta_{th,ind}$ for different ethanol proofs, at 1500 and 2100 rpm, when 30% of the engine torque is supplied by the alcohol.

The measured IMEP and $\eta_{th,ind}$ values are not changed appreciably from their

Table 5.3: IMEP and $\eta_{th,ind}$ at various Ethanol Proofs (40 Proof to 169.5 Proof), with 30% Torque Replacement, at 100% and 50% Load Conditions, at 1500 and 2100 rpm

Speed	Load %	% Torque From Alcohol	Alcohol Proof	IMEP, kPa		$\eta_{th,ind}$, %		% Error
				Expt.	Model	Expt.	Model	
1500	100	30	40	1042	1102	46.1	48.7	5.7
1500	100	30	60	1037	1112	45.8	49.1	7.2
1500	100	30	80	1039	1101	45.8	48.6	6.0
1500	100	30	100	1041	1085	45.9	47.9	4.3
1500	100	30	120	1042	1080	46.3	48.0	3.6
1500	100	30	140	1041	1080	45.4	47.2	3.8
1500	100	30	160	1037	1051	46.3	46.9	1.3
1500	100	30	169.5	1037	1056	46.0	46.9	1.9
1500	50	30	60	620	655	46.6	48.6	5.6
1500	50	30	80	620	633	47.5	48.5	2.1
1500	50	30	100	627	622	48.6	48.2	-0.8
1500	50	30	120	625	610	48.6	47.4	-2.5
1500	50	30	140	622	601	48.7	47.1	-3.3
1500	50	30	160	623	599	48.7	46.8	-4.0
1500	50	30	169.5	629	603	48.7	46.7	-4.1
2100	100	30	40	957	1027	45.7	49.1	7.2
2100	100	30	60	966	1005	47.9	49.8	4.0
2100	100	30	80	961	1017	46.4	49.1	5.9
2100	100	30	100	964	1012	46.4	48.7	5.0
2100	100	30	120	970	1002	46.3	47.9	3.2
2100	100	30	140	964	984	46.4	47.4	2.0
2100	100	30	160	964	975	46.5	47.0	1.1
2100	100	30	169.5	972	978	46.7	47.0	0.6
2100	50	30	40	621	682	45.6	50.2	9.9
2100	50	30	60	621	667	45.9	49.3	7.4
2100	50	30	80	619	638	46.9	48.5	3.1
2100	50	30	100	621	634	46.8	47.8	2.1
2100	50	30	120	619	625	46.9	47.4	0.9
2100	50	30	140	626	625	47.1	47.0	-0.2
2100	50	30	160	619	614	47.2	46.9	-0.7
2100	50	30	169.5	619	611	47.5	47.0	-1.2

corresponding diesel-only values. Model-predicted IMEP is from 4.1% lower to 9.9% higher than measured values. As suggested in a related work [55], the slight variations in the indicated thermal efficiency during alcohol fumigation at the low load conditions may be caused by experimental uncertainties.

Audible misfire with unstable engine operation was observed when 30% torque replacement with 40 proof ethanol was attempted at 50% of the full load operation at 1500 rpm, and the test was discontinued to prevent engine damage.

The exhaust temperature increased with the alcohol proof at both full load and 50% of full load operation at 1500 rpm, as shown in Figure 5.15. The lower fraction of water in higher proof alcohol results in a lower reduction of flame temperature and higher exhaust temperature. A similar trend of higher exhaust temperature with increasing alcohol proof was observed at 2100 rpm as shown in Figure 5.16.

The model-predicted exhaust temperature is also shown in Figures 5.15 and 5.16. The predicted exhaust temperatures show the correct trend of increasing temperature with increasing proof. The model-predicted exhaust temperatures are from 12.2% lower to 5.4% higher than the measured values.

The NO emission increased with the alcohol proof at 1500 rpm under 100% and 50% of the full load, as shown in Figure 5.17. The measured NO concentration obtained with 169.5 proof ethanol was lower than that from diesel-only operation, for both full load and 50% of full load operation. Similar observations were made at 2100 rpm, and the data is plotted in Figure 5.18.

Figure 5.18 shows the effect of ethanol fumigation at 2100 rpm and 100% load operation on exhaust NO emission, with 30% of the torque replaced by the alcohol.

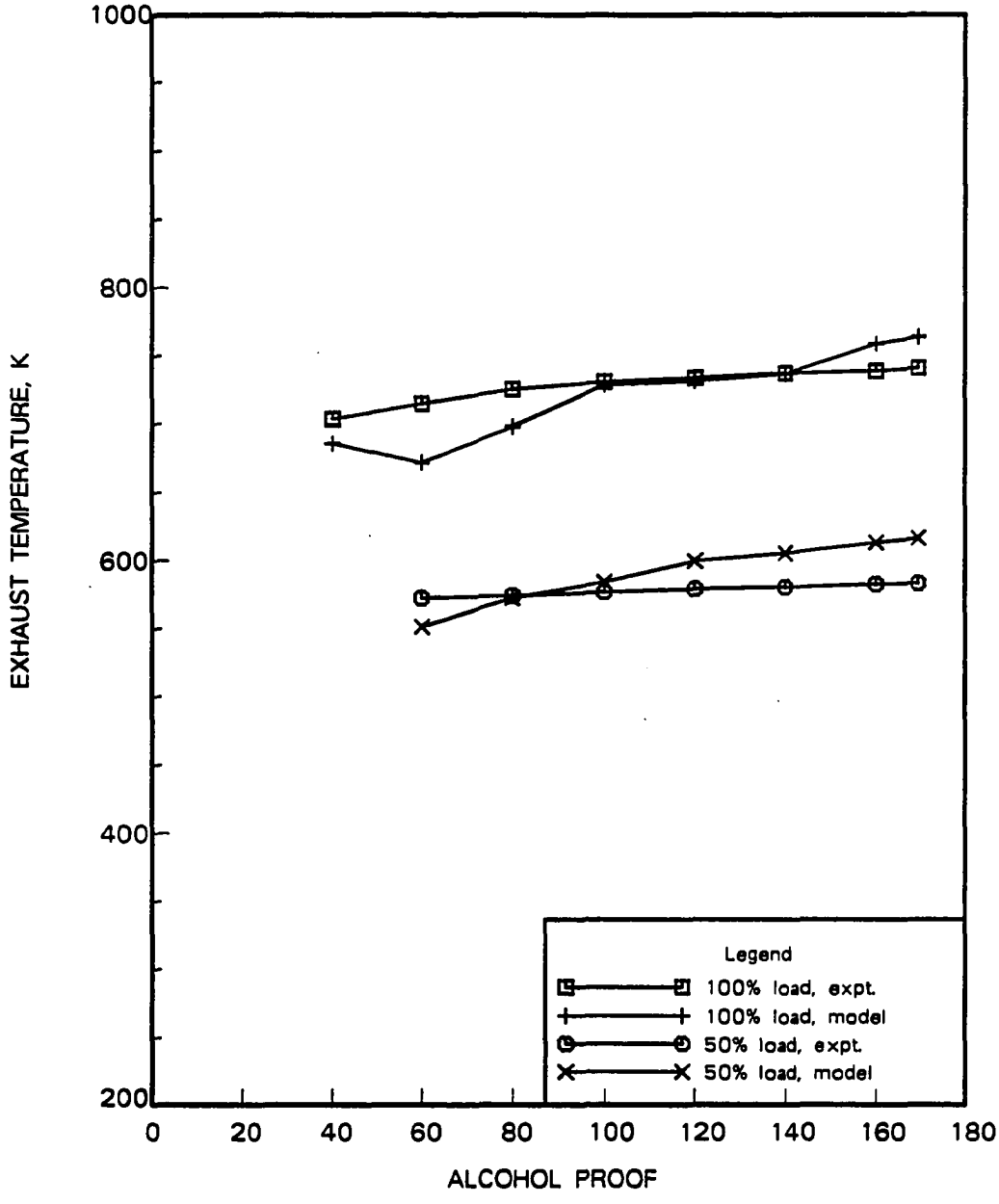

Figure 5.15: Exhaust Temperature versus Ethanol Proof at 1500 rpm, 30% Torque Replacement

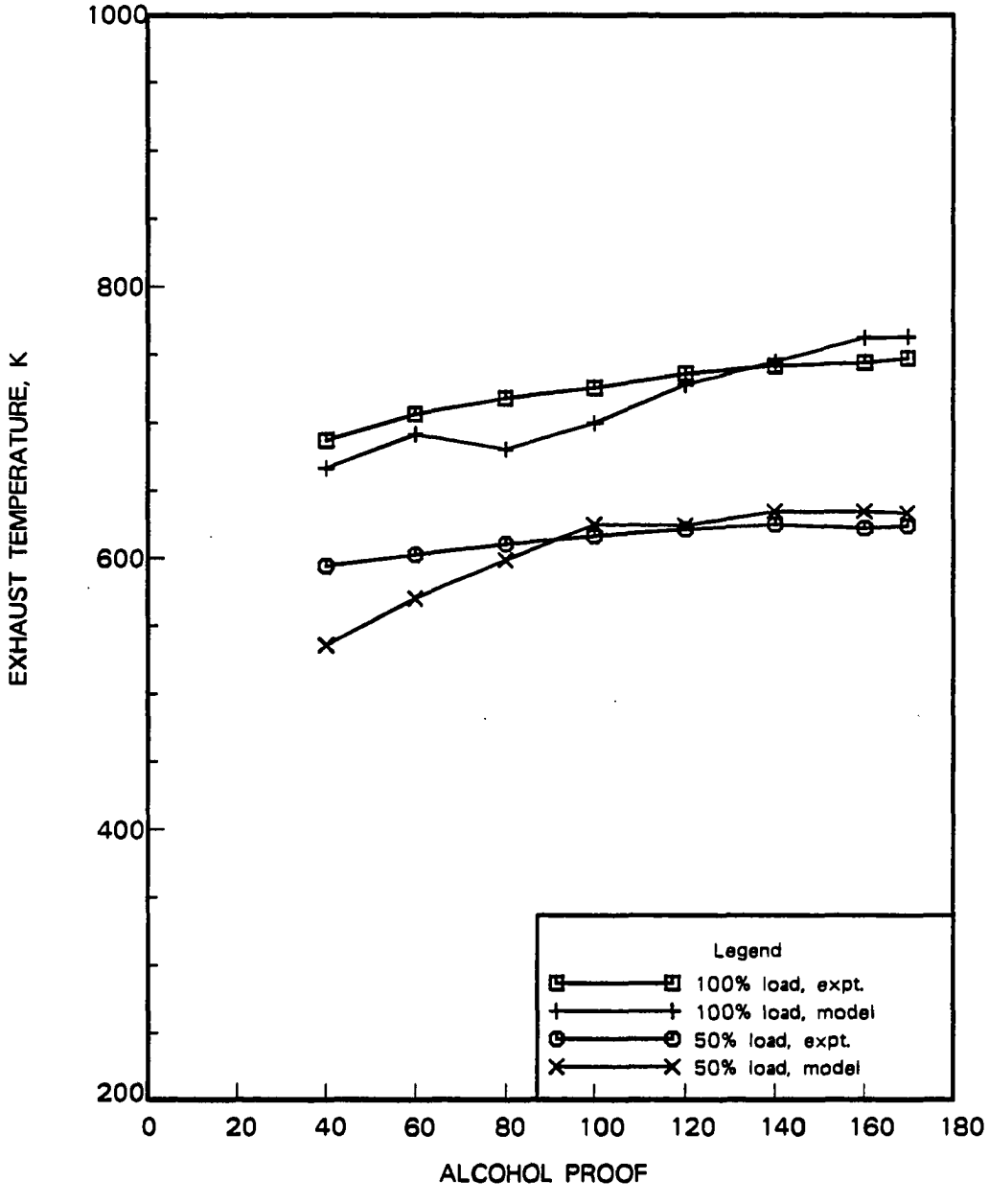

Figure 5.16: Exhaust Temperature versus Ethanol Proof at 2100 rpm. 30% Torque Replacement

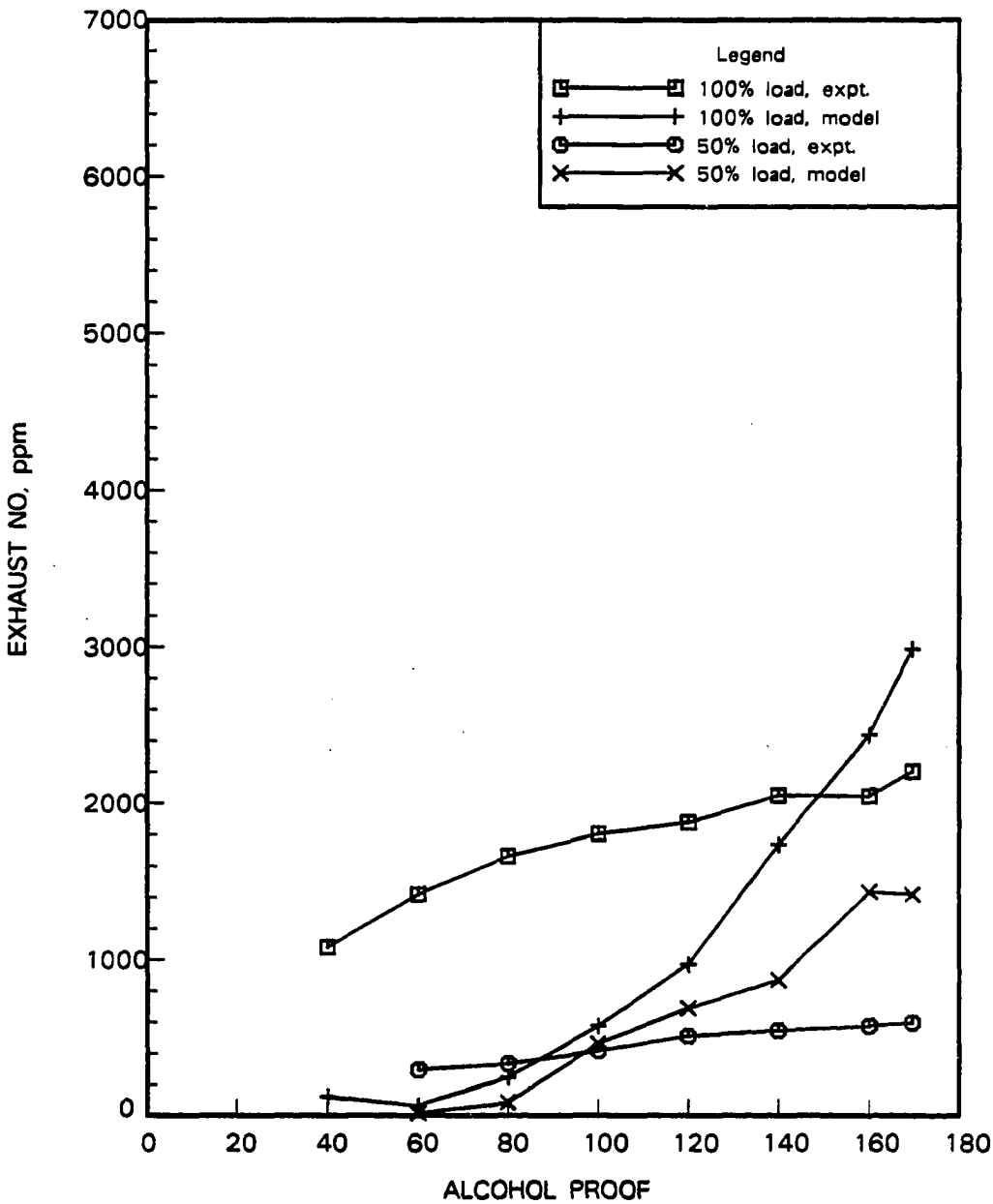

Figure 5.17: Exhaust NO Concentration versus Ethanol Proof at 1500 rpm, 30% Torque Replacement

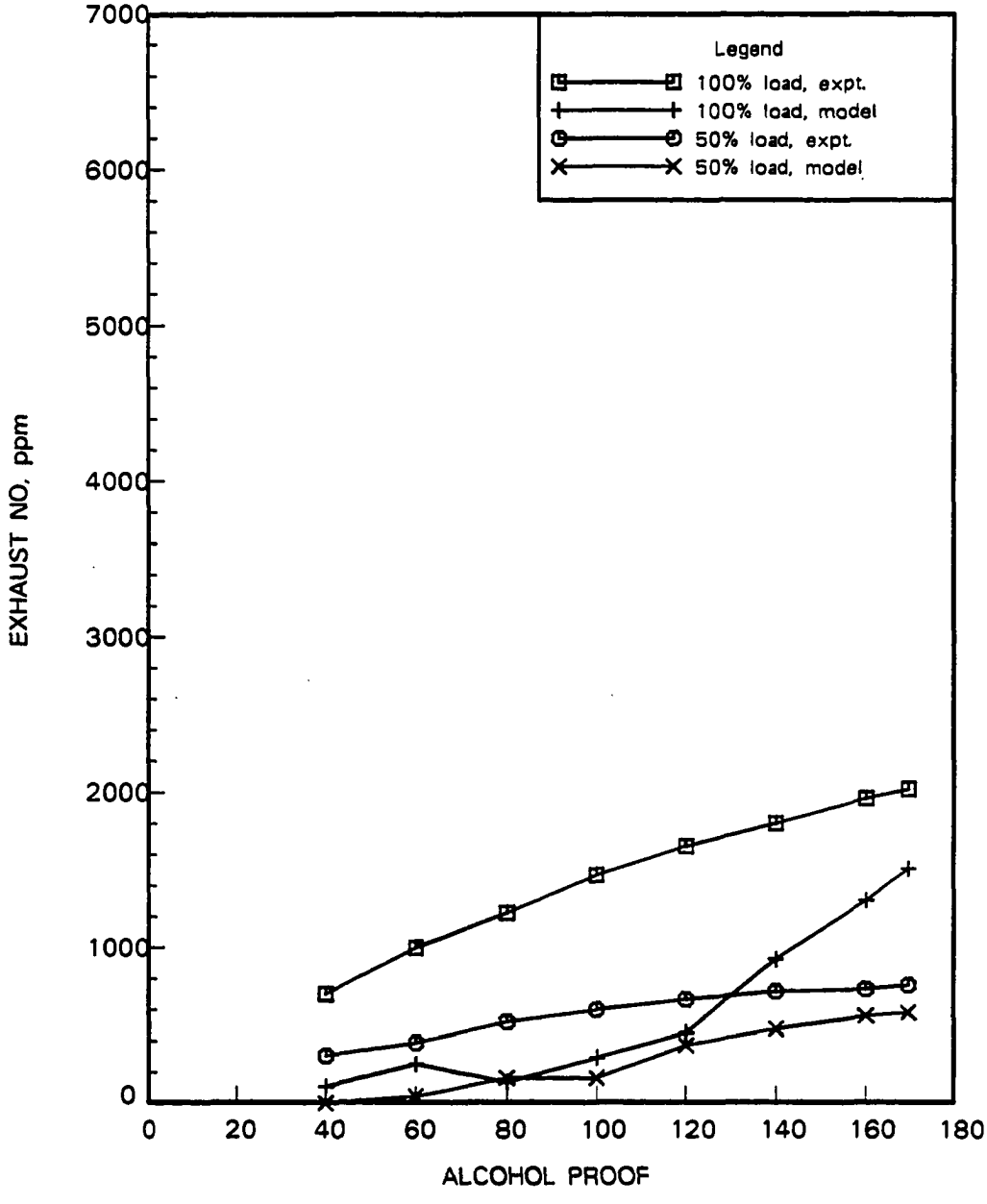

Figure 5.18: Exhaust NO Concentration versus Ethanol Proof at 2100 rpm, 30% Torque Replacement

The model over-predicts the reduction in NO emission with lowering the proof of alcohol used. Model predictions of NO emission are from 95% lower to 5% higher than the measured values.

Difficulties in predicting oxides of nitrogen in an ethanol fumigated diesel engine, were also encountered by Gao et al. [10] in their three zone model. Figure 5.19 reproduces the data published by Gao. Although the three zone model predicted proper trends and closely matched values of the oxides of nitrogen in the exhaust at 25% of full load, the predicted values are much higher than the measured values at the higher loads.

As stated in Section 5.2.2, CO and unburned HC increased substantially over their diesel-only values, with alcohol fumigation. The highest CO and unburned HC values were observed with 40 proof ethanol mixture. A gradual decrease in CO and HC levels was noted with increase in the ethanol proof. However, even with 169.5 proof ethanol fumigation, the CO level was about four to five times higher than the diesel-only value, and the unburned HC level was nearly double that of its diesel-only value. No discernible difference was seen in the smoke level with change in alcohol proof. Slight differences of 0.2 to 0.3 BSN in the smoke values at certain operating conditions may be due to the resolution of the smoke meter being only 0.1 units.

5.2.4 Comparison of ethanol and methanol

Comparisons of ethanol and methanol were made using the equivalent amount of methanol in water that matches a certain proof of ethanol, both in terms of lower heating value and enthalpy of vaporization. When compared on this basis, there is

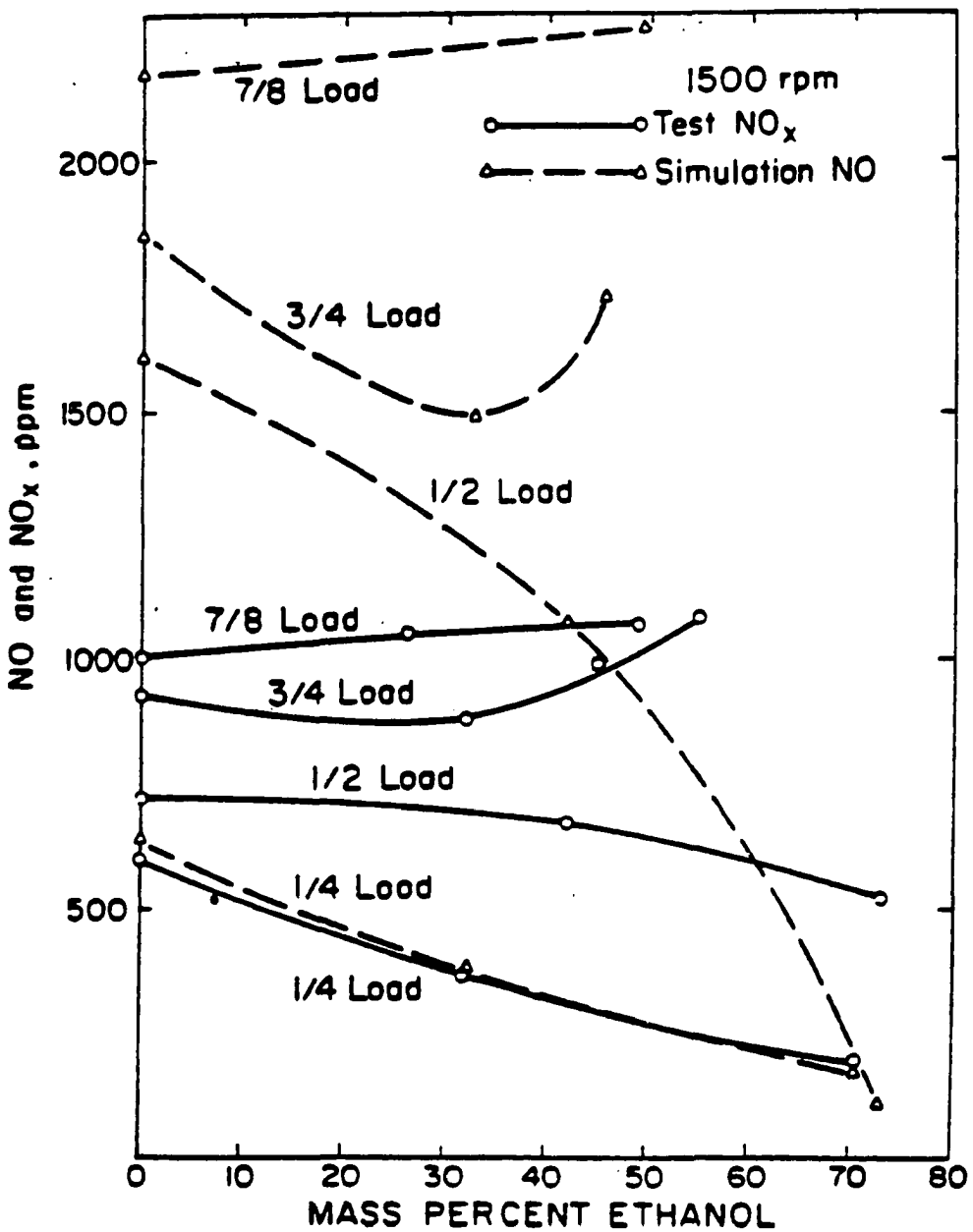

Figure 5.19: Comparison of Model-Predicted and Measured Nitrogen Oxides Emission (Reproduced from Gao et al. [10])

very little difference between the IMEP, $\eta_{th,ind}$, and emissions from the two alcohols. The calculation procedure used to determine the equivalent proofs and the definition of a new unit of proof for methanol (Pr.EEM) is described in Chapter 4.

Table 5.4 shows the data from tests at 1500 rpm, full load and 20% torque replacement, and Table 5.5 shows the data at 2100 rpm, full load and 30% torque replacement. The measured IMEP and $\eta_{th,ind}$ values for methanol fumigation are comparable to those for ethanol fumigation. The small differences in the measured IMEP and $\eta_{th,ind}$ values between the two alcohols, and between different proofs of alcohol at the same speed and load condition are within the range of uncertainty of the experimental data.

Model-predicted IMEP is from 0.8 to 5.0% higher for ethanol, and 1.5 to 11.1% higher for methanol, at 1500 rpm, 100% load, with 20% torque replacement. At 2100 rpm, 100% load, with 30% torque replacement, the model-predicted IMEP is from 0.6 to 7.2% higher for ethanol, and 2.6% lower to 12.0% higher for methanol.

The measured exhaust temperatures for equivalent proofs of the two alcohols were very nearly the same. Since the lower heating value and enthalpy of vaporization for equivalent proofs of the two alcohols was matched during fuel preparation, near equivalent exhaust temperatures were expected. Figure 5.20 and Figure 5.21 show the variation of exhaust temperature for the two alcohols, at the two different test conditions used for comparison. Both measured and model-predicted values are plotted in these figures. As in the case of ethanol fumigation, the exhaust temperature increases with increase in the Pr.EEM of the fumigated methanol.

At 1500 rpm, the model-predicted exhaust temperatures are from 5.7% lower to

Table 5.4: IMEP and $\eta_{th,ind}$ for Ethanol and Methanol Fumigation (40 Proof/Pr.EEM to 169.5 Proof/Pr.EEM), with 20% Torque Replacement at 1500 rpm, and 100% of Full Load

Ethanol	IMEP, kPa		$\eta_{th,ind}$, %		%	Methanol	IMEP, kPa		$\eta_{th,ind}$, %		%
Proof	Expt.	Model	Expt.	Model	Error	Pr. EEM	Expt.	Model	Expt.	Model	Error
40	1041	1037	45.7	47.8	4.4	40	1026	1140	45.1	50.1	11.1
80	1046	1091	46.1	48.1	4.3	80	1035	1096	45.3	48.0	5.9
100	1043	1075	46.0	47.5	3.1	100	1039	1085	45.5	47.5	4.4
120	1043	1065	46.1	47.1	2.2	120	1035	1073	45.6	47.3	3.6
140	1044	1064	46.0	46.9	1.8	140	1031	1046	46.1	46.8	1.5
160	1044	1055	46.0	46.5	1.1	160	1033	1061	45.6	46.9	2.7
169.5	1048	1056	45.9	46.3	0.8	169.5	1037	1067	45.5	46.8	2.9

Table 5.5: IMEP and $\eta_{th,ind}$ for Ethanol and Methanol Fumigation (40 Proof/Pr.EEM to 169.5 Proof/Pr.EEM), with 30% Torque Replacement at 2100 rpm, and 100% of Full Load

Ethanol	IMEP, kPa		$\eta_{th,ind}$, %		%	Methanol	IMEP, kPa		$\eta_{th,ind}$, %		%
Proof	Expt.	Model	Expt.	Model	Error	Pr. EEM	Expt.	Model	Expt.	Model	Error
40	957	1027	45.7	49.1	7.2	40	944	1057	45.4	50.9	12.0
60	962	1005	47.9	49.8	4.0	60	964	1000	47.0	48.7	3.6
80	961	1017	46.4	49.1	5.9	80	970	1047	46.5	50.2	7.9
100	964	1012	46.4	48.7	5.0	100	968	1029	46.5	49.4	6.3
120	970	1002	46.3	47.9	3.2	120	968	1018	46.5	48.6	5.1
140	964	984	46.4	47.4	2.0	140	972	947	49.6	48.3	-2.6
160	964	975	46.5	47.0	1.1	160	966	1003	46.3	48.2	3.8
169.5	972	978	46.7	47.0	0.6	169.5	963	990	46.1	47.5	2.8

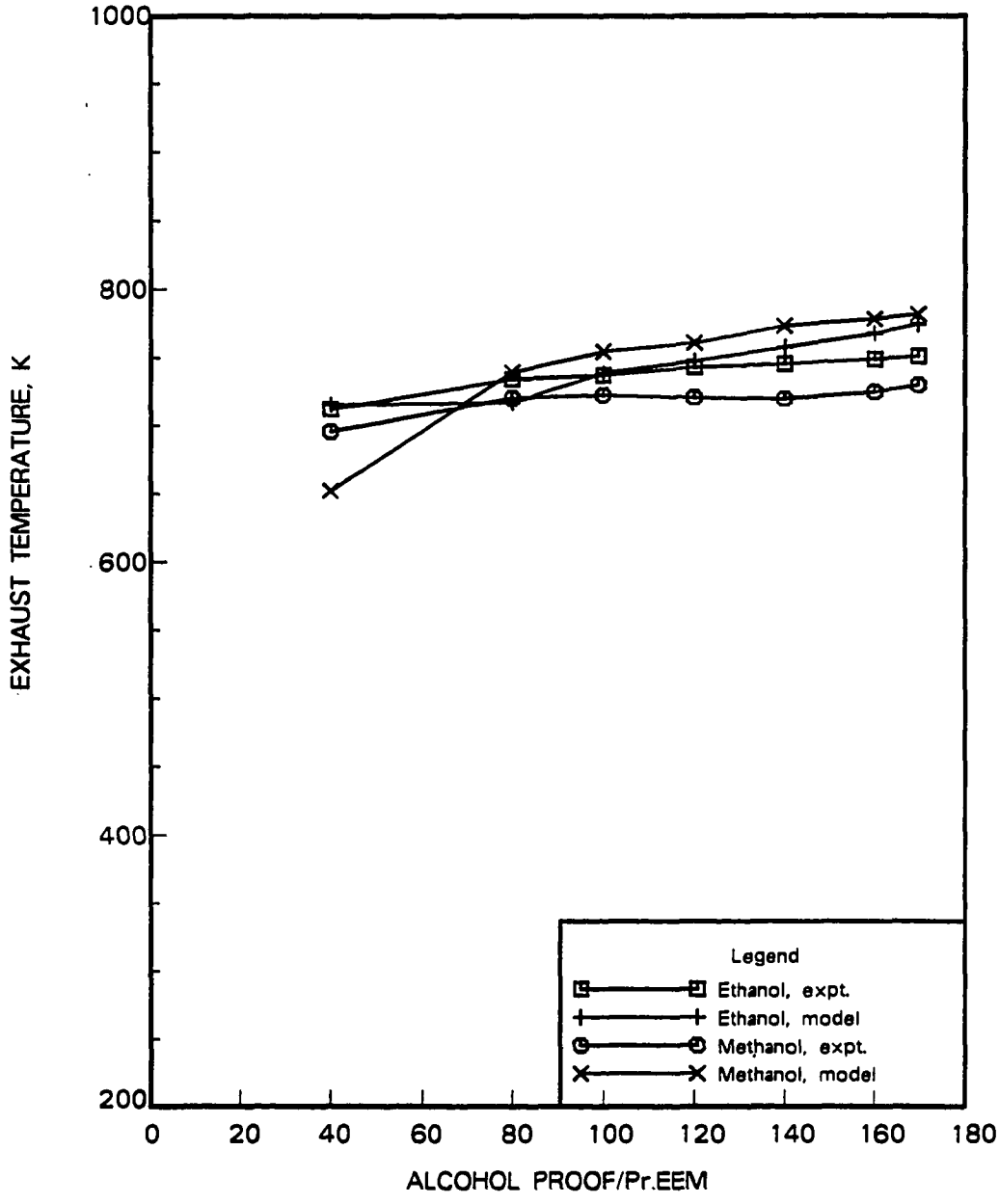

Figure 5.20: Exhaust Temperature versus Alcohol Proof, at 1500 rpm 100% Load, 20% Torque Replacement

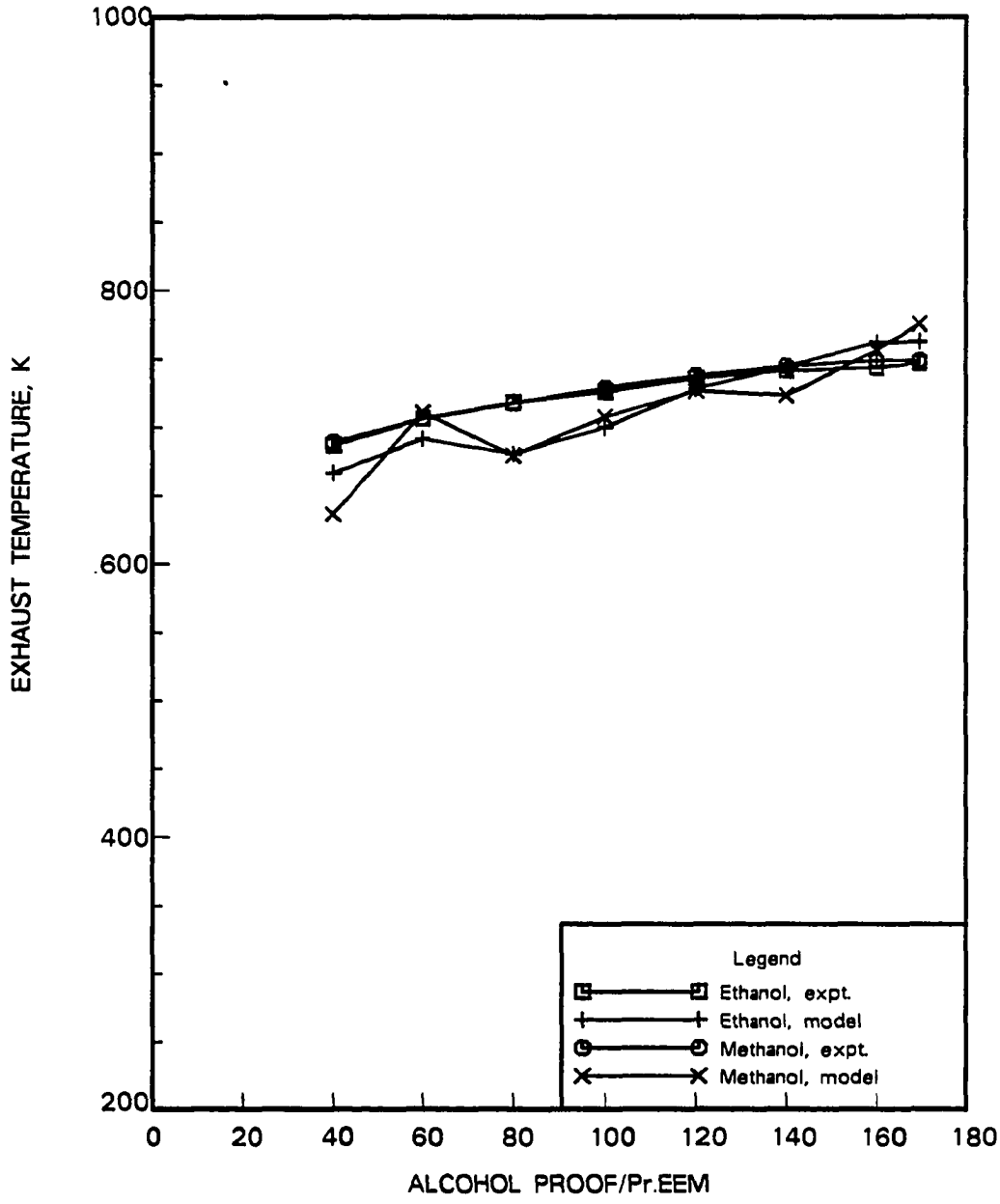

Figure 5.21: Exhaust Temperature versus Alcohol Proof, at 2100 rpm 100% Load, 30% Torque Replacement

4.7% higher for ethanol, and 9% lower to 8.6% higher for methanol. For comparisons at 2100 rpm, the model-predicted 8.2% lower to 3.8% higher exhaust temperatures for ethanol, and 12.2% lower to 5.4% higher values for methanol.

Figure 5.22 is a plot of the measured and model-predicted exhaust NO emission at 1500 rpm, 100% load, and 20% torque replacement, and Figure 5.23 shows the data at 2100 rpm, 100% load and 30% torque replacement. The exhaust NO concentration for the two alcohols with equivalent proofs is comparable within the limits of experimental uncertainties. The exhaust NO concentration increases with proof for both ethanol and methanol, due to lower amount of water fumigated with the alcohol and the resulting higher flame temperatures in the cylinder. This trend is observed at both test conditions used for comparisons.

Although the model-predicted proper trends in NO concentration for both methanol and ethanol, the reduction in NO levels at lower proofs is overpredicted by the model. At 1500 rpm, the general trend in exhaust NO level predicted by the model for both methanol and ethanol fumigation matches the experimental data. At 2100 rpm, the experimental data are very close for both ethanol and methanol and the model also predicts this. Although the level of NO predicted by the model does not match well with test data, and the sensitivity of the model to proof is greater than for the experimental data, the model does show the similarity in the performance of ethanol and methanol. The reason for poor NO prediction capability of the model is discussed in Section 5.3.4.

There was very little difference in the measured CO, unburned HC, and smoke levels between ethanol and methanol fumigation. The differences were within the

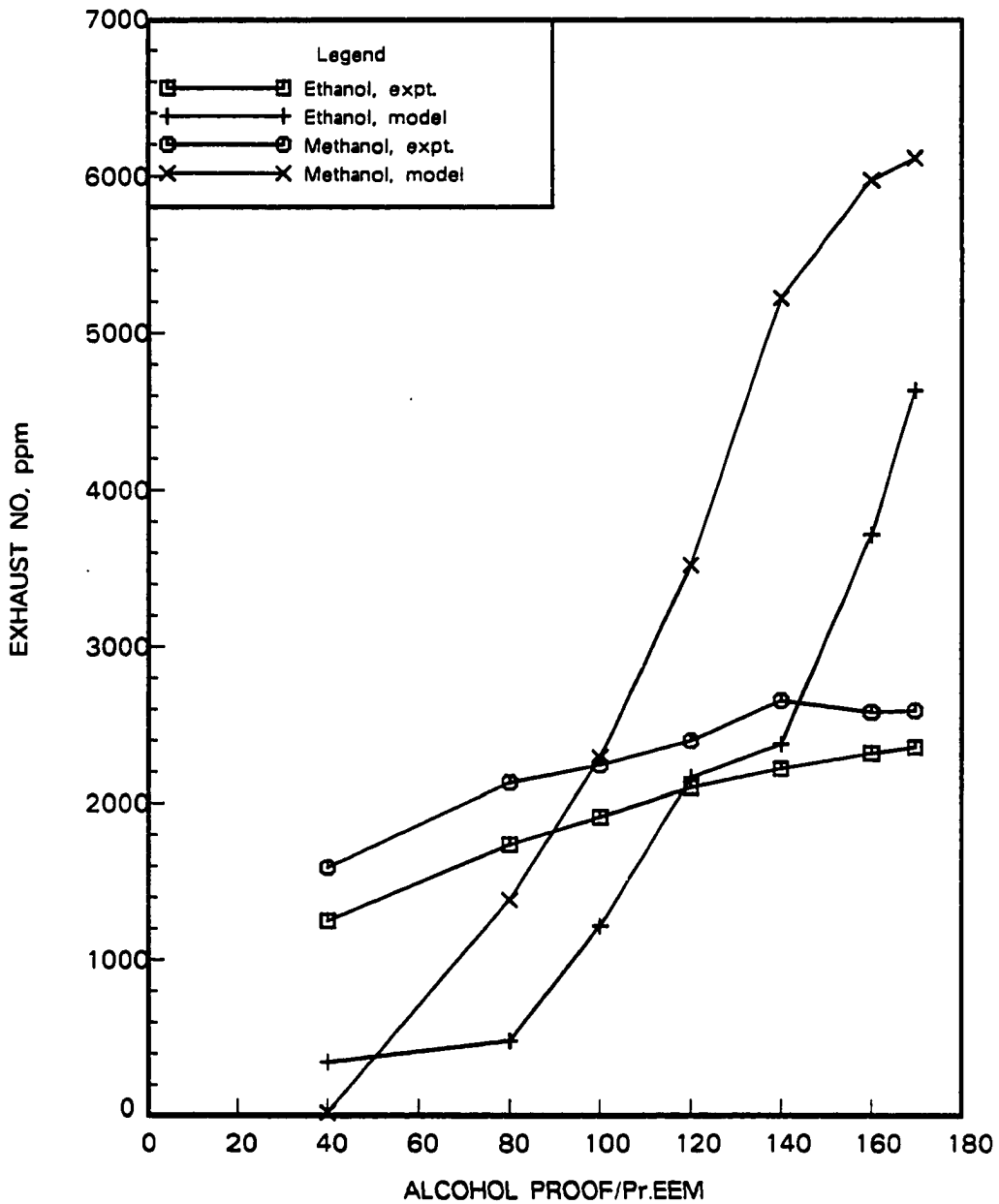

Figure 5.22: Exhaust NO Concentration versus Alcohol Proof, at 1500 rpm 100% Load, 20% Torque Replacement

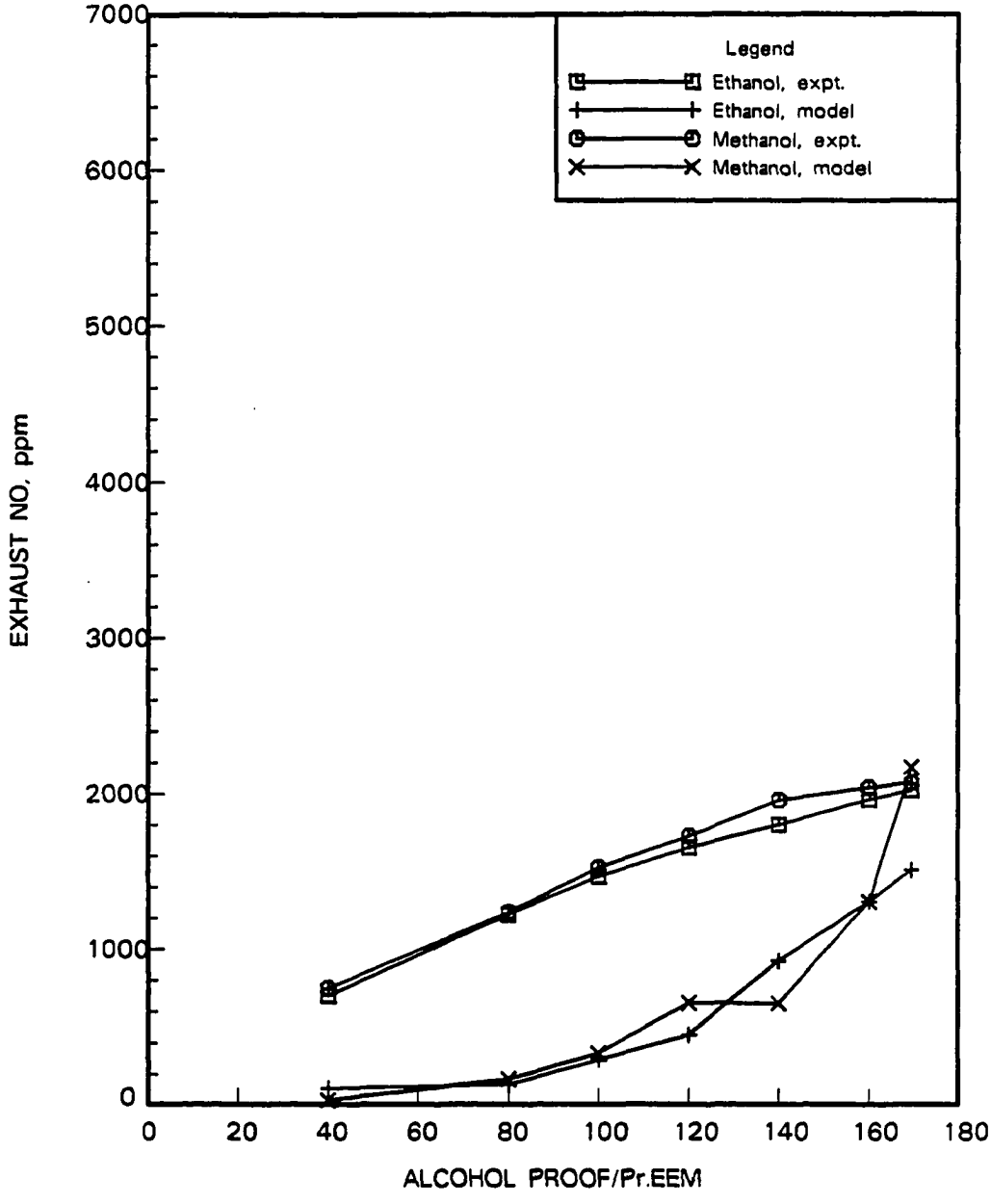

Figure 5.23: Exhaust NO Concentration versus Alcohol Proof, at 2100 rpm 100% Load, 30% Torque Replacement

range of uncertainty of the data.

5.2.5 Water injection

To investigate the role of water in the fumigated alcohol and water mixture, distilled water was injected into the intake manifold of the engine at two different operating conditions.

Table 5.6 shows the IMEP and $\eta_{th,ind}$ data with water injection at 1500 rpm and at two load conditions: 100% load and 75% load. For the 100% load case, the amount of water was gradually increased until the torque started to drop off and further tests were discontinued. At 75% of full load, water was added gradually until the load started to drop off and then the diesel fuel flow was increased to maintain the torque level constant. The IMEP and $\eta_{th,ind}$ values did not change considerably with water injection, under the conditions tested. At 1500 rpm the water flow rate could be increased to about 2.5 times the diesel fuel flow rate before the engine efficiency decreased. After this point, additional diesel fuel had to be injected to maintain the torque constant.

Table 5.6 also shows a comparison between model-predicted and measured values of IMEP and $\eta_{th,ind}$, with water injection at 100% and 75% load at 1500 rpm. The model-predicted IMEP values are within 0.7% to 11.0% higher than the experimental values.

Figure 5.24 shows the variation of exhaust temperature with water injection rate. Both measured and model-predicted values are given. As expected, the exhaust temperature decreased gradually with increasing rate of water injection at both the load

Table 5.6: IMEP and $\eta_{th,ind}$ for Water Fumigation at 1500 rpm, 100% and 75% of Full Load

Load, %	IMEP, kPa		$\eta_{th,ind}$, %		% Error
	Expt.	Model	Expt.	Model	
100	1016	1038	45.0	46.0	2.1
100	1020	1076	44.5	47.0	5.5
100	1022	1094	44.8	48.0	7.1
100	1014	1116	44.5	49.0	10.0
100	1007	1110	43.8	48.3	10.2
100	1003	1113	44.0	48.9	11.0
75	820	826	46.8	47.2	0.7
75	820	851	46.8	48.6	3.8
75	818	835	46.5	47.5	2.0
75	817	857	46.3	48.6	5.0

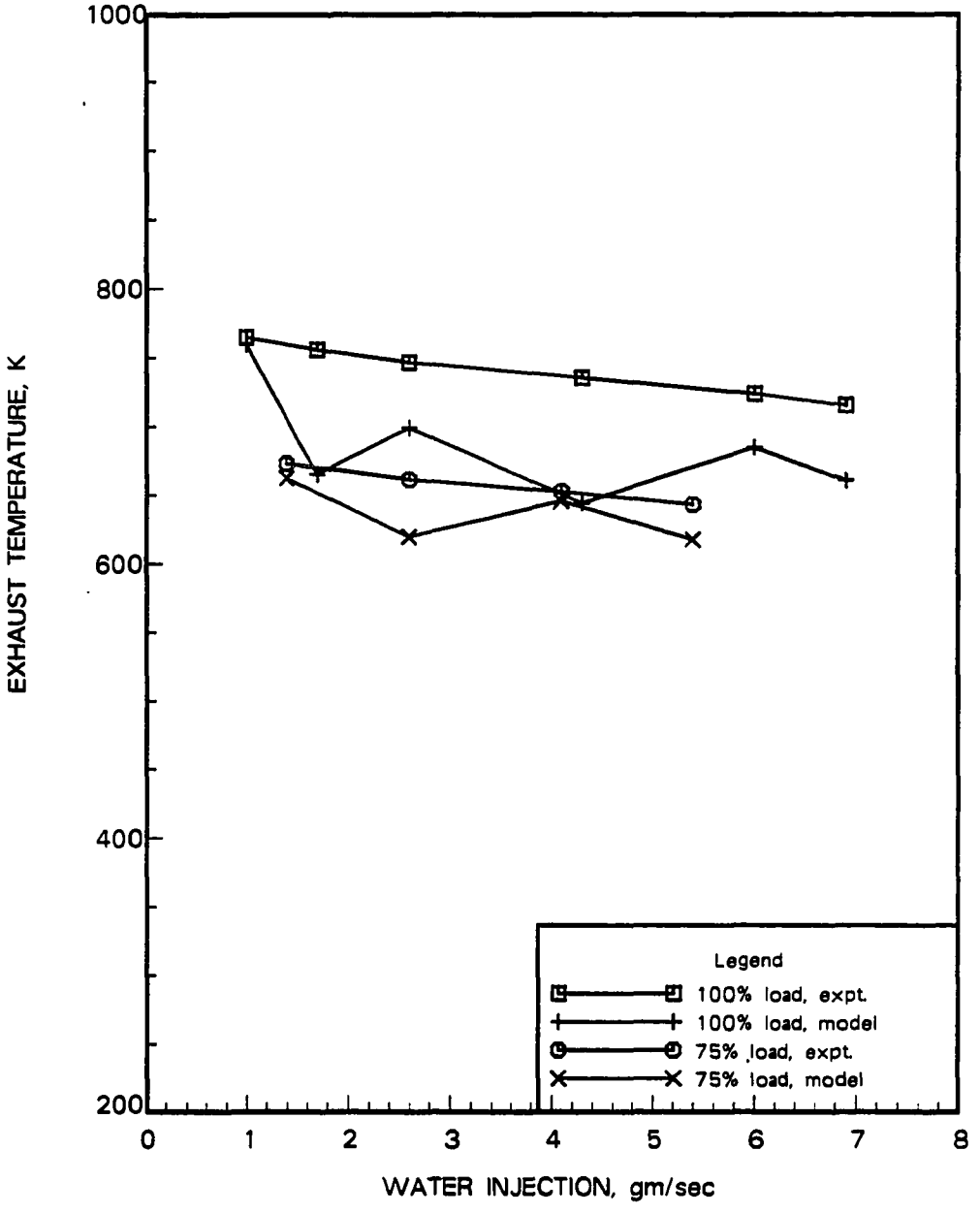

Figure 5.24: Exhaust Temperature versus Water Injection Rate, at 1500 rpm, 100% and 75% Load

conditions tested, due to lower flame temperatures caused by liquid water entering the individual cylinders.

The model correctly predicts the reduction in exhaust temperature with increased water flow rate. Model-predicted values of exhaust temperature are from 1% to 19% lower than the measured values.

The reduction in flame temperature caused by water injection resulted in lower exhaust NO emission, as shown in Figure 5.25. Model-predicted NO values are also plotted in this figure. The reduction in exhaust NO emission with water injection was observed at both 100% and 75% of full load operation at 1500 rpm. The model-predicted values are from 20% to 99% lower than the actual measured values. Section 5.3.4 provides an explanation for the overprediction in NO reduction.

At 100% load, the unburned hydrocarbons were not affected by water injection, the CO emissions increased gradually, and the smoke increased substantially. At 75% of full load, the hydrocarbon level increased with increasing water flow rate although the engine could tolerate some water injection without an increase in HC.

A comparison of the behavior of the engine and the multizone model, with and without alcohol fumigation, has been presented in this section. The reasons for the behavior of the engine have been discussed. The following section is a discussion of the positive aspects, and the various shortcomings of the present model.

5.3 Discussion

This section is divided into four subsections. The first subsection highlights the positive aspects of the present model. The second subsection provides an explanation

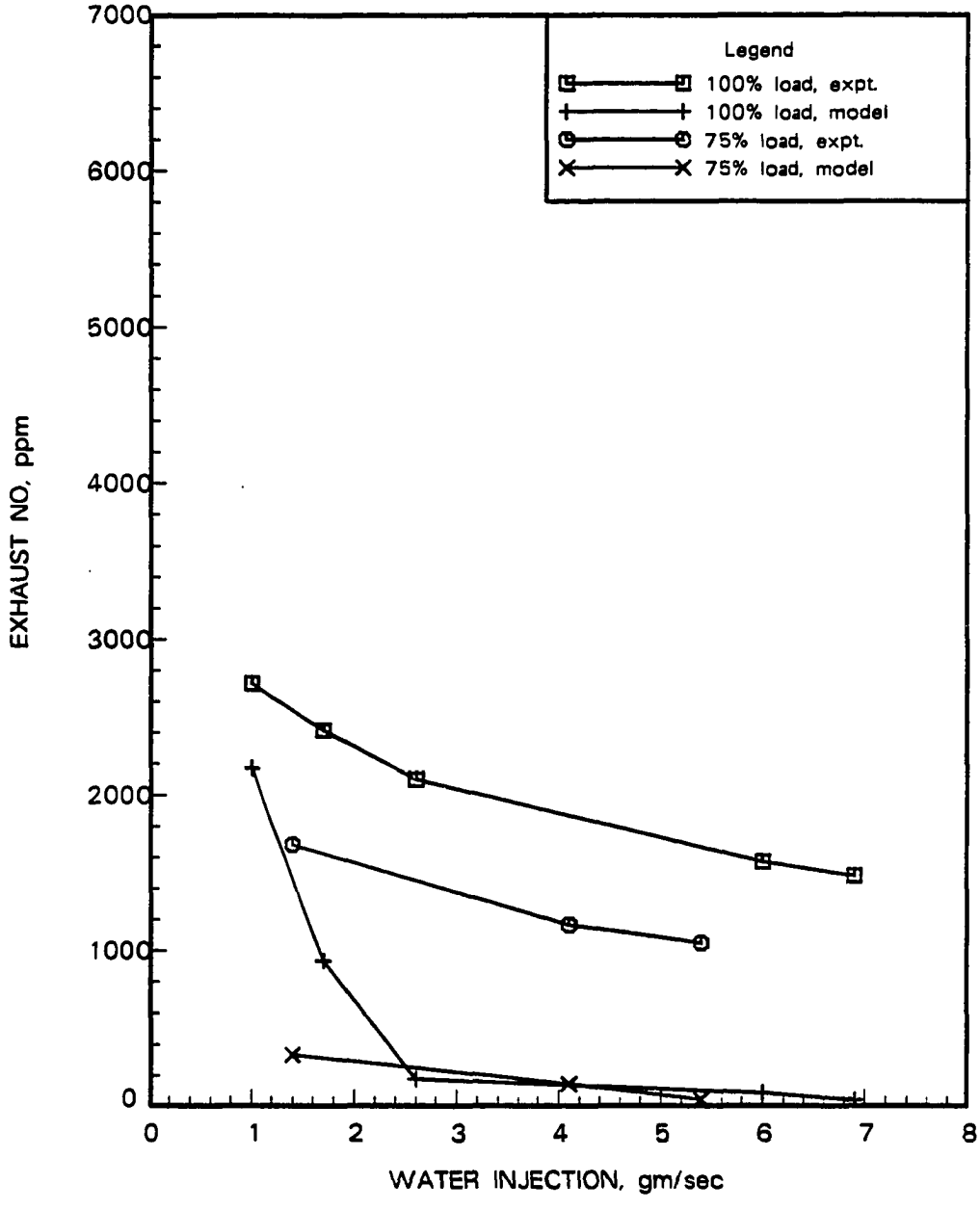

Figure 5.25: Exhaust NO Concentration versus Water Injection Rate, at 1500 rpm, 100% and 75% Load

for the failure of the model to predict changes in the indicated thermal efficiency with load. The causes for variations in the exhaust temperature, in excess of those due to experimental uncertainties, are given in the third subsection. The fourth subsection dicusses the reason for overpredicting reductions in exhaust NO level, with increase in percent torque replaced by alcohol, and decrease in the alcohol proof.

5.3.1 Capabilities of the model

The present multizone model was used to simulate one hundred and fifty different operating conditions and the model predictions were compared with the corresponding experimental data. The IMEP decreased with load as expected. This trend was observed at both the speeds, 1500 and 2100 rpm, used for comparing the model with experimental data, for both diesel-only, and alcohol fumigated operation. In general the agreement in IMEP between experiments and the model is best at higher loads. With alcohol fumigation the model predictions matched closely with experimental data, at higher proofs. The same trends apply to indicated thermal efficiency.

The model-predicted exhaust temperatures matched from 164 K lower to 60 K higher than measured temperatures, over a nominal temperature range of 500 to 917 K, for all the cases simulated. Specific trends in exhaust temperature were correctly predicted by the model. Model-predicted higher temperatures at higher loads, and lower temperatures with the fumigation of lower proofs of alcohol.

Although in-cylinder NO concentrations were not measured during actual engine tests, the model-predicted NO histories are quite reasonable when compared with other existing multizone models developed for diesel-only operation. Figure 5.26,

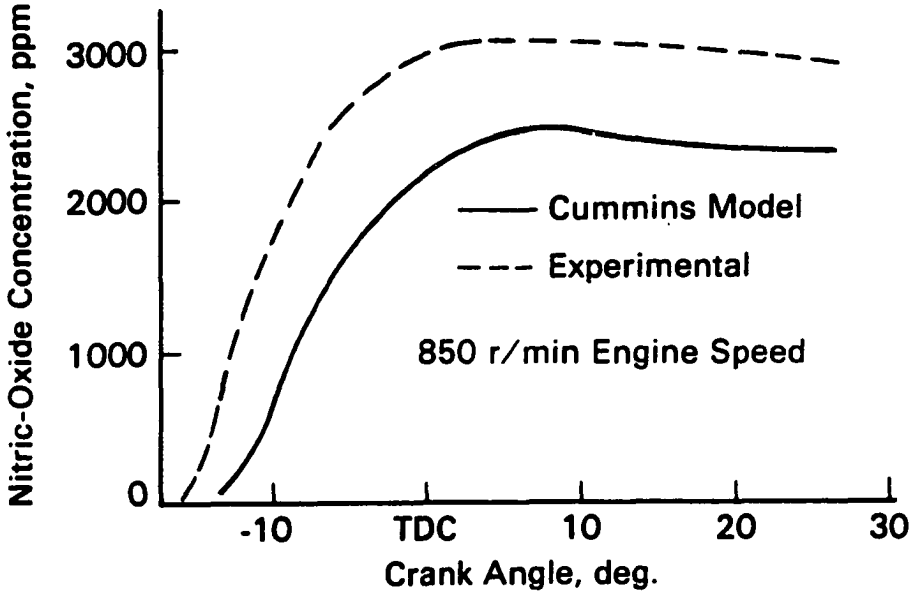

Figure 5.26: Nitric Oxide History in the Cylinder, Experimental and Model-Predicted Data (Reproduced from Shahed et al. [21])

reproduced from Shahed et al. [21] shows both the experimental NO history measured by Voiculescu and Borman [58] for diesel-only operation, and the corresponding model predicted history given by the multizone model of Shahed et al. [21]. The in-cylinder NO history predicted by the present model is given in Figure 5.3, and the general trend is very similar to those given in Figure 5.26. In the present cycle simulations, peak NO values were reached at 10 to 25 degrees after TDC, and beyond this the NO concentration remained nearly constant until the end of the cycle.

For diesel-only operation, the model-predicted NO values are from 15% lower to 117% higher than the measured values. No general conclusions can be made regarding the effect of speed or load on the difference between model predictions and test data. The multizone model of Chiu et al. [15] for diesel-only operation predicted NO values from 40% lower to 60% higher than measured values. In the published work of Chiu et al. [15] the effect of wall impingement has been ignored. The present model overpredicted reductions in NO emission with alcohol fumigation. With alcohol fumigation, the model predicted NO values from 99% lower to 150% higher than experimental values. In general the difference between model predictions and experimetal data of NO, is lower at medium proofs of alcohol, between 80 and 140 proof. At lower proofs the model overpredicts reduction in NO emission, and at higher proofs the model-predicted NO levels are higher than those measured. The three zone model of Gao et al. [10] predicted NO levels which matched closely with experimental data, at 25% of full load, at 1500 rpm. At higher loads, the model-predicted NO values were greatly exaggerated, and large differences between model data and measured values were observed.

5.3.2 Failure to predict higher thermal efficiencies at lower loads

In general, the increase in thermal efficiency with decreasing load is due to a shortened combustion duration. In the present model, the entrainment of alcohol, water and air into the wall zone continues up to the end of the expansion stroke. However, a major portion of combustion is completed at the end of phase three when the entire spray plume is transferred to the wall zone. Beyond this, only zone D and zone A are present in the cylinder. The equivalence ratio of zone D at the end of phase three is below stoichiometric and the mass of diesel fuel in zone A is negligible. This indicates that during the remaining part of the expansion stroke following the end of phase three, very little energy is released by combustion. Based on this concept, the crank angle corresponding to end of phase three has been used as a measure of the end of substantial energy release.

Theoretically, the end of phase three should occur later in the expansion stroke at higher loads, resulting in a longer combustion period. The crank angle data corresponding to the end of phase three, predicted by the model for four different loads: 100, 75, 50, and 25% of full load, at 1500 rpm, with diesel-only operation are given in Table 5.7. The end of phase three occurs between 367.3° and 368.4°, for all the four cases. This shows that a major portion of burning is completed very early in the expansion stroke, and that the crank position corresponding to this event does not change with load. Although diesel-only operation was used for the discussion here, the same behavior was observed with alcohol fumigated runs. Hence, a nearly constant value of thermal efficiency is predicted for all the four load conditions, at a fixed speed. This problem can be attributed to the single-zone wall impingement

Table 5.7: Effect of Load on the Timing of Phase 3 at 1500 rpm

Load %	Crank Angle at End of Phase 3 degrees	$\eta_{th,ind}$, %	
		Expt.	Model
100	368.4	45.6	45.9
75	367.9	46.3	45.7
50	367.3	49.1	46.3
25	367.3	50.3	45.1

model used to simulate the interaction between the spray plume and the wall zone, during phases two and three. A more detailed wall impingement model should show a greater effect of the quantity of fuel injected on the combustion duration.

5.3.3 Large discrepancy in exhaust temperature predictions

For diesel-only operation, the exhaust temperature predicted by the model is from 7.7% lower to 5.8% higher than the the measured values. On an absolute scale, the predicted exhaust temperature is from 73 K lower to 11 K higher, over a nominal temperature range of 458 K to 940 K. This difference is higher than the uncertainty in the measurements. However, part of the lack of agreement may be due to the difficulty of characterizing the exhaust temperature of a multicylinder engine, especially under fumigated operation. Exhaust temperature measurements for the two branches of the exhaust manifold show that the temperature of the gases leaving cylinders one and two are always higher than that for cylinders three and four, by 11 to 28 K. An average of the measurements made for the two branches, is used as the bulk exhaust temperature for the engine. The model assumes identical behavior for all the four cylinders, and predicts a uniform exhaust temperature. The discrepancy in the measured exhaust temperature between the cylinders, results in errors between the model predictions and measured values. In addition to this, the use of an assumed two-step exhaust process to represent the actual process is another source of error. With alcohol fumigation, the error in model-predicted exhaust temperature is from 17% lower to 10.2% higher than the measured values. Poor distribution of the fumigated alcohol and water mixture to the individual cylinders was observed at higher alcohol flow

rates, and the difference in the exhaust temperatures between the two branches of the manifold increased to about 28 to 39 K. With water injection this difference was as high as 45 to 56 K. The model-predicted exhaust temperature during simulation of water injected operation is 1% to 19% lower than the average of the measured values. Better mixing of the two exhaust plumes to obtain a single bulk exhaust temperature, uniform distribution of the fumigated mixture to the individual cylinders, and a better exhaust model for the flow through the exhaust valve will be necessary to improve the match between measurements and model predictions of exhaust temperature.

5.3.4 Poor NO prediction

The model overpredicts the reduction in exhaust NO level at higher torque replacements with alcohol, and with decreasing alcohol proofs at constant speed and load. To investigate this behavior of the model, the formation of NO in the cylinder was studied in detail at 1500 rpm, 100% load operation, for four different alcohol proofs (40, 80, 120 and 169.5) with 30% of the total torque supplied by the alcohol.

Figure 5.27 shows the NO history for the wall zone, zone D, and for the entire cylinder, for 80 proof ethanol fumigation. It is obvious that a major portion of the total cylinder NO is formed after TDC (top dead center), during the expansion stroke. Figure 5.27 indicates that over 90% of the total cylinder NO is contained in zone D. The wall zone, zone D, is created at about 5 to 7° prior to TDC.

The conditions prevailing in the wall zone are crucial for the formation of NO in the cylinder. Figure 5.28 shows that the peak NO concentration for the four different alcohol proofs is reached within 20° after TDC. The conditions in the wall zone,

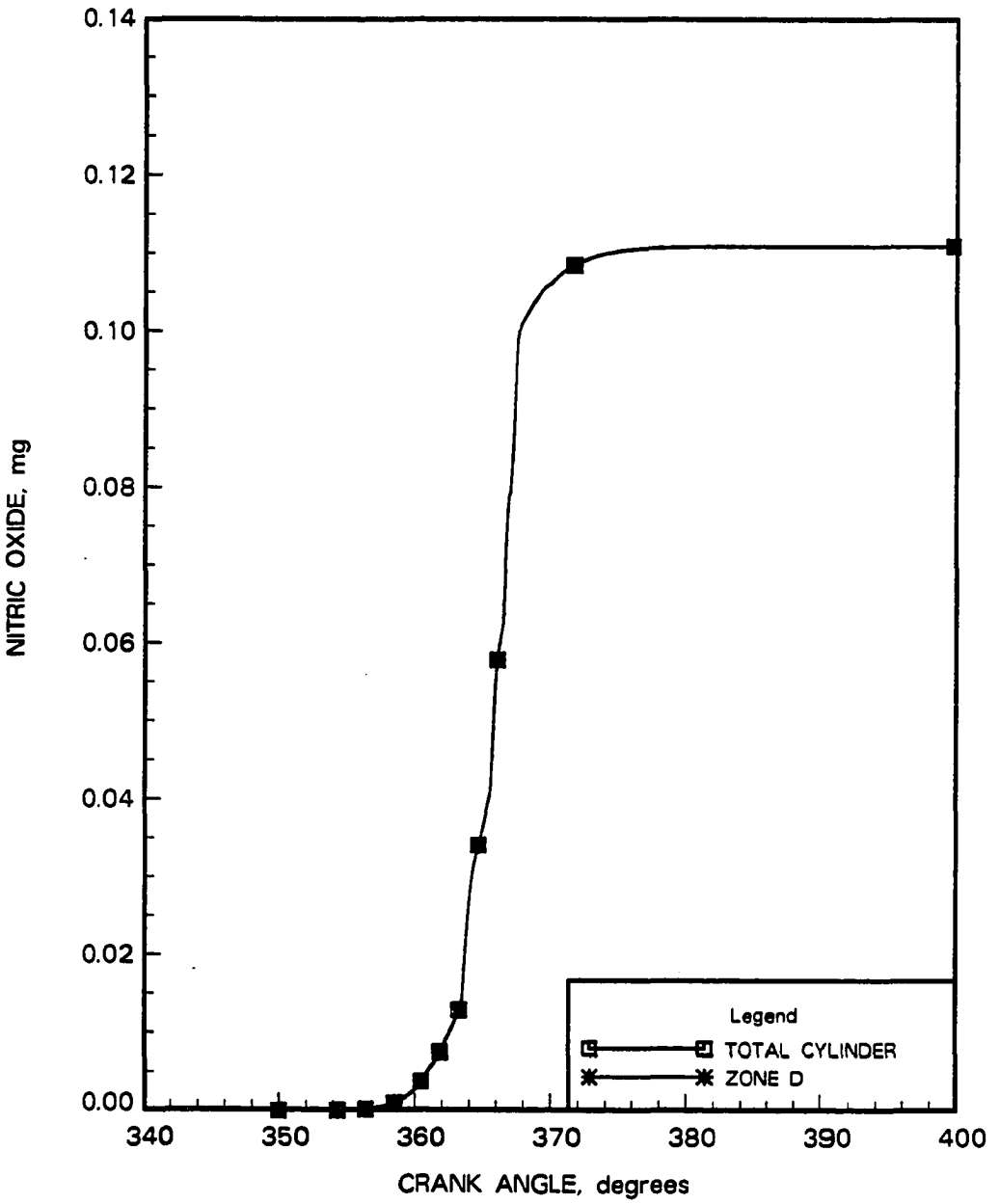

Figure 5.27: Nitric Oxide History in the Cylinder and the Wall Zone, at 1500 rpm. 80 Proof Ethanol, 30% Torque Replacement

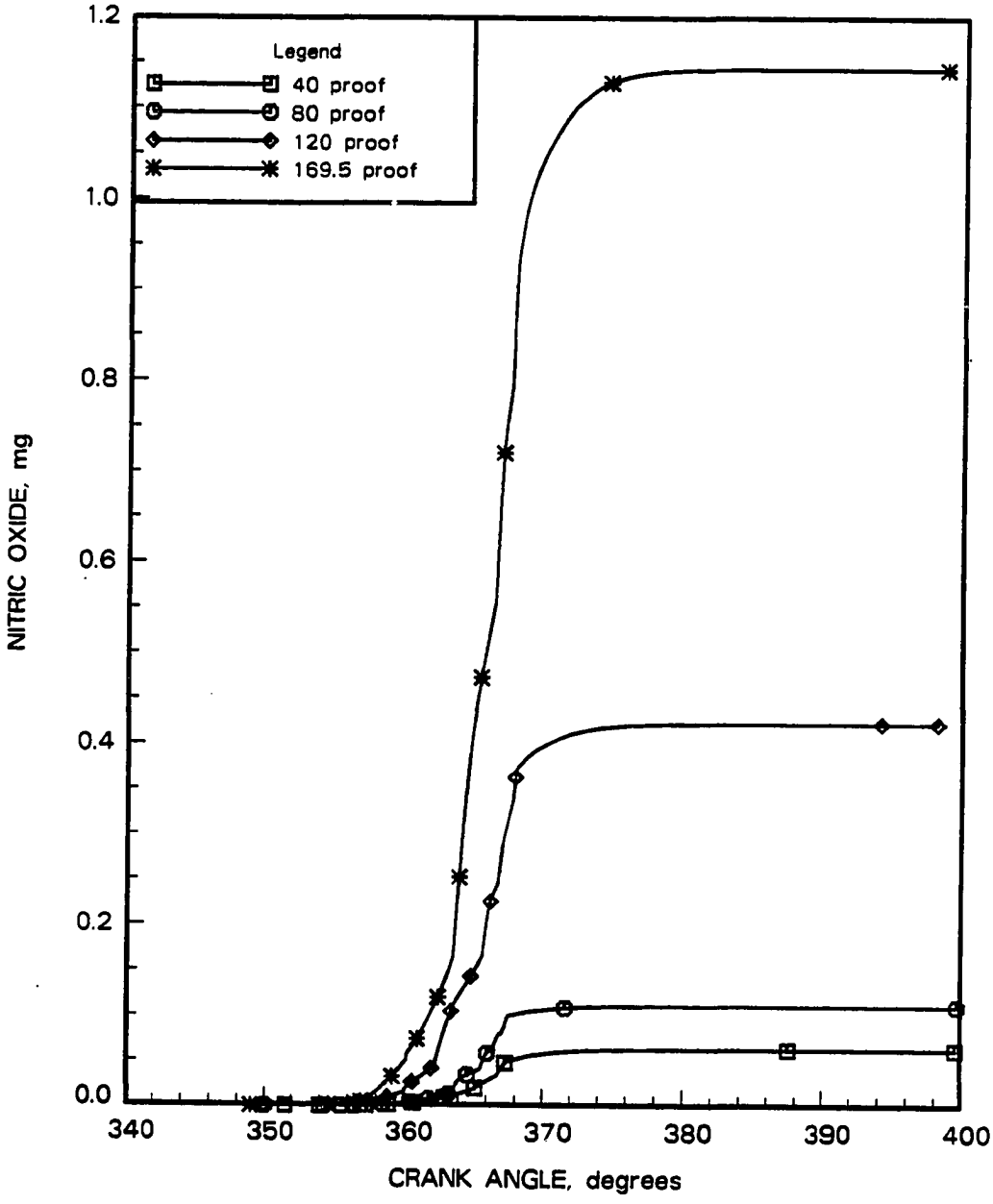

Figure 5.28: Variation of Nitric Oxide History in the Wall Zone, at 1500 rpm, for four different Ethanol Proofs, 30% Torque Replacement

between TDC and 20° after TDC, dictate the NO formation in the cylinder.

The NO kinetics are mainly governed by local equivalence ratio and temperature. Figure 5.29 and Figure 5.30 show the variations in the equivalence ratio and temperature with crank position, for the four different alcohol proofs.

The equivalence ratio of the wall zone remains nearly constant between 5° after TDC and the end of expansion. The equivalence ratio for the critical NO formation phase is around 0.66 to 0.70 for all the four cases. For the 40 proof alcohol case the equivalence ratio of the wall zone is 0.70, and for the other three proof levels, the equivalence ratio is between 0.66 and 0.67. Due to small variations in the equivalence ratio for the four different proof levels, it is unlikely that the change in equivalence ratio is responsible for the large differences in the NO level predicted by the model.

Temperature histories for the wall zone are given in Figure 5.30. For changes in the proof from 80 to 120, and 120 to 169.5, the temperature increase is 120 K, and 140 K respectively. The temperature increases by 20 K, for the proof increase from 40 to 80. Although the equivalence ratio is below stoichiometric, around 0.66 to 0.70 for all the four cases, the temperature difference causes different levels of NO formation. For the small temperature difference between 40 and 80 proof, the model correctly predicts a relatively modest increase in the NO concentration, from 126 ppm to 249 ppm. The large increases in the wall zone temperature increases the model-predicted NO level for the 120 proof ethanol fumigation to 970 ppm, and the value predicted for 169.5 proof ethanol to 2986 ppm.

In an actual engine, combustion in the wall zone is a distributed phenomena characteristic of a turbulent diffusion flame. Small packets of fuel and air burn under

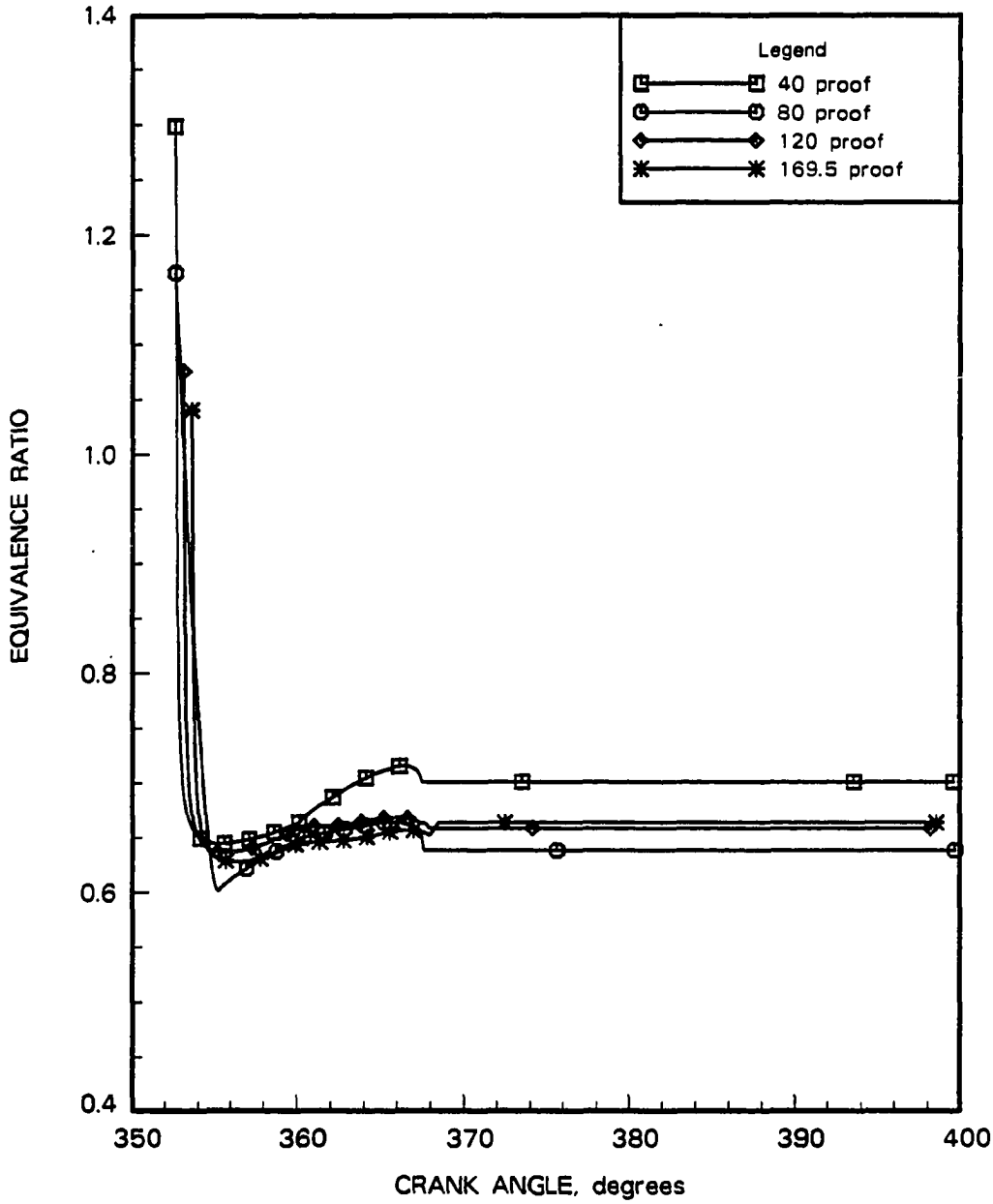

Figure 5.29: Equivalence Ratio History in the Wall Zone, at 1500 rpm, for four different Ethanol Proofs, 30% Torque Replacement

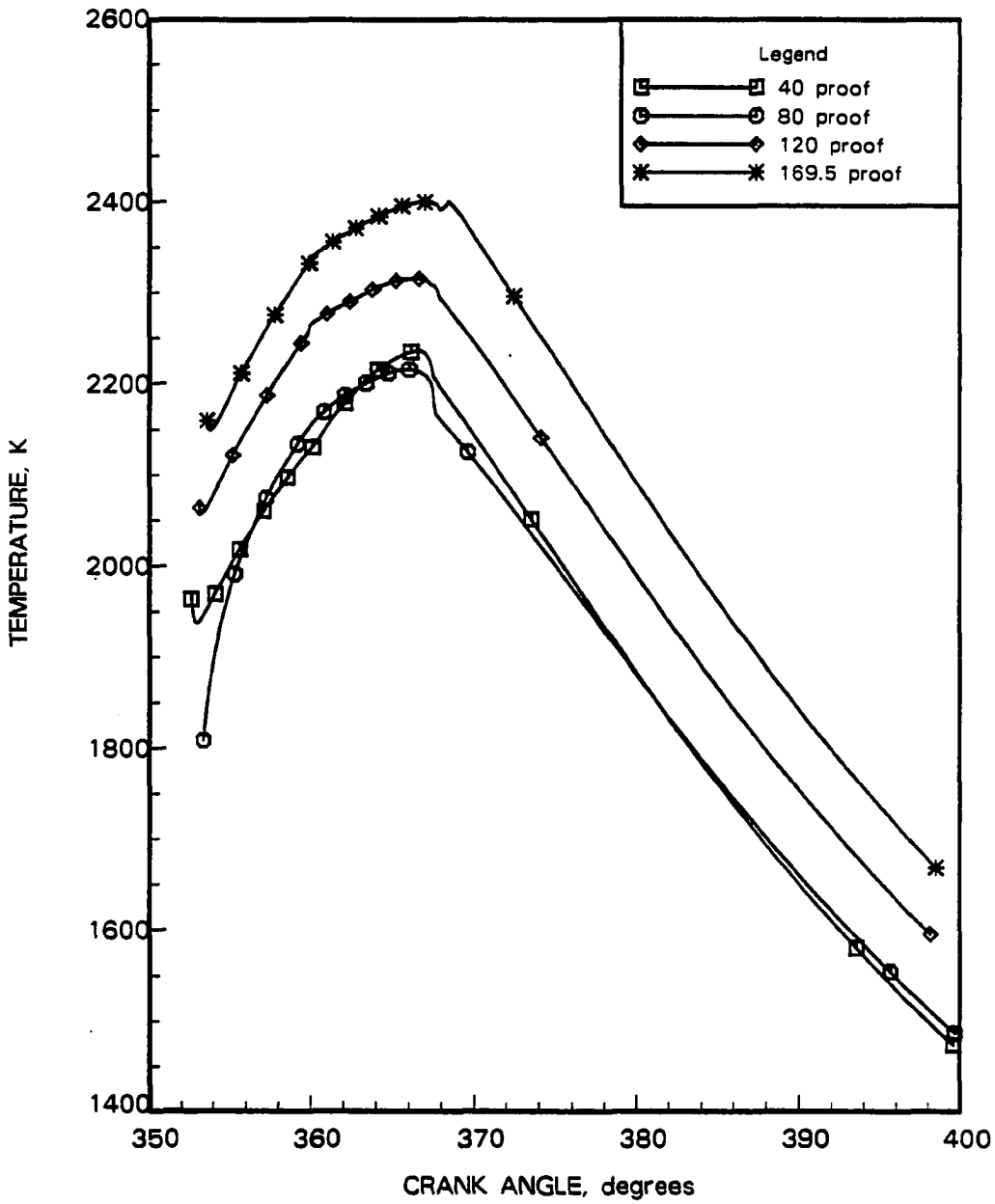

Figure 5.30: Temperature History in the Wall Zone, at 1500 rpm, for four different Ethanol Proofs, 30% Torque Replacement

conditions where the fuel-air mixture is nearly stoichiometric, resulting in higher NO production even at lower alcohol proofs. In the present model, the wall zone is treated as a single zone, with an overall lean equivalence ratio. This exaggerates the importance of the wall zone temperature. Fumigation of low proof alcohols with their larger fraction of water results in lower bulk temperatures during the cycle. Hence, NO formation is underpredicted at lower alcohol proofs.

Division of the wall zone into smaller zones, and accounting for combustion in the zones at equivalence ratios close to stoichiometric should enable the model to better predict the formation of nitric oxide.

The conclusions based on the present modeling effort, and attempts to validate the model using experimental data obtained on a fumigated diesel engine, are presented in the next chapter. Suggestions to improve the capability of the present model are also presented in the following chapter.

6. CONCLUSIONS

The objectives of this research were to develop a model to predict the performance and emission characteristics of a diesel engine fumigated with alcohol, and compare the performance predictions of the model with experimental data under a large variety of engine operating conditions to validate and improve the model. The purpose of this chapter is to summarize the model results as they relate to the objectives and then to propose recommendations for future research.

6.1 Summary

Comparison of model-predicted data with experimental measurements was carried out under a wide variety of operating conditions. Engine tests were conducted at two different speeds, and at four different loads at each speed. Both ethanol and methanol were used as the fumigated fuel. The alcohol proof was varied from 40 to 169.5 proof, and the alcohol flow was gradually increased to replace the engine's torque from 10 to 40%. Water was injected to isolate the effect of water contained in the fumigated alcohol on engine performance. The results are summarized below:

1. The model accurately predicted indicated mean effective pressure (IMEP) for both diesel-only and alcohol fumigated operation. Over the entire test matrix,

the model-predicted IMEP values are within 11% lower to 12% higher than experimental values.

2. The model does not predict changes in the indicated thermal efficiency with load. This is caused by the inability of the model to simulate longer combustion durations at higher loads.

3. The model correctly predicted trends in the exhaust temperature with changes in the engine speed and load and alcohol proof, for both diesel-only and alcohol fumigated operation.

4. The predicted exhaust temperatures are from 73 K lower to 11 K higher, for a nominal temperature range of 458 to 940 K, with diesel-only operation. With alcohol fumigation, the predicted values are within 105 K lower to 60 K higher than measured temperatures, for a nominal temperature range of 570 to 900 K.

5. With water injection, the model predictions matched fairly close with experimental data. Predicted IMEP is from 0.4% to 4.9% higher than measured values, and the exhaust temperature is within 9 K to 164 K lower than the measured temperature, over a nominal temperature range of 715 to 917 K.

6. The trends of exhaust NO were correctly predicted by the model. The NO level is predicted to decrease with load. With diesel-only operation, the model-predicted values of exhaust NO concentration are within -15% to +117% of the measured values. This is comparable to the NO prediction capability of other existing models for diesel combustion.

7. The model-predicted NO values for alcohol fumigated and water injected operation varied from -99% to +150% of the measured values. The use of a single-zone wall model has been suggested as the reason for the large discrepancies in the predicted NO levels.

6.2 Recommendations for Future Work

Several changes to the present multizone model are suggested in this section. These suggestions are based on the experience gained during the development, application, and verification of the model. The changes suggested here are expected to improve the capability of the model to better predict engine performance and emission characteristics.

6.2.1 Include heat transfer between individual zones

The formation of nitric oxide (NO) in the zones is a strong function of the zone temperature. To simplify the task of modeling, the heat transfer between the individual zones is neglected, as a first approximation in the present modeling work. Including the effect of heat transfer between the individual zones will provide more realistic temperature estimates for the zones resulting in better prediction of the formation of NO in the cylinder.

6.2.2 Improve the wall model

The wall model used for this study is based on several assumptions. A single wall zone with an equivalence ratio below stoichiometric is characteristic of the present

wall model.

The contents in the wall zone are heterogeneous, and the division of the wall zone into several smaller zones, allowing for combustion reactions close to stoichiometric should alleviate the problems in NO emission predictions.

Theoretically, the wall zone grows with time and the surface area of the zone would gradually increase, resulting in a proportional increase in the mass of alcohol. water and air mixture entrained from the lean zone. In order to model the entrainment on the basis of the shape of the wall zone, the wall zone structure proposed by Katsura et al. [59] in their recent work, could be used. Other wall jet models used by Dent and Mehta [11] and Mathur et al. [40] are based on experimental and theoretical efforts to understand the effect of wall impingement on entrainment and mixing. Meguerdichian and Watson [13] modified an existing correlation for a free jet to describe the wall jet. One or more of these approaches could improve the present wall model. resulting in better emission prediction capability.

In the present model. the wall zone is assumed to be a continuously growing. homogeneous mixture of burned products. To maintain the heterogenity in the cylinder contents, even after wall impingement, the wall zone can be divided into smaller zones in a method similar to that used for the main spray plume. This may also help to reduce the discrepancies in NO prediction.

6.2.3 Include premixed burning of alcohol-air mixture

A means of including premixed burning of the alcohol-air mixture in the spray is required to model the case of alcohol fumigation under high proof conditions.

6.2.4 Verify spray geometry

The penetration and cone angle of the diesel spray under conditions similar to those in the engine, must be confirmed with experiments in a constant volume bomb. This would help confirm and modify the correlations used in the present work.

6.2.5 Model other pollutants

Including sub-models to predict the formation of other pollutants such as carbon monoxide, particulates, and unburned hydrocarbons will help in identifying the sources for improving the present model, and greatly increase the usefulness of the model for engine development.

7. REFERENCES

[1] "*Federal Register*." Environmental Protection Agency, No. 51: 10607 (March 15, 1985).

[2] Amsden, A. A., Butler, T. D., O'Rourke, P. J., and Ramshan, J. D. "KIVA-A Comprehensive Model for 2-D and 3-D Engine Simulations." *SAE* Paper 850554 (1985).

[3] O'Rourke, P. J., and Amsden, A. A. "Three Dimensional Numerical Simulations of the UPS-292 Stratified Charge Engine." *SAE* Paper 870597 (1987).

[4] McKinley, T. J., Primus, R. J., O'Rourke, P. J., and Butler, T. D. "Comparison of Computed and Measured Air Motion in Circular and Square Piston Cups." *SAE* Paper 881612 (1988).

[5] Zur Loye, A. O., Siebers, D. L., McKinley, T. L., Ng, H. K., and Primus, R. J. "Cycle-Resolved LDV Measurements in a Motored Diesel Engine and Comparison with K-ε Model Predictions." *SAE* Paper 890618 (1989).

[6] Lyn, W. T. "Study of Burning Rate and Nature of Combustion in Diesel Engines." *Ninth Symposium (International) on Combustion. The Combustion Institute*, Pittsburgh, Pennsylvania (1963).

[7] Shipinski, J., Uyehara, O. A., and Myers, P. S. "Experimental Correlation Between Rate-of-Injection and Rate-of-Heat-Release in Disel Engines." *ASME* Paper 68-DGP-11 (1968).

[8] Kouremenos, D. A., Rakopoulos, C. D., and Hountalas, D. "Thermodynamic Analysis of Indirect Injection Diesel Engines by Two-zone Modeling of Combustion." *ASME Winter Annual Meeting*, Boston (1987).

[9] Van Gerpen, J. H., and Shapiro, H. N. "Second Law Analysis of Diesel Engine Combustion." *ASME Winter Annual Meeting*, Boston (1987).

[10] Gao, X., Chen, J., Je, Z., Foster, D., and Borman, G. "Ignition Delay and Heat Release Analysis of an Ethanol Fumigated Turbocharged Diesel Engine." *ASME* Paper No. 83-DGP-1 (1983).

[11] Dent, J. C., and Mehta, P. S. "Phenomenological Combustion Model for a Quiescent Chamber Diesel Engine." *SAE* Paper 811235 (1981).

[12] Dent, J. C., Mehta, P. S., and Swan, J. "A Predictive Model for Automotive DI Diesel Engine Performance and Smoke Emissions." *Instn. of Mech. Engrs. Conference.* "Diesel Engines for Passenger Cars and Light Duty Vehicles." London, England (1982).

[13] Meguerdichian, M., and Watson, N. "Prediction of Mixture Formation and Heat Release in Diesel Engines." *SAE* Paper 780225 (1978).

[14] Lipkea, W. H., and DeJoode, A. D. "A Model of a Direct Injection Diesel Combustion System for Use in Cycle Simulation and Optimization Studies." *SAE* Paper 870573 (1987).

[15] Chiu, W. S., Shahed, S. M., and Lyn, W. T. "A Transient Spray Mixing Model for Diesel Combustion." *SAE* Paper 760128 (1976).

[16] Rife, J., and Heywood, J. B. "Photographic and Performance Studies of Diesel Combustion with a Rapid Compression Machine." *SAE* Paper 740948 (1974).

[17] Jiang, Q., and Van Gerpen, J. H. "Prediction of Nitric Oxide Emissions from an Alcohol Fumigated Diesel Engine." *ISU-ERI-Ames* Report No. 89251, Engineering Research Institute, Iowa State University (1989).

[18] Dent, J.C. "A Basis for Comparison of Various Experimental Methods for Studying Spray Penetration." *SAE* Paper 710571 (1971).

[19] Hiroyasu, H., Kadota, T., and Arai, M. "Supplementary Comments: Fuel Spray Characterization in Diesel Engines." *Combustion Modeling in Reciprocating Engines*, J.N. Mattavi and C.A. Amann (Eds.), Plenum Press, New York (1980).

[20] Patrick, M. A. "Experimental Investigation of Mixing and Flow in a Round Turbulent Jet Injected Perpendicularly into a Transverse Stream." *Trans. Instn. Chem. Engrs.*, 45: 16-31 (1967).

[21] Shahed, S. M., Flynn, P. F., and Lyn, W. T. "A Model for the Formation of Emissions in a Direct-Injection Diesel Engine." *Combustion Modeling in Reciprocating Engines*, J. N. Mattavi and C. A. Amann (Eds.), Plenum Press, New York (1980).

[22] Shahed, S. M., Chiu, W. S., and Lyn, W. T. "A Mathematical Model of Diesel Combustion." *Instn. of Mech. Engrs. Conference.* "Combustion in Engines." Paper No. C 94/75, Cranfield, England (1975).

[23] Wakuri, Y., Fujii, M., Amitani, T., and Tsuneya, R. "Studies on the Penetration of Fuel Spray in a Diesel Engine." *Bulletin of JSME*, 3, No. 9: 123-130 (1960).

[24] Wilson, M., and Wallace, F. J. "A Comprehensive Phenomenological Model of the Jet Mixing Process in D.I. Diesel Engines." *SAE* Paper 861273 (1986).

[25] Adler, D., and Baron, A. "Prediction of a Three-dimensional Circular Jet in a Crossflow." *AIAA Journal*, 17: 2 (1978).

[26] Gupta, A. K., Mehta, P. S., and Gupta, C. P. "Model for Predicting Air-Fuel Mixing and Combustion for Direct Injection Diesel Engine." *SAE* Paper 860331 (1986).

[27] Abramovich, G.N. *The Theory of Turbulent Jets.*, The M.I.T. Press, MIT, Cambridge, Massachusetts (1963).

[28] Hoult, D. P., and Weil, J. C. "Turbulent Plume in a Laminar Crossflow." *Atmosperic Environment*, 6. Pergamon Press, Cambridge, England (1972).

[29] Hardenberg, H.O., and Hase, F.W. "An Empirical Formula for Computing the Pressure Rise Delay of a Fuel from its Cetane Number and from the Relevant Parameters of Direct-Injection Diesel Engines." *SAE* Paper 790493 (1979).

[30] Ferguson, C. R. "*Internal Combustion Engines - Applied Thermosciences.*" John Wiley and Sons, New York (1985).

[31] Lyn, W. T., and Valdmanis, E. "The effects of Physical Factors on Ignition Delay." *Proceedings of the Instn. of Mech. Engrs.*, Automobile Division, 181, England (1967).

[32] Eichelberg, G. "Some New Investigations on Old Combustion Engine Problems-II." *Engineering* 149: 547-549 (1939).

[33] Woschni, G. "A Universally Applicable Equation for the Instantaneous Heat Transfer Coefficient in the Internal Combustion Engine." *SAE* Paper 670931 (1967).

[34] Annand, W.J.D. "Heat Transfer in the Cylinders of Reciprocating Internal Combustion Engines." *Proceedings of the Instn. of Mech. Engrs.*, 177, No. 36: 973-990, England (1963).

[35] Kyriakides, S. C., Dent, J. C., and Mehta, P. S. "Phenomenological Diesel Combustion Model Including Smoke and NO Emission." *SAE* Paper 860330 (1986).

[36] Hayes, T. K., Savage, L. D., White, R. A., and Sorenson, S. C. "The Effect of Fumigation of Different Ethanol Proofs on a Turbocharged Diesel Engine." *SAE* Paper 880497 (1988).

[37] Van Meter, D., Van Gerpen, J. H., and Ottikkutti, P. "Performance and Emission Evaluation of Diesel Fuel Additive." *ISU-ERI-Ames* Report No. 88144. Engineering Research Institute, Iowa State University (1987).

[38] Valdmanis, E., and Wulfhorst, D. E. "The Effect of Emulsified Fuels and Water Induction on Diesel Combustion." *SAE* Paper 700736 (1970).

[39] Karim, G. A., and Zhaoda, Y. "An Analytical Model for Knock in Dual Fuel Engines of the Compression Ignition Type." *SAE* Paper 880151 (1988).

[40] Mathur, H. B., Gajendra Babu, M. K., and Prasad, Y. N. "A Thermodynamic Simulation Model for a Dual Fuel Open Combustion Chamber Compression Ignition Engine." *SAE* Paper 861275 (1986).

[41] Whitehouse, N. D., and Way, R. "Rate of Heat Release in Diesel Engines and its Correlation with Fuel Injection Data." *Proceedings of the Instn. of Mech. Engrs.*, 184, Pt. 3(J), England (1970).

[42] Glassman, I. *Combustion*. Second Ed. Academic Press Inc., New York (1987).

[43] Chigier, N.A., "The Atomization of Liquid Fuel Sprays." pp 183-200 in *Energy and Combustion Science*, N. Chigier (Ed.). Pergamon Press, Oxford, England (1976).

[44] Wallace, F.J., and Horner, J. "Droplet Histories in a Mixed-out Fuel-Air Field in High Swirl Diesel Type Combustion Chambers." *The Journal of Thermal Engineering*, Indian Soc. of Mech. Engrs., No. 1, 2, 1-16 (1981).

[45] Packer, J.P., Wallace, F.J., Adler, D., and Karimi, E.R. "Diesel Fuel Jet Mixing Under High Swirl Conditions." *Instn. of Mech. Engrs. Intl. Conference.* "Combustion in Engineering." Paper No. C 80/83, London, England (1983).

[46] Hiroyasu, H., and Kadota, T. "Fuel Droplet Size Distribution in Diesel Combustion Chamber." *SAE* Paper 740715 (1974).

[47] Hay, N., and Jones, P.L. "Comparison of the Various Correlations for Spray Penetration." *SAE* Paper 720776 (1972).

[48] *Petroleum Measurement Tables.* American Edn. ASTM, Philadelphia (1952).

[49] Taylor, D. H. C. *The Analysis of Fuel Spray Penetration and Distribution in a Medium Speed Diesel Engine Using Optical Techniques*, Ph.D. Dissertation, Loughborough University of Technology, England (1967).

[50] Williams, P. W. *Numerical Computation.* ELBS, The Camelot Press, Southampton, Great Britain (1980).

[51] Olikara, C., and Borman, G. L. "A Computer Program for Calculating Properties of Equilibrium Combustion Products with some Applications to I.C. Engines." *SAE* Paper 750468 (1975).

[52] Westenberg, A. A. "Kinetics of NO and CO in Lean, Premixed Hydrocarbon-Air Flames." *Combustion Science and Technology.* 4, No. 2: 59-64 (1971).

[53] "*Gauging Manual.*" Department of the Treasury, Bureau of Alcohol, Tobacco, and Firearms, U. S. Govt. Printing Office, Washington, D.C. (1978).

[54] Alkidas, A. C. "Relationship Between Smoke Measurements and Particulate Measurements." *SAE* Paper 840412 (1984).

[55] Jiang, Q., Ottikkutti, P., Van Gerpen, J., Van Meter, D. "The Effect of Alcohol Fumigation on Diesel Flame Temperature and Emissions." *SAE* Paper to be presented at the SAE Intl. Congress and Exposition, Detroit, Feb. 1990.

[56] Heisey, J. B., and Lestz, S. S. "Aqueous Alcohol Fumigation of a Single Cylinder DI Diesel Engine." *SAE* Paper 811208 (1981).

[57] Chen, J., Gussert, D., Gao, X., Gupta, C., and Foster, D., "Ethanol Fumigation of a Turbocharged Diesel Engine." *SAE* Paper 810680 (1981).

[58] Voiculescu, I. A., and Borman, G. L. "An Experimental Study of Diesel Engine Cylinder-Averaged NO_X Histories." *SAE* Paper 780228 (1978).

[59] Katsura, N., Saito, M., Senda, J., and Fujimoto, H. "Characteristics of a Diesel Spray Impinging on a Flat Wall." *SAE* Paper 890264 (1989).

[60] "*JANAF Thermochemical Tables.*" The Advanced Research Projects Agency, Washington, D.C., 1965.

[61] Krieger, R. B., and Borman, G. L. "The Computation of Apparent Heat Release for Internal Combustion Engines." *ASME* Paper 66-WA/DGP-4 (1966).

[62] Rossini, F. D., Pitzer, K. S., Arnett, R. L., Braun, R. M., and Primentel, G. C. "*Selected Values of Physical and Thermodynamic Properties of Hydrocarbons and Related Compounds.*" Carnegie Press, Carnegie Institute of Technology, Pittsburgh, Pennsylvania (1953).

[63] Green, J. H. S. "Thermodynamic Properties of the Normal Alcohols, C_1-C_{12}." *Journal of Applied Chemistry* 11: 397-404 (1961).

[64] Caretto, L. S. "Mathematical Modeling of Pollutant Formation." pp 49-73 in *Energy and Combustion Science*, N. Chigier (Ed.). Pergamon Press, New York (1976).

[65] Newhall, H. K., and Shahed, S. M. "Kinetics of Nitric Oxide Formation in High-Pressure Flames." *Thirteenth Symposium (International) on Combustion. The Combustion Institute*, Pittsburgh, Pennsylvania (1971).

[66] Baulch, D. L., Drysdale, D. D., Horne, D. G., and Lloyd, A. C. "*Evaluated Kinetic Data for High Temperature Reactions.*" Vol. 2. Butterworths, London, England (1973).

[67] Bowman, C. T. "Kinetics of Pollutant Formation and Destruction in Combustion." pp 35-47 in *Energy and Combustion Science.*, N. Chigier (Ed.). Pergamon Press, New York (1976).

8. APPENDIX A: EVALUATION OF PROPERTIES OF EQUILIBRIUM COMBUSTION PRODUCTS

This appendix describes the procedure used for obtaining the thermodynamic properties for zones containing equilibrium combustion products. The procedure for evaluating the properties of high pressure, high temperature air is also discussed.

A computer program called PER, which was developed by Olikara and Borman [51], is used to calculate the thermodynamic properties. PER deals with the the gas phase products of combustion of fuels containing C, H, O, and N atoms, burned in air. The program consists of two separate sections. The first section deals with the calculation of the concentrations of the equilibrium products of combustion species. The second section evaluates the thermodynamic properties u and R of the products, and their derivatives with respect to temperature, pressure, and equivalence ratio.

The combustion reaction is represented by the chemical reaction;

$$\begin{aligned} & x_{13}\left[C_nH_mO_lN_k + \frac{(n+\frac{m}{4}-\frac{l}{2})}{\phi}(O_2 + 3.7274N_2 + 0.0444Ar + jH_2O)\right] \\ \longrightarrow\ & x_1H + x_2O + x_3N + x_4H_2 + x_5OH + x_6CO + x_7NO + x_8O_2 \\ +\ & x_9H_2O + x_{10}CO_2 + x_{11}N_2 + x_{12}Ar \end{aligned} \tag{8.1}$$

The fuel is represented by the general molecule $C_nH_mO_lN_k$. The moles of water vapor per 4.7718 moles of dry air, contained in the intake air is given by j.

The equivalence ratio of the reacted mixture is represented by ϕ. x_1 through x_{12} are the mole fractions of the product species, and x_{13} is the moles of fuel required to produce one mole of products. The program requires as input, the fuel composition data, n, m, l, k, the system pressure, and temperature, and the equivalence ratio of the reacting fuel-air mixture.

The first section of the program solves for the thirteen unknowns (x_1 through x_{13}) in the chemical equation, using thirteen mathematical equations. Atom balances for the elements C, H, O, N, and Ar give five equations. The mole fraction of all the products must add up to unity and this results in the sixth equation. Equilibrium reaction equations among the products provides an additional set of seven equations. The thirteen equations are reduced by mathematical manipulations to four non-linear equations, and an iterative procedure is used to solve them.

The second section which deals with the calculation of enthalpy and internal energy of the equilibrium combustion products, obtains the values of the specific heats and the heats of formation of the individual species from the JANAF thermochemical tables [60]. Knowing the mole fractions of the species from the results of the first section, the specific enthalpy of the product, h, the average molecular weight, M, and the specific gas constant, R, are obtained from mass fraction weighted averages of the corresponding properties of the individual species.

The absolute internal energy of the product mixture with reference to 0 Kelvin is obtained using;

$$u = h - RT \tag{8.2}$$

The partial derivatives of the properties M, R, h, and u with respect to T, p, and o

are also calculated by differentiating the expressions with respect to the corresponding property.

The equilibrium constants and thermodynamic property data used in the subroutine PER are available for a temperature range between 167 K and 4000 K, and use of the property program is limited to this temperature range. The program cannot account for the formation of free carbon. For values of equivalence ratio exceeding the ratio

$$\left(\frac{n + 0.25m - 0.5l}{0.5n - 0.5l}\right) \tag{8.3}$$

free carbon will be formed. Hence the program is limited to values between zero and the limiting equivalence ratio defined above, for a given fuel. The products of combustion are assumed to be ideal gases.

PER can also be used to obtain the properties of pure air at a given pressure and temperature, by setting the equivalence ratio equal to zero. However, a non-zero number must be supplied for n and m, the moles of C and H in the fuel to allow the property program to function. The values of n and m do not affect the final property values for air, calculated by the property program.

In the present model, PER is called by the subroutine BURNDGAS that calculates the equilibrium thermodynamic properties and their derivatives for the individual zones containing burned products. The total moles of carbon, hydrogen, oxygen, and nitrogen in the zone, cylinder pressure, zone temperature, and the zone equivalence ratio are supplied as inputs to PER through a common statement named BLOC of the form:

```
.. COMMON /BLOC/ AN,AM,AL,AK,AJ,PHI,T,P,KLO,IERR,XEQ(13)
```

PROP is another named common statement:

```
      COMMON /PROP/ AVM,R,H,U,S,DRT,DHT,DUT,DST.DRP,DHP,DUP,DSP,
     &              DRF,DHF,DUF,DSF
```

PROP returns the required properties such as the molecular weight of the burned products in the zone, specific gas constant, specific enthalpy, specific internal energy, specific entropy, and their derivatives with respect to temperature, pressure, and equivalence ratio.

9. APPENDIX B: UNBURNED MIXTURE PROPERTY EVALUATION

This appendix outlines the procedure for evaluating the thermodynamic properties of an unburned mixture of diesel fuel vapor, alcohol vapor, water vapor, and air under both rich and lean conditions. The techniques used to express the properties of the mixture in terms of the properties of the constituents is explained, and the method for obtaining the molecular weight, gas constant, enthalpy, and internal energy of the constituents is described.

9.1 Mixture Properties

In the present model of a fumigated diesel engine, the cylinder contains a mixture of diesel fuel vapor, alcohol vapor, water vapor and air. The presence of residual gases in the cylinder is neglected. The water in the alcohol and water mixture evaporates and can be combined with the moisture present in the intake air.

The specific internal energy u of the individual components can be obtained by using the relationship: $u = h - RT$, where, h is the total specific enthalpy, R is the specific gas constant of the component, given by Ru/M. Ru is the universal gas constant and M is the molecular weight of the component. The specific heat at constant volume $C'v$ for the individual components can be obtained from $C'v = C'p - R$.

If the principal thermodynamic properties h_i and $C'p_i$ for the individual components of the unburned mixture are available, they can be combined to obtain the overall mixture properties. Let,

m_{dsl} = mass of diesel fuel

m_{eth} = mass of ethanol fuel

m_{wat} = mass of water added with the fumigated alcohol plus the mass of water vapor in the intake air

m_{air} = mass of dry air

α = the ratio of mass of alcohol to mass of dry air

β = the ratio of mass of water to mass of dry air

γ = the ratio of mass of diesel fuel to mass of dry air.

For the case of alcohol fumigation, which is the focus of this study, the ratio of alcohol to air, and water to air at any location in the cylinder is assumed uniform. and hence the values of α and β are constant for all the zones in the cylinder. The mass fraction y_i of each component in the mixture can be given by

$$y_{dsl} = \frac{\gamma}{(1+\alpha+\beta+\gamma)} \tag{9.1}$$

$$y_{eth} = \frac{\alpha}{(1+\alpha+\beta+\gamma)} \tag{9.2}$$

$$y_{wat} = \frac{\beta}{(1+\alpha+\beta+\gamma)} \tag{9.3}$$

$$y_{air} = \frac{1}{(1+\alpha+\beta+\gamma)} \tag{9.4}$$

If R_{dsl}, R_{eth}, R_{wat}, and R_{air} denote the specific gas constants of the individual

components, the specific gas constant of the mixture can be given by

$$R_{mix} = \sum_{i=1}^{4} y_i R_i \tag{9.5}$$

Hence,

$$R_{mix} = y_{dsl}R_{dsl} + y_{eth}R_{eth} + y_{wat}R_{wat} + y_{air}R_{air} \tag{9.6}$$

Similar expressions can be written for h_{mix}, and u_{mix}.

$$h_{mix} = y_{dsl}h_{dsl} + y_{eth}h_{eth} + y_{wat}h_{wat} + y_{air}h_{air} \tag{9.7}$$

$$u_{mix} = y_{dsl}u_{dsl} + y_{eth}u_{eth} + y_{wat}u_{wat} + y_{air}u_{air} \tag{9.8}$$

The average molecular weight of the unburned mixture is obtained from

$$M_{mix} = \frac{R_{mix}}{R_u} \tag{9.9}$$

For single fuel operation R_{mix}, h_{mix}, and u_{mix} are functions of pressure, temperature, and equivalence ratio. The equivalence ratio for a single fuel, is defined as the ratio of the actual fuel-air ratio to the stoichiometric fuel-air ratio. At moderate pressures, corresponding to those in an operating engine, R_{mix}, h_{mix}, and u_{mix} are weak functions of pressure and hence their dependence on pressure is usually neglected [61]. In a fumigated engine, R_{mix}, h_{mix}, and u_{mix} are functions of temperature, α, β, and γ. As mentioned above, α, and β remain fixed for a given operating condition. Based on these assumptions, R_{mix}, h_{mix}, and u_{mix} are functions of zone temperature and the mass ratio of diesel fuel to dry air, γ, in the zone.

To calculate the partial derivative $\partial R_{mix}/\partial T$ it is possible to use the expression for R_{mix} given by Equation 9.5. Differentiating Equation 9.5 with respect to

temperature gives

$$\frac{\partial R_{mix}}{\partial T} = \sum_{i=1}^{4} \frac{\partial y_i}{\partial T} R_i + \sum_{i=1}^{4} y_i \frac{\partial R_i}{\partial T} \tag{9.10}$$

For a zone containing unburned mixture, there is no chemical reaction and the composition of the zone remains fixed. Hence y_i's do not change with zone temperature, and the term $\partial y_i/\partial T$ is zero. Also, R_i is defined as the universal gas constant Ru divided by the molecular weight of the component, M_i. Both Ru and M_i are fixed, so R_i for the individual components of the mixture is a constant and is independent of temperature T. Hence, the term $\partial R_i/\partial T$ in Equation 9.10 is zero and $\partial R_{mix}/\partial T$ also becomes zero.

The mixture enthalpy, hmix, is expressed as:

$$h_{mix} = \sum_{i=1}^{4} y_i h_i \tag{9.11}$$

Differentiating Equation 9.11 with respect to temperature, and recognizing that $\partial y_i/\partial T$ is zero gives

$$\frac{\partial h_{mix}}{\partial T} = \sum_{i=1}^{4} y_i \frac{\partial h_i}{\partial T} = \sum_{i=1}^{4} y_i C_{p_i} \tag{9.12}$$

The values of C_{p_i} at a specific temperature for all the components can be obtained from the polynomial fits to published data.

The specific internal energy of the mixture, u_{mix}, can be expressed as:

$$u_{mix} = \sum_{i=1}^{4} y_i u_i \tag{9.13}$$

following a procedure similar to that for $\partial h_{mix}/\partial T$ above, an expression can be obtained for $\partial u_{mix}/\partial T$:

$$\frac{\partial u_{mix}}{\partial T} = \sum_{i=1}^{4} y_i C_{v_i} \tag{9.14}$$

The value of Cv_i for the individual components can be obtained from the relationship:

$$Cv_i = Cp_i - R_i \tag{9.15}$$

Since, R_{mix} for the unburned mixture does not depend on pressure or temperature, the partial derivatives $\partial R_{mix}/\partial p$, and $\partial R_{mix}/\partial T$, are zero. However, the value of R_{mix} is strongly dependent on the composition of the mixture. In the present situation, α, β, and γ specify the mixture composition. For a specified operating condition, the values of α, and β are fixed over the entire engine cycle, so the effect of change in α and β on the thermodynamic properties is ignored. However, γ does change so the derivative of R_{mix} and u_{mix} with respect to γ are needed. To obtain $\partial R_{mix}/\partial\gamma$, Equation 9.5 is differentiated to obtain

$$\frac{\partial R_{mix}}{\partial \gamma} = \sum_{i=1}^{4} \frac{\partial y_i}{\partial \gamma} R_i + \sum_{i=1}^{4} y_i \frac{\partial R_i}{\partial \gamma} \tag{9.16}$$

R_i denotes the gas constant of the individual component and is not a function of γ, so $\partial R_i/\partial\gamma$ is zero. Equation 9.16 becomes

$$\frac{\partial R_{mix}}{\partial \gamma} = \sum_{i=1}^{4} \frac{\partial y_i}{\partial \gamma} R_i \tag{9.17}$$

Equations 9.1, 9.2, 9.3, and 9.4 provide expressions for y_{dsl}, y_{eth}, y_{wat}, and y_{air}, respectively. These expressions can be differentiated with respect to γ to provide the values of $\partial y_i/\partial\gamma$ needed in Equation 9.17. If these derivatives are substituted into Equation 9.17, the following expression is obtained for $\partial R_{mix}/\partial\gamma$

$$\frac{\partial R_{mix}}{\partial \gamma} = \frac{1}{(1+\alpha+\beta+\gamma)^2}\left[(1+\alpha+\beta)R_{dsl} - \alpha R_{eth} - \beta R_{wat} - R_{air}\right] \tag{9.18}$$

The internal energy of the unburned mixture is also dependent on the ratio of the mass of diesel to the mass of air in the respective zones. By following a procedure

similar to that for $\partial R_{mix}/\partial\gamma$, the partial derivative $\partial u_{mix}/\partial\gamma$ can be expressed as

$$\frac{\partial u_{mix}}{\partial\gamma} = \frac{1}{(1+\alpha+\beta+\gamma)^2}\left[(1+\alpha+\beta)u_{dsl} - \alpha u_{eth} - \beta u_{wat} - u_{air}\right] \qquad (9.19)$$

Each of the expressions for mixture properties requires the properties of the individual components. The method for evaluating the thermodynamic properties of the individual components of the unburned mixture is described below.

Diesel Fuel Properties:

The specific enthalpy of diesel fuel was obtained by combining data from the actual diesel fuel analysis and the table of properties for hydrocarbons [62]. A chemical analysis of two batches of diesel fuel used for the engine tests was obtained, and the table of data is given in Appendix G. The averaged chemical composition of the two batches of diesel fuel used for the engine tests is $C_{13.78}H_{24.26}$ and the average lower heating value of the fuel is 42361.82 kJ/kg.

Based on the lower heating value of $C_{13.78}H_{24.26}$, the heat of formation of $C_{13.78}H_{24.26}$ at 298.15 K was calculated to be -73777.5 cal/gmole of fuel. In the present model, the thermodynamic datum temperature for evaluating the various thermodynamic properties is 0 K. Hence, the heat of formation h_f^0 of $C_{13.78}H_{24.26}$ was needed at a reference temperature of 0 K. This required that the enthalpy change of the diesel fuel from 0 K to 298.15 K be known. Normal dodecane, $C_{12}H_{26}$, is often used to represent diesel fuel and is considered to possess combustion properties very similar to that of No. 2 grade diesel fuel. The sensible enthalpy Δh, of n-dodecane can be obtained from the property table, for temperatures ranging from 0 K to 1300 K, with a reference temperature of 0 K [62].

The sensible enthalpy Δh of n-dodecane for the temperature range of 0 K to 1300 K obtained from the property table can be fit to a fourth degree polynomial:

$$\Delta h_{C_{12}H_{26}} = 2568.522 - 3746.896T_c + 140278.7T_c^2 - 53285.59T_c^3 + 9027.444T_c^4 \quad (9.20)$$

where, T_c=T(in Kelvin)/1000.

Knowing the heat of formation of $C_{13.78}H_{24.26}$ at 298.15 K, and the sensible enthalpy Δh of n-dodecane from 0 K to 298.15 K, the enthalpy of formation h_f^0 of $C_{13.78}H_{24.26}$ at 0 K was found to be -58346.6 cal/gmole. The total specific enthalpy of the actual diesel fuel at any temperature is given by the general expression

$$h(T) = h_f^0 + \Delta h(T) \quad (9.21)$$

Cp_{dsl} was obtained by differentiating Equation 9.20 for $\Delta h_{C_{12}H_{26}}$ with respect to temperature:

$$Cp_{dsl} = -3.747 + 280.557T_c - 159.857T_c^2 + 36.110T_c^3 \quad (9.22)$$

where, Cp_{dsl} is in units of cal/gmole/K.

Alcohol Properties:

The thermodynamic properties of methanol and ethanol were obtained from Green [63]. Green [63] lists the heats of formation of methanol and ethanol vapor at the reference temperature of 0 K as 45.34 kcal/gmole and 51.95 kcal/gmole respectively. The sensible enthalpy, for methanol and ethanol over a temperature range of 273.18 K to 1000 K are tabulated by Green [63]. This enthalpy data can be used to develop a polynomial expression for Δh. A polynomial for Cp can be obtained by

differentiating the equation for Δh with respect to temperature. The polynomials for Δh and Cp, for both methanol and ethanol vapor are:

Methanol:

$$\Delta h_{meth} = 888.68 - 1308.43T_c + 19849.40T_c^2 - 12789.20T_c^3 + 7351.73T_c^4 - 1939.66T_c^5 \quad (9.23)$$

$$Cp_{meth} = 1.308 + 38.979T_c - 38.368T_c^2 + 29.407T_c^3 - 9.698T_c^4 \quad (9.24)$$

Ethanol:

$$\Delta h_{eth} = 904.59 + 173.0T_c + 30951.99T_c^2 - 12778.08T_c^3 + 2519.69T_c^4 \quad (9.25)$$

$$Cp_{eth} = 0.173 + 61.904T_c - 38.334T_c^2 + 100.788T_c^3 \quad (9.26)$$

where,

T_c = $T_K/1000.0$,

T_K = temperature in Kelvin,

Δh = sensible enthalpy in cal/gmole, and

Cp = specific heat at constant pressure in cal/gmole/K.

Knowing the heat of formation h_f^0 and the sensible enthalpy Δh, at any given temperature, the total specific enthalpy h can be obtained from Equation 9.21.

Water Vapor Properties:

The enthalpy and specific heat of water vapor are obtained from the JANAF thermochemical tables [60]. The heat of formation of water vapor with reference to 0 K is -57101 cal/gmole. The sensible enthalpy of water vapor, Δh_{wat} with reference to

0 K for a temperature range of 300 K to 1300 K was fit to a third degree polynomial:

$$\Delta h_{wat} = 103.663 + 7268.936T_c - 1048.797T_c^2 + 159.439T_c^3 \qquad (9.27)$$

As with diesel fuel and alcohol, the total enthalpy is obtained by adding the enthalpy of formation to the sensible enthalpy as shown in Equation 9.21. The specific heat at constant pressure $C'p_{wat}$ is given by

$$C'p_{wat} = \frac{(7268.936 + 2097.594T_c + 478.3164T_c^2)}{1000} \qquad (9.28)$$

where, $C'p_{wat}$ is in cal/gmole/K.

Air Properties:

The principal thermodynamic properties for dry air can be obtained from the thermodynamic property routine for equilibrium combustion products PER as described in Appendix A.

Summary:

The equations discussed in this appendix are coded into a Fortran subroutine MIXPROP. The inputs to this property routine are pressure, in bars, temperature in Kelvin, an alcohol indicator, to specify if methanol or ethanol is used, and the mass ratios α, β, and γ. The properties returned by MIXPROP are, R_{mix} in kJ/kg/K, h_{mix} in kJ/kg, u_{mix} in kJ/kg, $\partial h_{mix}/\partial T$ in kJ/kg/K, $\partial u_{mix}/\partial T$ in kJ/kg/K, $\partial R_{mix}/\partial \gamma$ in kJ/kg/K, and $\partial u_{mix}/\partial \gamma$ in kJ/kg. The partial derivatives $\partial R_{mix}/\partial p$, $\partial h_{mix}/\partial p$, and $\partial u_{mix}/\partial p$ are assumed zero, since, R_{mix}, h_{mix}, and u_{mix} for an unburned mixture are very weak functions of pressure. The inputs to MIXPROP

from the calling program, and the properties returned by MIXPROP are handled by using a labelled subroutine declaration:

```
      SUBROUTINE MIXPROP (pz,Tz,INDALC,alphap,betap,gamap,Rmix,
     &                    Hmix,Umix,DHTmix, DUTmix,DRGmix,DUGmix)
```

10. APPENDIX C: BURNED GAS PROPERTY EVALUATION FOR TWO FUELS

The procedure used for obtaining the properties of the products of combustion for the two fuels is explained in this appendix.

In a conventional diesel engine, only a single fuel is burned in air. For single fuel hydrocarbon-air combustion, the equivalence ratio ϕ is defined as the actual fuel-air ratio divided by the stoichiometric fuel-air ratio. The stoichiometric fuel-air ratio is the exact mass of air required to burn one mole of fuel completely to form carbon dioxide and water. The thermodynamic properties and their partial derivatives for the burned products of combustion for the case of single fuel can be obtained by using the property routine for combustion products, PER, described in Appendix A. This same subroutine can be used for the case of two fuels but the input arguments must be modified to reflect both fuels. The steps required to use PER to calculate the properties for the combustion products of two fuels in air follows.

To utilize PER for obtaining the properties of the equilibrium products of combustion, the two fuels must be combined into an equivalent pseudo-fuel molecule. To illustrate the process of combining two fuels, an example involving diesel fuel, $C_{13.78}H_{24.26}$, and ethanol-water mixture, is considered. In general terms the reac-

tion in the standard form required by PER is

$$X_1' C_{13.78} H_{24.26} + X_2' C_2 H_5 OH + X_3' H_2 O + 1(O_2 + 3.7274 N_2 + 0.0444 Ar + j H_2 O) \longrightarrow (\text{Equilibrium Products of Combustion}) \quad (10.1)$$

where X_1', X_2', and X_3' are the moles of $C_{13.78}H_{24.26}$, C_2H_5OH, and H_2O based on the measured flow rates of diesel fuel, ethanol, water, and dry air for the specified engine operating condition. Thus, X_1', X_2', and X_3' can be given by

$$X_1' = 4.7718\gamma(\frac{M_{air}}{M_{dsl}}) \quad (10.2)$$

$$X_2' = 4.7718\alpha(\frac{M_{air}}{M_{eth}}) \quad (10.3)$$

$$X_3' = 4.7718\beta(\frac{M_{air}}{M_{wat}}) \quad (10.4)$$

where α, β, and γ are the mass ratios of alcohol to air, water to air and diesel fuel to air, respectively, and M_{dsl}, M_{eth}, M_{wat}, and M_{air} are the molecular weights of diesel fuel, ethanol, water and air, respectively. For a specific operating condition of the engine, α, and β are uniform throughout the cylinder for the entire cycle. The diesel fuel and ethanol can be combined to form an equivalent fuel, $C_{n_{eq}} H_{m_{eq}} O_{l_{eq}} N_{k_{eq}}$. The number of moles of carbon, hydrogen, oxygen, and nitrogen in the equivalent fuel are:

$$C = n_{eq} = n_{dsl} X_1' + n_{eth} X_2' \quad (10.5)$$

$$H = m_{eq} = m_{dsl} X_1' + m_{eth} X_2' + m_{wat} X_3' \quad (10.6)$$

$$O = l_{eq} = 0.0 + l_{eth} X_2' + l_{wat} X_3' \quad (10.7)$$

$$N = k_{eq} = 0.0 \quad (10.8)$$

For the case of diesel fuel and ethanol, l_{dsl}, k_{dsl}, k_{eth}, and k_{wat} are zero. The equivalence ratio of the equivalent fuel depends on the mole fractions of the individual fuels, and can be represented by the functional relationship

$$\phi_{eq} = f(X_1', X_2', X_3') \tag{10.9}$$

The mole fractions can be expressed in terms of the moles of carbon, hydrogen, and oxygen in the equivalent fuel. Once the equivalent hydrocarbon fuel is obtained, the equivalence ratio ϕ_{eq} for this pseudo-fuel can be obtained by combining Equations 10.5, 10.6, 10.7, and 10.9 to give the following expression

$$\phi_{eq} = n_{eq} + (\frac{m_{eq}}{4}) - (\frac{l_{eq}}{2}) \tag{10.10}$$

PER can now be called with the calculated values of n_{eq}, m_{eq}, l_{eq}, k_{eq}, and o_{eq}, at the specified cylinder pressure, and the zone temperature. PER then provides the equilibrium concentrations of the product species, the average molecular weight of the product gas, M_{gas}, the thermodynamic properties; R_{gas}, h_{gas}, u_{gas}, and their partial derivatives; $\partial R_{gas}/\partial p$, $\partial h_{gas}/\partial p$, $\partial u_{gas}/\partial p$, $\partial R_{gas}/\partial T$, $\partial h_{gas}/\partial T$, and $\partial u_{gas}/\partial T$.

For the products of single-fuel combustion, the properties, of the products are functions of p, T, and ϕ. But in the two fuel case, ϕ_{eq} is dependent on the mass ratios, α, β, and γ. Hence, the properties R_{gas}, h_{gas}, and u_{gas} of the products are functions of p, T, α, β, and γ. The values of α and β do not change during a particular operating condition. Hence, the partial derivatives of R_{gas}, h_{gas}, and u_{gas} with respect to α, and β are not calculated.

One method to determine the partial derivatives of R_{gas} and u_{gas} with respect to γ is to modify the equations for $\partial R/\partial \phi$, and $\partial u/\partial \phi$, in PER. A simpler method

for obtaining these partial derivatives is to use a simple finite-differencing procedure such that

$$\frac{\partial R_{gas}}{\partial \gamma} \cong \frac{\Delta R}{\Delta \gamma} = \frac{R(\gamma + \Delta\gamma) - R(\gamma - \Delta\gamma)}{2(\Delta\gamma)} \tag{10.11}$$

The value of $\Delta\gamma$ can be set to be a very small fraction of γ. A number of values for this fraction were investigated and the use of 0.001 has been found to give the best results.

In the present model, the subroutine BURNDGAS is used to combine the diesel fuel and the alcohol-water mixture to form an equivalent pseudo-fuel, and calculate the equivalence ratio ϕ_{eq} for the individual zones. BURNDGAS calls the subroutine PER to obtain the product species concentration, the average molecular weight of the products M_{gas}, thermodynamic properties R_{gas}, h_{gas}, and u_{gas}, and their partial derivatives with respect to p, and T. The inputs to BURNDGAS are the cylinder pressure in bars, zone temperature in Kelvin, an alcohol indicator to specify if methanol or ethanol is used, and the mass ratios α, β, and γ. The properties returned by BURNDGAS are, R_{gas} in kJ/kg/K, h_{gas} in kJ/kg, u_{gas} in kJ/kg, $\partial R_{gas}/\partial p$ in kJ/kg/K/bar, $\partial h_{gas}/\partial p$ in kJ/kg/bar, $\partial u_{gas}/\partial p$ in kJ/kg/bar, $\partial R_{gas}/\partial T$ in kJ/kg/K^2, $\partial h_{gas}/\partial T$ in kJ/kg/K, $\partial u_{gas}/\partial T$ in kJ/kg/K, $\partial R_{gas}/\partial \gamma$ in kJ/kg/K, and $\partial u_{gas}/\partial \gamma$ in kJ/kg. The inputs to BURNDGAS from the calling program, and the properties returned by BURNDGAS are transferred by a labelled subroutine declaration:

```
SUBROUTINE BURNDGAS (pz,Tz,INDALC,alphap,betap,gamap,AVMgas,Rgas,
&                    Hgas,Ugas,DRTgas, DHTgas,DUTgas,DRPgas,
&                    DHPgas,DUPgas,DRGgas, DUGgas,X1gas,X2gas,
```

```
&                                X3gas,X5gas.X7gas, X8gas,X11gas)
```

X1gas, X2gas, X3gas, X5gas, X7gas, X8gas, and X11gas are the equilibrium concentrations of H, O, N, OH, NO, O_2, and N_2 in moles per mole of the product, returned by PER.

The procedure developed to obtain the thermodynamic properties and their partial derivatives for the equilibrium products of combustion in a fumigated engine has been described in this appendix. In addition, the subroutine BURNDGAS also provides the equilibrium concentrations of seven species in the product. The concentrations of six of these species are used to determine the rate of formation or destruction of nitric oxide as described in Appendix F.

11. APPENDIX D: INSTANTANEOUS BURNING OF NEWLY CREATED ZONES

In the present multizone transient spray model, the combustion of newly evolved B_i zones is assumed to occur instantaneously as discussed in Chapter 3. The burning of a new B_i zone affects the thermodynamic states of the other non-burning zones such as, zone A, and zone C, and the zones containing previously burned products such as, zone D, and the previously formed B_i zones. A systematic procedure to set-up the relevant thermodynamic equations for each zone in the cylinder, and solve these equations simultaneously has been developed. The method used in the present model to determine the final states of all the zones in the cylinder, after the instantaneous combustion of a newly created B_i zone, is described in this appendix.

The newly created B_i zones are bounded by the rich core boundary with an equivalence ratio corresponding to the rich limit of combustion (assumed to be 3.0 for fumigated operation with diesel and alcohol), and the inner boundary of a previously formed B_i zone. The inner boundary of the previously formed B_i zone has an equivalence ratio between the rich and lean limit, with a value closer to the rich limit. The overall equivalence ratio of this new zone, though rich, is within the flammability limit and hence is capable of spontaneous combustion. It is assumed for the purpose of this model that as long as the B_i zone is part of the rich core zone, it

does not burn. When the zone has acquired enough diesel fuel from the core zone C, it is capable of separation from zone C. The zone is then recognized as a new B_i zone, with the value of i, incremented by one over the zone formed in the last crank step. The zone division process is only capable of indicating the formation of new B_i zones. Once the new B_i zone is formed it is burned instantaneously. The process of instantaneous burning of the new B_i zone is governed by the fundamental laws of thermodynamics. If the thermodynamic state of the unburned B_i zone is specified, the final state of this zone after instantaneous burning can be obtained by solving the necessary thermodynamic equations.

Consider the burning of a newly evolved B_i zone at a fixed crank position θ, with $i = n - 3$ where, n is the total number of zones formed at θ. The zones, A, C, D, and previously burned B_i zones, with $i = 4$ to $i = n - 1$ do not undergo any chemical reaction during the instantaneous combustion of the new B_i zone. The instantaneous nature of the burning process means that the total cylinder volume does not change during burning, and hence no work is done. Also, there is no time for heat transfer to occur, and the mass of the cylinder contents and the mass of individual zones is conserved. Hence, the first law energy equation becomes:

$$\Delta U = 0 \tag{11.1}$$

This implies that the total internal energy of the cylinder contents after the instantaneous burning of zone B_{n-3}, should be equal to the total internal energy of the cylinder before burning.

$$\sum_{i=1}^{n} U_{F,i} = \sum_{i=1}^{n} U_{I,i} \tag{11.2}$$

where, the subscript F refers to the final state of the zones at the end of combustion, and the subscript I refers to the initial state of the zones before combustion of zone B_{n-3}. The initial total internal energy of the cylinder can be obtained from the property routines for the unburned mixture, and the burned products.

The total final internal energy of the cylinder must be obtained to compare with the total initial internal energy of the cylinder. The condition at which the two quantities are equal, defines the final state of the individual zones after zone B_{n-3} is burned completely. In order to obtain the final internal energy of the individual zones, the final cylinder pressure, and the temperatures of the individual zones are required. The diesel to air mass ratio of the zones remains constant during the process, as there is no mass transfer between the zones. For the n zones in the cylinder the number of unknowns to be determined at the end of the burning of zone B_{n-3} will be (2n−1). The final cylinder pressure p_F, the final temperatures, $T_{F,i}$, and volumes, $V_{F,i}$ for each of the n zones. A first guess for the final cylinder pressure is assumed to be slightly higher than the initial cylinder pressure before the instantaneous combustion of zone B_{n-3}.

In the absence of heat transfer isentropic compression is assumed for all the non-burning zones. The contents in each zone are assumed to behave as an ideal gas. Combining the ideal gas equation, and the equation for an isentropic process, the final temperature of each zone is calculated. The specific internal energy of the individual zones is then obtained from either MIXPROP or BURNDGAS, detailed in Appendices B, and C respectively. The total final internal energy of the cylinder contents is calculated and compared with the total initial internal energy. If the final

internal energy is lower than the initial internal energy, the final cylinder pressure is incremented slightly, and the process of calculating the new final internal energy is repeated. Thus an iterative procedure involving the final cylinder pressure is used to obtain the final state of all the zones in the cylinder. The details of this iterative process follow.

During the instantaneous burning of zone B_{n-3}, the chemical composition of all the other zones is unchanged. There is no heat transfer between the zones, and there is no mass transferred across the boundary of any of the zones. Hence, all zones other than zone B_{n-3} can be assumed to undergo an isentropic process represented by

$$T_{F,i} = T_{I,i}(\frac{p_F}{p_I})^{\frac{(k_{F,i}-1)}{k_{F,i}}} \tag{11.3}$$

where, $T_{I,i}$ is the initial temperature of zone i, p_I is the initial cylinder pressure, p_F is the assumed final cylinder pressure, and $k_{I,i}$ is the isentropic exponent for zone i evaluated at the final pressure and temperature. In practice $k_{F,i}$ is very nearly equal to $k_{I,i}$. The isentropic exponent k_i of the zone i, is the ratio of the specific heat at constant pressure, Cp, to the specific heat at constant volume, Cv. These properties are provided by the property routines for the unburned mixture, and the burned products. The isentropic exponent k_i is a constant for the non-reacting zones, hence k_i and k_f are equal. For the previously burned zones, variation in the cylinder pressure and zone temperature resulting from the instantaneous burning of the new B_i zone cause changes in the zone composition.

The volume of each zone can be computed from the ideal gas equation:

$$V_i = \frac{m_i R_i T_i}{p} \tag{11.4}$$

The sum of the volumes of all the zones must equal the cylinder volume, V_{cyl}, at the specified crank position.

$$V_{cyl} = \sum_{i=1}^{n} V_i \tag{11.5}$$

Substituting for V_i from Equation 11.4 in Equation 11.5:

$$V_{cyl} = \sum_{i=1}^{n} \frac{m_i R_i T_i}{p} \tag{11.6}$$

The post-combustion volume of the newly burned zone is estimated by subtracting the volumes of the other zones from the total cylinder volume. Then the post-combustion temperature of this zone can be calculated using the ideal gas equation with the gas constant estimated from the previous iteration.

With the calculation of the updated final temperature of the burning zone, B_{n-3}, the final pressure P_F, and the final temperature $T_{F,i}$ of all the n zones is available. The final specific internal energy $u_{F,i}$ of all the zones is then obtained from the property routines for unburned mixture or burned products, as the case may be. The values of P_F, $T_{F,i}$ and the diesel to air ratio γ_i, are the inputs to the property routines to obtain $u_{F,i}$ for all the zones. The total final internal energy of the cylinder contents is given by

$$U_F = \sum_{i=1}^{n} m_i u_{F,i} \tag{11.7}$$

The error between the final and initial total internal energy is calculated using

$$\%Error = \frac{(U_I - U_F)}{U_I} \times 100 \tag{11.8}$$

If the error is less than 0.01%, it is assumed that convergence has occurred, and the final cylinder pressure, and the final zone temperatures represent the right solution. If the error is larger than 0.01%, the final cylinder pressure can be incremented

slightly and the solution procedure is repeated beginning with Equation 11.3. To speed convergence of the solution process, the Secant Method [50], of guessing new p_F values is adopted in the present model.

The Fortran subroutine used to model the process of instantaneous combustion of the newly evolved B_i zones is BURNBZ. The main program calls BURNBZ immediately after a new B_i zone is formed. The cylinder pressure, zone temperatures, and zone volumes after the instantaneous combustion of the new B_i zone are returned by BURNBZ to the main program.

12. APPENDIX E: WALL IMPINGEMENT MODEL

In the present multizone model, the burned products of combustion at the spray tip impinge on the wall. A new wall zone, zone D, is initiated to form as soon as the spray reaches the wall The spray contents impinging on the wall are removed from the spray plume and added to a wall zone, zone D. This mass transfer process is assumed to occur instantaneously. Once zone D is formed, the mass removed from the spray is mixed with the mass previously existing in zone D. This mixing process is also assumed to be instantaneous. As the combustion proceeds more and more of the mass is transferred to zone D and an increasing number of B_i zones are depleted. The final states of the zones in the spray plume at the end of the instantaneous transfer and mixing process are determined by the present model. A Fortran subroutine MIXINGZ has been developed to model the instantaneous mass transfer and mixing processes. This subroutine determines the cylinder pressure, individual zone temperatures, and zone volumes at the end of mixing in zone D. The techniques used to model the effects of wall impingement, and the underlying assumptions are described in this appendix.

12.1 Division of the Combustion Period into Discrete Phases

In the present model, the entire combustion period is divided into five discrete phases. In the first phase, fresh fuel is injected into the spray, and the spray tip is not

at the bowl wall. In this phase there is no mass transfer from the spray to the wall zone. Hence, the wall zone, does not exist during the first phase. The second phase begins when the spray tip just impinges on the wall. Diesel fuel injection continues during this phase. The model assumes that the mass of diesel fuel contained in the spray plume is a constant during the second phase. By this approach a pseudo-steady spray is modeled, such that the mass of diesel fuel entering the tail of the spray plume is equal to the mass of burned diesel fuel leaving the spray plume at the tip of the spray. To maintain a pseudo-steady spray, the burned B_i zones are gradually stripped from the tip of the spray and transferred to the wall zone, zone D. The B_i zones transferred to zone D, have been previously burned and contain burned products. The mass of contents transferred from these burned B_i zones to zone D, is in proportion to the mass of diesel fuel required to be transferred out of the spray plume to maintain a pseudo-steady state. At the end of diesel injection, phase three begins, and the spray plume begins to move away from the fuel nozzle towards the bowl wall.

During the third phase, diesel fuel is stripped off from the spray plume at a constant rate corresponding to the injection rate during the last one degree of the diesel injection period. Although no additional diesel fuel is added to the core zone, additional B_i zones continue to form. The newly formed B_i zones are instantaneously burned as described in Appendix D. When all the B_i zones and the C zone have been transferred to zone D, only two discrete zones, zone A, and zone D, remain in the cylinder.

Phase four begins when the cylinder consists of only zone A, and zone D. The

entrainment rates of the mixture of air, water, and alcohol from zone A to all the B_i zones, and zone C are prescribed by the spray correlations discussed in Chapter 3 (Multizone Spray Model). The transfer of the mixture of air, water, and alcohol from zone A, to zone D, is assumed to be:

$$m_{awa,A-D} = \frac{m_{dsl,A}(\theta_1) + m_{awa,A}(\theta_1)}{K_{AD}}(\theta_2 - \theta_1) \qquad (12.1)$$

where $m_{awa,A-D}$ is the mass of air, water, and alcohol transferred from zone A to zone D, between crank angles θ_1 and θ_2. K_{AD} is a constant assumed by the present model and is given a value of 30. Use of Equation 12.1 gradually empties zone A and when all the air, water, and alcohol has been transferred to zone D, the small quantity of diesel fuel in zone A, is also completely transferred to zone D. The complete transfer of zone A into zone D, ends phase four. In phase five the entire cylinder is made up of one homogeneous zone, zone D, and phase five is continued up to opening of the exhaust valve.

12.2 Instantaneous Mixing in Zone D

The transfer of previously burned B_i zones to zone D is modeled with an instantaneous mixing process. The spray model predicts the formation of new B_i zones, and the newly evolved B_i zones are burned instantaneously as explained in Appendix D. In the absence of wall impingement, as in phase one, the burning of the new B_i zone is followed by a volume change in the cylinder, as the crank is rotated to the next new B_i zone formation point. But when the spray is impinging on the wall, the process of volume change, together with the transfer of mass from one or more B_i zones to zone D, results in a more complex solution procedure to obtain the re-

quired thermodynamic properties of the cylinder contents. A simplification that can be applied to the process without significantly affecting the final solution is to assume instantaneous transfer of B_i zones to zone, D, followed by cylinder volume change between two consecutive new B_i zone formation crank positions. For better results, the mass of diesel required to form new B_i zones is kept small enough, so that additional B_i zones are formed between small increments in the crank position.

The cylinder pressure p_I, zone temperatures $T_{I,i}$, zone volumes $V_{I,i}$, and the zone masses $m_{dsl_{I,i}}$ and $m_{awa_{I,i}}$ are specified by the final values of these parameters at the end of instantaneous burning of the latest B_i zone. The subscript I refers to the initial state of the zones before the instantaneous mixing process. The subscripts *dsl*, and *awa* refer to diesel and the air, water, and alcohol mixture in each zone, i. The transfer of zones from the spray plume to zone D, takes place instantaneously at a fixed crank position. Consider the transfer of m zones from the tip of the spray plume into zone D, at the beginning of phase two. Before zone D is inititated the spray plume contained $n-2$ zones: zone C, and all the B_i zones. Zone A, is outside of the spray plume and is not considered as part of the spray. After the instantaneous transfer of m B_i zones to zone D, the spray will contain $n-2-m$ zones. The wall zone, zone D, is assigned a zone number of $i=3$, and is just formed at the beginning of phase two. The newly created wall zone, zone D, contains m zones, that are well mixed after they are transferred into zone D, and hence zone D, is treated as a single well mixed homogeneous zone. The total number of zones in the cylinder after the instantaneous transfer and mixing becomes $3+n-3-m$. The unburned zones, zone A, and zone C, do not undergo any chemical reaction during the instantaneous

transfer of B_i zones to zone D. The B_i zones which are not transferred to zone D, may undergo chemical reaction due to the change in the conditions of the cylinder contents as a result of the instantaneous transfer and mixing. However, the chemical reaction in the B_i zones will follow a shifting equilibrium. The instantaneous nature of the transfer process requires that the total cylinder volume does not change during mixing, and hence no work is done by or on the engine shaft. Also there is no time for heat transfer to occur, and the total mass of the cylinder contents, and the masses of zone A, zone C, and the B_i zones that are not transferred to zone D, are conserved. The first law energy equation becomes:

$$\Delta U = 0 \tag{12.2}$$

for the entire cylinder. This implies that the total internal energy of the cylinder contents after the instantaneous transfer and mixing, should be equal to the total internal energy of the cylinder before the transfer.

$$\sum_{i=1}^{n} U_{F,i} = \sum_{i=1}^{n} U_{I,i} \tag{12.3}$$

where, the subscript F refers to the final state of the zones at the end of instantaneous transfer and mixing process, and the subscript I refers to the initial state of the zones before the mass transfer and mixing processes.

The total final internal energy of the cylinder must be obtained to compare with the total initial internal energy of the cylinder. The thermodynamic condition at which the two quantities are equal, defines the final state of the individual zones, after the instantaneous transfer and mixing is completed. In order to obtain the final specific internal energy of the individual zones, the final cylinder pressure, the final

temperatures of the individual zones, and the final mass of each zone are required. The diesel to air ratio of all the unaffected zones remains constant during the transfer process. The mass and diesel to air ratio of the zones completely transferred to zone D is zero. Based on the total mass transferred to zone D, the mass remaining in the partly transferred B_i zone is evaluated. The diesel to air ratio in the partly transferred zone is maintained at its initial diesel to air ratio. The diesel to air ratio of zone D is calculated from the total mass of diesel fuel and total mass of air transferred. The alcohol to air ratio, and the water to air ratio in zone D will be equal to the fixed values of these mass ratios in the entire cylinder. The mass ratios of alcohol to air, and water to air, in the cylinder will remain fixed throughout the cylinder over the entire cycle, for a specified engine operating condition. After the transfer process, let the final number of zones in the cylinder be n_F. The unknowns to be solved for at the end of mixing are: final cylinder pressure p_F, the final temperatures $T_{F,i}$, and the final volumes $V_{F,i}$ for the n_F zones. The total number of unknowns is $2n_F+1$. The final cylinder pressure is assumed to be slightly higher than the initial cylinder pressure before the instantaneous mixing process.

In the absence of heat transfer, isentropic compression is assumed for all the non-burning zones. The contents in each zone are assumed to behave as an ideal gas. Combining the ideal gas equation, and the equation for an isentropic process, the final temperature of each zone is calculated. The specific internal energy of the individual zones is then obtained from either MIXPROP or BURNDGAS, described in Appendices B, and C respectively. The total final internal energy of the cylinder contents is calculated and compared with the total initial internal energy. If the final

internal energy is lower than the initial internal energy, the final cylinder pressure is incremented slightly, and the process of calculating the new final internal energy is repeated. Thus, an iterative procedure involving the final cylinder pressure, is used to obtain the final state of all the zones in the cylinder. The details of this iterative process follow.

12.3 Solution Procedure to Obtain Final Conditions

During the instantaneous transfer process, the chemical composition of the unburned zones; zone A, and zone C, is unchanged. The change in the temperature of these unburned zones is quite small and hence the change in values of the specific heats Cp and Cv is negligible, and a constant ratio of specific heats can be assumed. By definition k represents the ratio of specific heats for an isentropic process between the initial and final states of the burned zones. For the burned B_i zones that are not transferred to zone D, the composition of the burned products changes because of chemical reaction at the end of the instantaneous transfer process due to a temperature change caused by a change in the cylinder pressure. The temperature of these burned zones, due to a slight change in the cylinder pressure, changes slightly. The reactions occurring in the burned zones due to a slight change in the temperature can be assumed to follow an isentropic process during the instantaneous mass transfer to zone D. The final temperature $T_{F,i}$ of all existing zones, except zone D, is given by

$$T_{F,i} = T_{I,i}\left(\frac{p_F}{p_I}\right)^{\left(\frac{k_{F,i}-1}{k_F}\right)} \tag{12.4}$$

where, $T_{I,i}$ is the initial temperature of zone i, p_I is the initial cylinder pressure, p_F is the guessed final cylinder pressure, and $k_{F,i}$ is the isentropic exponent for zone i, evaluated at the final pressure and temperature. In practice $k_{F,i}$ is very nearly equal to $k_{I,i}$. k_i is the ratio of specific heats. The specific heat at constant pressure, Cp, and the specific heat at constant volume, Cv, are provided by the property routines for the unburned mixture, and the burned products. For the burned zones transferred to zone D, the masses are zero and hence these zones will not be considered for further calculations. The isentropic condition cannot be applied to zone D, since there is mass transfer and mixing in zone D, resulting in a considerable degree of chemical reaction and change in temperature. At the beginning of phase two, zone D is initiated to form and the initial temperature of zone D is assumed to be equal to the temperature of the burned B_i zone that is transferred into it, first. At future crank positions, the temperature of zone D at the previous crank step is used as a first guess for the final zone temperature. An initial guessed temperature is required for the iterative solution procedure used in the present mixing model. The iterations are carried out with slightly incremented values of the final cylinder pressure, p_F, as explained earlier in this appendix.

The volume of each zone can be computed from the ideal gas equation:

$$V_i = \frac{m_i R_i T_i}{p} \tag{12.5}$$

The sum of the volumes of all the zones must equal the cylinder volume, V_{cyl}, at the specified crank position.

$$V_{cyl} = \sum_{i=1}^{n_f} V_i \tag{12.6}$$

Substituting for V_i from Equation 12.5 in Equation 12.6

$$V_{cyl} = \sum_{i=1}^{n_f} \frac{m_i R_i T_i}{p} \tag{12.7}$$

The post-mixing volume of the zones completely transferred to zone D is zero. The volume of zone D at the end of mixing is estimated by subtracting the volume of the other zones from the total cylinder volume. Then the post-mixing temperature of zone D, can be calculated using the ideal gas equation, with the gas constant estimated during the previous iteration. The final diesel to air ratio of zone D is calculated at the end of the mixing process.

For the burned zone which is partially transferred to zone D, the final zone mass is obtained by the mass balance relation:

$$m_{f,i} = m_{I,i} - m_{f,D} - m_{i,D} - \sum_{i=4}^{k_w} m_{I,i} \tag{12.8}$$

where, the subscript k_w refers to the burned zone currently at the bowl wall. The final mass of zones not transferred to zone D, is kept equal to the initial mass of the respective zones.

With the calculation of the updated final temperature of the wall zone, zone D, the final cylinder pressure p_F, and the final temperatures $T_{F,i}$ of all the n zones is available. However, the temperature $T_{F,i}$ for the burned zones completely transferred to zone D, will be of no interest. The final specific internal energy $u_{F,i}$ of all the zones is then obtained from the property routines for unburned mixture or burned products, as the case may be. The values of p_F, $T_{F,i}$ and the diesel to air mass ratio for the individual zones $\gamma_{F,i}$ are the inputs to the property routines to obtain $u_{F,i}$

for all the zones. The total final internal energy for the cylinder is given by:

$$U_F = \sum_{i=1}^{n_F} m_{F,i} u_{F,i} \tag{12.9}$$

The error between the final and initial total internal energy is calculated using

$$\%Error = \frac{(U_I - U_F)}{U_I} \times 100 \tag{12.10}$$

If the error is less than 0.01%, it is assumed that convergence has occurred, and the final cylinder pressure, and the final zone temperatures represent the right solution. If the error is larger than 0.01%, the final cylinder pressure can be incremented slightly and the solution procedure is repeated beginning with Equation 12.4. For speedier convergence of the solution process, the Secant Method [50] of guessing new p_F values is adopted in the present model.

The main program calls the wall model subroutine MIXINGZ, during phase two, and phase three of the engine cycle, after each newly evolved B_i zone is burned. The final cylinder pressure, final zone temperatures, and final zone volumes of all the zones in the cylinder, are returned by MIXINGZ to the main program.

13. APPENDIX F: MODELING THE FORMATION OF NITRIC OXIDE

Oxides of nitrogen (NO_X) are considered to be a major source of air pollution and their level in engine exhaust is regulated by the Environmental Protection Agency. Current regulations for heavy-duty diesel engines limit the exhaust concentration of NO_X to 6.0 grams/BHP-Hr, under standardized transient engine test conditions [1]. The 1991 regulations reduce this limit to 5.0 grams/BHP-Hr, and more stringent regulations are possible beyond the 1990s. Modifications to existing diesel engines or the development of newer engines to meet the upcoming stringent regulations for NO_X will be expensive and tedious. Computer models of diesel engine combustion can help to reduce engine development time and these models can provide estimates of NO_X production. The procedure used in the present work to model the formation of NO_X in the individual zones, and in the entire cylinder is described in this appendix.

Of the various oxides of nitrogen, nitric oxide (NO) and nitrogen dioxide (NO_2) are the major species emitted from combustion processes [64]. Under most conditions, NO is present in much larger concentration than NO_2. Hence, the present model focuses on the formation of NO.

The formation of NO_X in the cylinder is dependent on both excess air and temperature. In the present model, instantaneous cylinder NO is calculated over the

entire cycle, and the NO concentration in the cylinder corresponding to exhaust valve opening is compared with experimentally obtained exhaust NO level. The kinetics of NO in the engine cylinder have been modeled, using simplified schemes, by other researchers [22], [64], and [65].

Nitric oxide can be formed in three different modes:

a) fuel NO - from nitrogen containing fuels,

b) prompt NO - from reactions of fuel-based radicals with nitrogen during the combustion reaction, and

c) thermal NO - from reactions of oxygen and nitrogen in the cylinder.

Since neither diesel fuel nor alcohol contain nitrogen, the formation of fuel NO is ignored in the present model. Also, the amount of prompt NO [64] is small compared to thermal NO and hence prompt NO is not accounted for in the present model.

Thermal NO is known to form by a set of three coupled reactions called the extended Zeldovich mechanism [52]:

$$O + N_2 \rightleftharpoons NO + N \tag{13.1}$$

$$N + O_2 \rightleftharpoons NO + O \tag{13.2}$$

$$N + OH \rightleftharpoons NO + H \tag{13.3}$$

The species involved in these reactions are H, N, O, N_2, O_2, OH, and NO. The instantaneous concentration of these seven species can be expressed in terms of the chemical reaction rates and the concentrations of other species. By combining the expressions for the instantaneous concentration of the individual species, and assuming that because of the high combustion temperatures, the concentrations of H, N,

Table 13.1: Table of Reaction Rate Constants

	Reaction	Rate Constant $cm^3/mole/sec$	Temperature Range K	
1-f	$O + N_2 \longrightarrow NO + N$	$7.60 \times 10^{13} exp(-38,000/T)$	2000	5000
1-b	$NO + N \longrightarrow O + N_2$	1.60×10^{13}	300	5000
2-f	$N + O_2 \longrightarrow NO + O$	$6.40 \times 10^{9} exp(-19,500/T)$	300	3000
2-b	$NO + O \longrightarrow N + O_2$	$1.50 \times 10^{3} exp(-19,500/T)$	1000	3000
3-f	$N + OH \longrightarrow NO + H$	1.00×10^{14}	300	2500
3-b	$NO + H \longrightarrow N + OH$	$2.00 \times 10^{14} exp(-23,650/T)$	2200	4500

O, N_2, O_2, and OH in each zone are at their equilibrium values, the rate of change of NO concentration at constant volume is given by:

$$\begin{aligned} \frac{d[NO]_V}{dt} &= \left(2k_{f,1}k_{f,2}[O][N_2][O_2] - 2k_{b,1}k_{b,2}[NO]^2[O]\right. \\ &+ \left. 2k_{f,1}k_{f,3}[O][N_2][OH] - 2k_{b,1}k_{b,2}[NO]^2[H]\right) \\ &/ \left(k_{b,1}[NO] + k_{f,2}[O]_2 + k_{f,3}[OH]\right) \end{aligned} \tag{13.4}$$

The concentration of NO used in the above expression is the value of NO at the previous time step. For the first time step, the value of NO in the zone is assumed to be zero. Subscripts k_f and k_b refer to the forward and backward reaction rate constants, respectively.

The rate constants used in the present model are based on those suggested by Baulch et al. [66] and Bowman [67], and are provided in Table 13.1.

In an actual engine the cylinder volume changes with time, and hence the instantaneous NO concentration is a function of both the cylinder volume and the reaction

rates. The rate of change of NO concentration in the cylinder is given by

$$\frac{d[NO]}{dt} = \frac{d[NO]_V}{dt} - \frac{NO}{V_{cyl}}\frac{dV_{cyl}}{dt} \tag{13.5}$$

where, $\frac{d[NO]_V}{dt}$ represents the rate of change of NO concentration due to reaction kinetics, at constant volume, obtained from Equation 13.4. The rate of change of cylinder volume is given by $\frac{dV_{cyl}}{dt}$, where V_{cyl} is the instantaneous cylinder volume.

A partial equilibrium approximation has been used for determining the initial conditions. In this approximation, it is assumed that the concentrations of O_2, N_2, O, N, H, and OH in the burned zones are equal to their equilibrium values, and the NO formation rate is much slower than the combustion rate. Nitric oxide formation rates can be calculated from Equation 13.4 utilizing equilibrium values of temperatures and concentrations of O_2, N_2, O, N, H, and OH. The equilibrium concentrations of O_2, N_2, O, N, H, and OH in the previously burned zones are obtained from PER [51] as detailed in Appendix C. The initial value of NO for newly burned zones is assumed to be zero.

Equations 13.4 and 13.5 are written for each zone, and are solved along with the thermodynamic equations for cylinder pressure and the zone volumes. The values of NO concentration obtained for the individual zones are combined to obtain the total NO concentration in the cylinder. The NO concentrations are obtained only for the burned zones, since NO will not form in the low temperature unburned zones. The value of exhaust NO concentration is given by the value of cylinder NO level at the time of exhaust valve opening. Typical plots of NO history, and comparisons with experimental data are given in Chapter 5.

As discussed in Chapter 3, the combustion period of the engine cycle is divided

into five discrete phases. During phases two and three, the spray impinges on the wall and the previously burned zones from the spray plume are transferred to the wall zone, zone D. The burned zones transferred to zone D contain oxides of nitrogen as a result of combustion. If a burned zone is completely transferred to zone D, the entire nitric oxide, in units of moles, is added to the moles of nitric oxide present in zone D prior to the instantaneous mass transfer process. If only a part of a burned zone is transferred to zone D, a corresponding mass weighted fraction of the moles of nitric oxide from this burned zone is instantaneously transferred to zone D. During phase four and phase five, all of the nitric oxide in the cylinder is present in zone D.

In this appendix the sub-model used to calculate the nitric oxide concentration in the cylinder has been described. The method used in the present model to obtain the nitric oxide concentration in the cylinder during the different phases of the combustion process has been included in subroutine THERMOZ. The derivative equations for the rate of change of nitric oxide concentration in each zone in the cylinder are integrated in THERMOZ along with the differential form of the thermodynamic equations. The instantaneous zone temperatures, T_i, used in the calculation of reaction rates for the individual zones from the rate equations in Table 13.1, and the instantaneous zone volumes, V_i, are obtained from the solution procedure in THERMOZ.

14. APPENDIX G: DIESEL FUEL PROPERTIES

Fuel analyzed by Phoenix Chemical Laboratory, Inc., Chicago. Illinois. August 3, 1988.

	Sample #1 08 May '88 to 30 May '88.	Sample #2 31 May '88 to 08 June '88.
Carbon, %	86.75	86.83
Hydrogen, %	12.98	12.66
Carbon/Hydrogen Ratio	6.683	6.859
Molecular Weight	192	188
API Gravity at 60°F.	32.6	33.2
Hydrocarbon Types		
(D875) %(V/V)		
Saturates	69.2	68.9
Olefins	2.4	3.0
Aromatics	28.4	28.1
Sulphur, %	0.19	0.25
Heat of Combustion, BTU/lb.		
Gross	19,380	19,408
Net	18,196	18,253
Heat of Combustion, BTU/gal.		
Gross	139,148	138,845
Net	130,647	130,582

Distillation, °F		
Initial Boiling Point	350	356
5%	391	396
10%	418	417
20%	448	446
30%	472	467
40%	493	487
50%	511	507
60%	531	526
70%	550	546
80%	573	568
90%	603	599
95%	628	626
End Point	646	644
Recovery, %	98.0	98.0
Residue, %	1.9	1.9
Loss, %	0.1	0.1

The diesel fuel data required for use in the multizone model are: carbon/hydrogen ratio on a weight basis, molecular weight in kg/kmole, and the net heat of combustion (or the lower heating value) in BTU/lb. The data for the two separate batches of fuel were averaged and used in the model. The average values used are

$$\text{Carbon/Hydrogen ratio} = 6.771$$

$$\text{Molecular weight} = 190$$

$$\text{Net heat of combustion} = 18224.5$$

Based on the average carbon to hydrogen ratio and the average molecular weight the chemical formula of the diesel fuel molecule is found to be $C_{13.78}H_{24.26}$.